

12-2017

Development of a Direct-Contact Triculture Model of the Human Blood Brain Barrier and Potential Applications as a Preclinical Drug Screening Tool

Aimable Ngendahimana
Purdue University

Follow this and additional works at: https://docs.lib.purdue.edu/open_access_dissertations

Recommended Citation

Ngendahimana, Aimable, "Development of a Direct-Contact Triculture Model of the Human Blood Brain Barrier and Potential Applications as a Preclinical Drug Screening Tool" (2017). *Open Access Dissertations*. 1609.
https://docs.lib.purdue.edu/open_access_dissertations/1609

This document has been made available through Purdue e-Pubs, a service of the Purdue University Libraries. Please contact epubs@purdue.edu for additional information.

**DEVELOPMENT OF A DIRECT-CONTACT TRICULTURE MODEL OF
THE HUMAN BLOOD-BRAIN BARRIER AND POTENTIAL
APPLICATIONS AS A PRECLINICAL DRUG SCREENING TOOL**

by

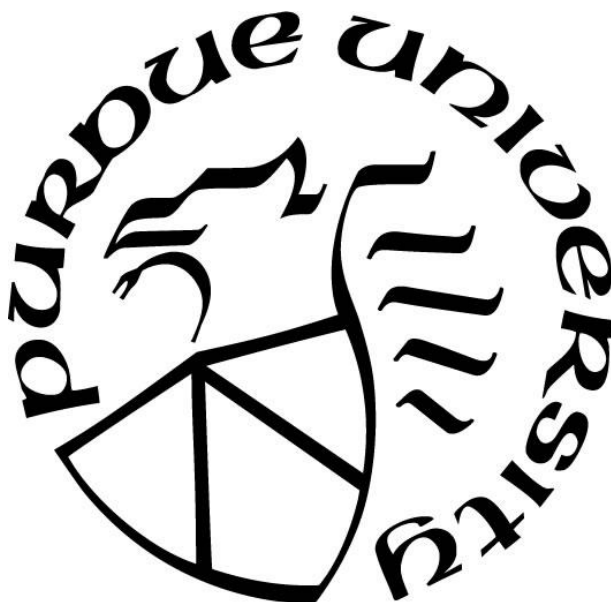
Aimable Ngendahimana

A Dissertation

Submitted to the Faculty of Purdue University

In Partial Fulfillment of the Requirements for the degree of

Doctor of Philosophy



Department of Industrial & Physical Pharmacy

West Lafayette, Indiana

December 2017

**THE PURDUE UNIVERSITY GRADUATE SCHOOL
STATEMENT OF COMMITTEE APPROVAL**

Dr. Gregory T. Knipp, Chair

Department of Industrial and Physical Pharmacy

Dr. Rodolfo Pinal

Department of Industrial and Physical Pharmacy

Dr. Stephen R. Byrn

Department of Industrial and Physical Pharmacy

Dr. Dea Herrera-Ruiz

Faculty of Pharmacy, Universidad autonoma Del estado de Mexico

Approved by:

Dr. Rodolfo Pinal

Head of the Graduate Program

*This thesis is dedicated to my parents (**Benithe Uwamwiza and Esaie Ngendahimana**), my American-grandparents (Professor **Helen Kholer and Ronald B. Stauffer**), and to my siblings (**Pascasie, David, and Valentine**). From Karura-Nairobi, to Baraton University, to Youngstown State University and now at Purdue, you have seen me through thin and thick! You have unconditionally encouraged me to achieve my academic dreams. For that, I would like to say **asanteni sana!***

ACKNOWLEDGMENTS

First, I would like to thank my advisor Dr. Gregory T. Knipp for his guidance over the last five years. I thank him for his patience and support while I worked on a subject that has baffled many BBB-scientists for so long. I believe that methods developed in Dr. Knipp's lab can expedite positive outcomes in CNS-drug discovery and development. I am glad to have worked on one of these methods.

Secondly, I wish to express gratitude to my committee members, former and current, (Dr. Elizabeth M. Topp, Dr. Stephen R. Byrn, Dr. Keith Chadwick, Dr. Rodolfo Pinal and Dr. Dea Ruiz-Herrera). You have enlightened me in many ways; your advice has permanently strengthened my understanding of scientific research and scientific progress. It is my plan to follow your excellent examples as leaders in the discipline of pharmaceutical research.

My experiences in the department of industrial and physical pharmacy involved teaching responsibilities in parenteral-products labs and pharmaceutical formulation and manufacturing. I would like to acknowledge Dr. Tonglei Li and Dr. Tony Zhou for their excellent mentorship for me as a graduate Teaching Assistant. The skills that I gained as your Teaching Assistant will surely propel me to higher levels of professionalism.

I would like to thank Mary Ellen Hurt for so many reasons. For five years, she has persistently watched out to make sure that I succeed in the program. I thank you exceedingly Mary Ellen!

Equally important, I would like to express my thanks to Dr. V. Jo Davisson and Dr. Jean-Christophe Rochet. You have inspired me directly or indirectly through classes and personal interactions. Through you, I have learned a lot and my plan is to follow your example.

In closing, I would like to thank all my friends and colleagues in the IPPH program for having made my stay enjoyable here at Purdue. I hope that we will stay connected even when I leave. Thank you!

TABLE OF CONTENTS

LIST OF TABLES	ix
LIST OF FIGURES	x
LIST OF ABBREVIATIONS.....	xviii
ABSTRACT.....	xx
CHAPTER 1. JUSTIFICATION FOR THE DEVELOPMENT OF A LAYERED DIRECT- CONTACT TRICULTURE MODEL OF THE BLOOD-BRAIN BARRIER.....	1
1.1 Summary.....	1
1.2 Introduction.....	2
1.3 Blood-brain barrier glial unit	3
1.4 BBB transport properties	4
1.4.1 Cell-cell junctions	5
1.4.1.1 Junctional protein complexes	5
1.4.1.2 Peg & socket junctions	6
1.4.1.3 Gap junctions	6
1.4.2 Cell transmigration	7
1.4.3 Vesicular transport.....	7
1.4.4 Membrane transporters	8
1.4.5 Lipophilic diffusion	9
1.5 Mimicking the BBB function in a <i>Transwell</i> TM	10
1.6 Specific research aims.....	11
1.7 Concluding remarks	15
1.8 References.....	16
CHAPTER 2. IMPROVED PARACELLULAR TIGHTNESS IN THE DIRECT-CONTACT TRICULTURE MODEL OF THE BLOOD-BRAIN BARRIER.....	21
2.1 Summary.....	21
2.2 Introduction.....	23
2.3 Hypothesis.....	26
2.4 Test Parameters.....	26
2.4.1 Trans-Endothelial Electrical Resistance (TEER)	27

2.4.2	Permeability coefficients	27
2.5	Materials and methods	28
2.5.1	Cells and cell growth materials.....	28
2.5.2	Cell seeding	29
2.5.3	TEER measurement.....	30
2.5.4	Test compounds.....	30
2.5.5	Permeability assays under monocultures of the hCMEC/D3 cells.....	31
2.5.6	Permeability assays under cocultures of the hCMEC/D3 cells with pericytes.....	33
2.5.7	Permeability assays under cocultures of the hCMEC/D3 cells with Astrocytes	34
2.5.8	Permeability assays under tricultures of the hCMEC/D3 cells with pericytes and astrocytes	34
2.5.9	Statistical Analysis.....	34
2.6	Results and discussion	35
2.6.1	Selection of the cell-seeding density ratio for the triculture model.....	35
2.6.2	Selection of the day for performing permeability assays	37
2.6.3	Microscopic examination in triculture seeding.....	38
2.6.4	Relative paracellular tightness in the BBB triculture	41
2.6.5	Relative permeability of mannitol in the coculture of astrocytes with pericytes	44
2.6.6	Size-dependent permeability of paracellular marker compounds	46
2.7	Conclusions.....	48
2.8	Acknowledgements.....	48
2.9	References.....	48
CHAPTER 3. ANALYSIS OF THE MULTILAYERED CONFIGURATION OF THE TRICULTURE MODEL OF A HUMAN BLOOD-BRAIN BARRIER		53
3.1	Summary.....	53
3.2	Introduction.....	54
3.3	Hypothesis.....	58
3.4	Cell specific features.....	58
3.4.1	Cell specific morphologies	58
3.4.2	Cell-cell junctions.....	59
3.4.3	Internal cell organelles.....	59

3.5	Materials and imaging techniques	60
3.5.1	Materials	60
3.5.2	Imaging techniques	61
3.5.2.1	A brief description of phase contrast microscopy	61
3.5.2.2	Application of phase contrast during preparation of a BBB triculture.....	61
3.5.2.3	A brief description of transmission electron microscopy (TEM).....	62
3.5.2.4	Application of TEM in imaging the BBB triculture.....	62
3.5.3	A brief description of the fluorescence microscopy	63
3.5.3.1	Application of confocal microscopy in visualizing optical sections of a BBB triculture	64
3.6	Results.....	65
3.7	Discussion.....	72
3.7.1	Cell morphologies and arrangements during preparation of a triculture model of the BBB	72
3.7.2	Analysis of cell-cell junctions and cell organelles	73
3.7.3	The expression pattern of F-actin in the BBB cells: astrocytes, pericytes and the hCMEC/D3.....	77
3.8	Conclusions.....	78
3.9	Acknowledgements.....	78
3.10	References	78
CHAPTER 4. POTENTIAL APPLICATIONS OF THE BLOOD-BRAIN BARRIER TRICULTURE MODEL AS A DRUG ABSORPTION AND PERMEABILITY SCREENING TOOL		
4.1	Summary.....	83
4.2	Introduction.....	84
4.3	Hypothesis.....	88
4.4	Test parameters	88
4.4.1	Mole fraction absorbed.....	88
4.4.2	Permeability of transcellular permeants	89
4.5	Materials and Methods.....	92
4.5.1	Materials	92

4.5.2	Enhancement of Digoxin Absorption by a Pgp/BCRP inhibitor	93
4.5.3	Permeability assays for transcellular permeants	93
4.5.3.1	Control assay in the monocultures of hCMEC/D3 cells.....	93
4.5.3.2	Assay in the triculture model of the human BBB.....	94
4.5.4	Statistical analysis.....	95
4.6	Results and discussion	95
4.6.1	Effects of elacridar on the absorption of digoxin	95
4.6.2	Permeability of hydrophilic transcellular permeants	98
4.6.3	Permeability of lipophilic transcellular permeants	100
4.6.4	A basic permeability ranking scale for transcellular permeants	101
4.7	Conclusions.....	103
4.8	Acknowledgement	104
4.9	References.....	104
CHAPTER 5. DISSERTATION HIGHLIGHTS AND LONG-TERM PERSPECTIVES ON		
THE DEVELOPMENT OF LAYERED CELL CULTURE MODELS OF THE HUMAN		
BLOOD-BRAIN BARRIER.....		
5.1	Dissertation highlights	110
5.2	Long-term strategies for advancing the triculture-methodology	113
5.2.1	High throughput implementation of the triculture methodology.....	114
5.2.2	Inclusion of brain neurons in the direct-contact triculture model of the blood-brain barrier	116
5.2.3	Development of <i>In Vitro In Vivo</i> correlation models, refinements and commercialization	117
5.3	A declaration of conflict of interests.....	119
5.4	References.....	119
APPENDIX A. SUPPLEMENTAL DATA ON THE BASAL CULTURE OF ASTROCYTES		
AND PERICYTES.....		
APPENDIX B. SUPPLEMENTAL TEM MICROGRAPHS OF THE BBB TRICULTURE... 123		

LIST OF TABLES

Table 2.1. The Physicochemical properties for the tested paracellular permeants.	32
Table 2.2. Selection of a seeding density ratio. A = astrocytes, P = pericytes, E = hCMEC/D3 cells	36
Table 2.3. The Formation of tight cell-cell junctions in a monoculture of hCMEC/D3. A sudden reduction in the mannitol permeability across the hCMEC/D3 culture at the end of 144 hours indicated a reduced cell-cell junctional space.....	38
Table 4.1. Pgp probe substrate (digoxin) and inhibitor (elacridar)	891
Table 4.2. Transcellular test-permeants	913

LIST OF FIGURES

Figure 1.1. A neuroprotective BBB. The bright green arrow shows a neuron (**N**), the light blue arrow shows an astrocyte (**A**), the black arrow shows a pericytes (**P**) and the purple arrow shows a BBB-endothelium. It is notable that for a neuronal drug delivery to be attained, a drug molecule would have to be transported past the BBB-endothelium, the extracellular matrix, and pericytes or astrocytes. Cell-cell junctions (molecular channels) that connect neurons, astrocytes, pericytes and the BBB-endothelium may provide an alternative transport pathway to circumvent tight junctions, extracellular enzymes, and CFS clearance in neuronal drug delivery. An *in vitro*- multicellular model of the BBB that allows for unlimited and direct interactions between the cellular constituents of the BBB-glia unit would be useful in preclinical CNS-drug delivery studies.....12

Figure 1.2. The lack of optimal cell-cell interactions in the conventional methodology when modeling the BBB-glia unit on a *Transwell*TM support. EC stands for Endothelial Cells, PC for pericytes, and AC for astrocytes. A thick membrane filter support limits the formation of cell-cell junctions between ECs and PCs. In addition, ACs are seeded at the bottom surface where they are largely separated from ECs and PCs. Therefore, optimal cell-cell channels such as gap junctions, peg-socket junctions may not be formed between ACs, PCs and ECs. Figure 1.2 was reproduced with permission from Elsevier [Cerruti et al. 2011].....13

Figure 1.3. A direct-contact triculture methodology for mimicking the BBB-glia unit on a *Transwell*TM support. Configuration (**A**) involves seeding the triculture on the apical surface, (**B**) is an inversed configuration of (**A**), and (**C**) is configuration (**A**) seeded on the basolateral surface of a transwell membrane. The proposed methodology leads to a spatial arrangement that would allow for additional cellular components of the neurovascular unit to be added in the model.....14

Figure 2.1. The BBB-glia vascular unit. **AF** stands for Astrocytic-Foot process, **E** stands for endothelial cell, and **P** stands for pericyte. It is noteworthy that blood inside the endothelial capillary lumen does not cross the paracellular space of the endothelial cells. The junctional space of the endothelial cells (blue region) is filled with tight junctions that restrict free passage of cells, serum proteins and molecules circulating in the capillary lumen from accessing the brain parenchyma. 23

Figure 2.2. The BBB-culture models examined in the present study: (1) is the hCMEC/D3 monoculture representing a section of the BBB-glia vascular unit (2), the hCMEC/D3 co-culture with pericytes; a partial representation of the BBB-glia vascular unit and (3) the hCMEC/D3-triculture, which fully mimics the BBB-glia unit as it contains all physiologically relevant cell layers formed by endothelial, pericytes and astrocytes. 26

Figure 2.3. Step I: Preparation of a layer of astrocytes in the course of seeding a direct-contact triculture. Prior to seeding, the suspended astrocytes were sheared up and down using a Pasteur pipette to ensure that no cell clumps were seeded on the transwell membrane. Initially a seeding volume of .250mL was used to seed astrocytes at a density of 4×10^4 cells/cm² (**Panel A**). Cells were left in the sterile hood for 30 minutes in order to settle down on the surface of the membrane. An additional .250mL of astrocytes media was then added on the apical chamber where the astrocytes were seeded. The basolateral chamber was filled with 1.5 mL of astrocytes media. The astrocytes culture was then set in a sterile incubator. The astrocytes culture expanded and changed the morphology from round circular cells to a sharp-ended morphology at the end of 48 hours (**panel B**)..... 39

Figure 2.4. Step II: Culturing a layer of pericytes on top of the astrocytes prepared in step I. Pericytes were prepared in the same way as astrocytes in step I. **Panel A** shows pericytes settling on a base-culture of astrocytes. Pericytes were dispersed well to avoid formation of unwanted overgrowth. **Panel B** shows pericytes growing in the co-culture at the end of 48 hours. Though the new culture looks distinct from the astrocytes culture, it was difficult to visualize a distinct layer of pericytes due to poor phase contrast in an inverted light microscope. 40

Figure 2.5. Step III: Culturing a layer of hCMEC/D3 cells after step II. **Panel A** is a micrograph showing the hCMEC/D3 cells seeded at 8×10^4 cells/cm², on top of a co-culture of pericytes & astrocytes prepared in step II. The hCMEC/D3 cells was left to grow on a base of astrocytes and pericytes for 6 days. The resulting triculture was stained on day 7 using hematoxylin. A light micrograph of the triculture after staining is shown in panel **B**..... 41

Figure 2.6. A comparison of paracellular tightness in the mono-, co- and triculture models of the BBB. TEER values (**Panel A**) indicated that the direct-contact triculture shows more resistance to the flux of conducting ions in comparison to the mono- or co-cultures (one-way ANOVA; n

=12, p-values were 0.001 and 0.004 respectively. The higher resistance in the triculture was confirmed using the permeability of sucrose. The hCMEC/D3 monoculture was less restrictive to sucrose permeation in comparison to the co-cultures of hCMEC/D3 with pericytes or with astrocytes and the triculture as shown in **Panel B** (one way ANOVA; n = 6, p-values were < 0.001 in each comparison where the hCMEC/D3 monoculture was used in the control experiment). A Turkey's post hoc test showed that a significant difference in the mean permeability values existed only between the hCMEC/D3 monoculture control versus co- and tricultures examined in this study..... 43

Figure 2.7. Permeability of mannitol across mono- or co-cultures of astrocytes and pericytes. The apparent permeability of mannitol is lower in the co-culture of astrocytes and pericytes in comparison to the astrocytes or pericytes alone (**Panel A**). The effective permeability of mannitol (**Panel B**) in the culture of pericytes could not be determined since it was equal to that of a free filter membrane containing no cell layers. The effective permeability of mannitol across layers of pericytes and astrocytes in a coculture, was significantly lower in comparison to monoculture of astrocytes alone as shown in Panel B (T-test: n = 6, p-value = 0.002) 45

Figure 2.8. Size-dependent reduction of paracellular permeability through the triculture. In comparing mono- and tri-cultures, the decrease in permeability was 1.5-fold for mannitol, 2.4-fold for sucrose, 4.5-fold for PEG-4000, and 8-fold for Inulin-5000. The larger compounds would be much more restricted in the triculture than in the monoculture models of the BBB system. T-tests indicated a higher paracellular tightening in the triculture model for all four marker compounds employed in this study (n = 5, p-values were less than 0.05 in all the cases).....47

Figure 3.1. A reference TEM micrograph of a Blood-Brain Barrier specimen from the rat. Panel A represents the actual micrograph and Panel B is a pictorial representation of the micrograph in panel A. The cross-sectional BBB micrograph of a rat, as presented in the micrograph, consists of a single endothelium that forms a lumen of the blood capillary. The BBB endothelium locks its peripheral ends by forming tight-junctions. The BBB endothelium shows prominent cell organelles in the cytoplasm including mitochondria, vacuoles, nucleus, and the nucleolus. Numerous regions of the capillary lumen seem to be budding off the endothelial surface. Pericytes that surround the BBB capillary seem to be relatively smaller than endothelium. The surrounding astrocytes are

more transparent to the beam of electrons, and they have a heterogeneous morphology that lack prominent nuclei and other cell organelles [Farkas et al., 2001, image reproduced with permission from Elsevier] 56

Figure 3.2. A cross-sectional TEM micrograph of a human BBB. The BBB capillary is associated with a single pericyte. The BBB endothelium forms cytoplasmic extensions that loop to form a capillary lumen stabilized by tight junctions. Pericytes do not form a lumen nor tight junctions similar in a similar way to the BBB endothelium [Garbuzova-Davis et al., 2012, image reproduced with permission from Elsevier]..... 57

Figure 3.3. A schematic representation for the cross-sectional features of a typical human cell grown on a filter membrane: (1) Nucleolus, (2) Nucleus, (3) Cytosol, (4) Endoplasmic reticulum, (5) Golgi body, (6) Vacuole, (7) Microfilament, (8) Mitochondrion, (9) Microtubules (10) Junctional complex, (11) Filter-support (12) Cell membrane. Sizes and distributions of the cell organelles can vary across different types of cells depending on their functions or environment. 60

Figure 3.4. Formation of distinct cell-layers during BBB triculture preparation. (A) Sub-confluent layer of astrocytes formed after two days (48 hours) shows cells with a characteristic morphology for the astrocytes. (B) A sub-confluent layer of pericytes laid over the astrocytes layer at the end of two days (48hrs) post-seeding. (C) A confluent-layer of hCMEC/D3 cells laid over the underneath coculture of astrocytes and pericytes (prepared as described in panels A and B) at the end of six days post-seeding. 65

Figure 3.5. Ultrastructural features in the monoculture of hCMEC/D3 cells. **Panel A** shows tight junctions formed between two adjacent hCMEC/D3 cells (**red arrow**) and an exosome budding off the hCMEC/D3 cell (**blue arrow**). **Panel B** shows an overlapping cell-cell junction forming a minute contact points (**orange arrow**) and a larger nucleus occupying most of the cytoplasmic space (**white arrow**). Panel C shows the formation of numerous vacuoles (**green arrow**), a large exosome (**blue arrow**) and a fusing cell-cell junction (**orange arrow**). 66

Figure 3.6. Ultrastructural features in the monoculture of pericytes. **Panel A** shows wide cell-cell junctions between two adjacent pericytes (**orange arrow**), and a highly transparent vesicle

containing granular materials in its lumen (**green arrow**). **Panel B** shows an overlapping cell-cell junction between two adjacent pericytes (**orange arrow**), a prominent rough endoplasmic reticulum (**red-pink arrow**) and highly transparent exosomes (**blue arrow**). **Panel C** shows a prominent nucleolus structure at the center of a pericyte nucleus (**dark blue arrow**). 67

Figure 3.7. Ultrastructural features in the monoculture of astrocytes. **Panel A** shows a stellate projection from the body center of an astrocyte (**orange arrow**) and a swollen body center (**blue arrow**). **Panel B** shows an elongated projection from the body-center of an astrocyte. **Panel C** shows a swollen end-section of an astrocyte (**green-yellow arrow**) 68

Figure 3.8. Cross-sectional arrangement of cells in the triculture model, part I. **Panel A** shows a multicellular structure composed of closely associated cells at the top layer, which could be endothelial (**E**), or pericytes (**P**). The middle section in **Panel A** contains dispersed cells containing a prominent nucleus (PN); these could be disordered pericytes separated by a swollen astrocyte (**A**) between them. The bottom layer in **panel A** consists of cells lacking a prominent nucleus, or formation of vesicles; these could be astrocytes with sharp stellate ends. **Panel B** shows a well-contrasted micrograph of the triculture model. Note that the top layer of cells formed a continuous thin membrane; this is a property of BMECs/BBB endothelium. Also note that though certain cells in the middle section resemble endothelial cells at the top, they do not form a continuous wall; this is a property of pericytes (there is also a large nucleolus in the cells assigned as pericytes). There is a large extracellular space denoted by a **double-headed yellow arrow** in the micrographs. This space could be due to the formation of excess extracellular matrix 69

Figure 3.9. Cross-sectional arrangement of the BBB cells in the triculture model, part II. **Panel (A)** shows junctional contacts between two endothelial cells (**red arrow**), and a high population of vacuoles (green) in the two adjacent endothelial cells. The middle and basal layers in **panel (A)** show prominent mitochondria characteristic of astrocytes at the BBB in vivo (**maroon arrow**). **Panel (B)** shows middle and basal layers containing cells with prominently large nucleus and nucleolus (dark blue arrow). Cells in the basal layer of **panel (B)** formed widened cell-cell junctions (white arrow). **Panel (C)** shows cells that form a continuous cell layer (characteristic of BMECs, see **red arrow**) at the top layer, a cell in the middle layer that lacks connections with adjacent cells

(a characteristic of pericytes) and a basal layer of cells that have long sharp projections, lacking prominent vesicles (a characteristic of astrocytes) 70

Figure 3.10. Fluorescent patterns of F-actin in the cytoskeletons of astrocytes (**Panel A**), pericytes (**Panel B**) and the hCMEC/D3 cells (**Panel C**). The fluorescence pattern in the astrocytes is more diffuse in a pattern that shows a stellate morphology (**Panel A**). The fluorescence pattern in the pericytes showed a discrete arrangement of the F-actin bundles (**Panel B**). The hCMEC/D3 cells showed a more diffuse fluorescent pattern reflecting their spindle-shaped morphology (**Panel C**) 71

Figure 3.11. Fluorescent optical sections in the BBB triculture. **Panel A** shows a faint optical section showing the expression pattern of F-actin in the hCMEC/D3 section. **Panel B** shows a clearer optical section showing mixed features of astrocytes and hCMEC/D3 cells, all projected in the same plane..... 71

Figure 4.1. Transcellular transport systems at the BBB-glia unit. BCRP stands for Breast Cancer Resistance Protein. MRP1, -2, -3, -4 stands for Multidrug Resistance associated-Protein 1, -2, -3, -4. GLUT1 stands for Glucose Transporter 1. Pgp stand for P-glycoprotein transporter. LAT1 stands for Large neutral-Amino Acid Transporter. CRT1-Creatinine Transporter 1, ASCT1-neutral Amino Transporter 1, OCTN 1, -2 stands for Organic Cation/Carnitine Transporter 1, -2 and SNAT3 stands for Special Amino Acid Transporter 3. Note that transport out of the brain is more favored than transport into the brain parenchyma.....90

Figure 4.2. A comparison of drug-interactions (elacridar and digoxin) in the AP-coculture versus hCMEC/D3 monocultures, and the triculture containing hCMEC/D3 cells on a basement of pericytes layered directly on the astrocytes. AP stands for Astrocytes Pericytes coculture. The confidence intervals (CI) for the difference in the mean molar fraction absorbed indicated a significant difference for values obtained under the hCMEC/D3 monoculture (n=6, at 95% CI = 0.06 ± 0.009), and for values obtained under the AP-coculture (n=6, at 95% CI = 0.04 ± 0.007). There was no significant increase of digoxin absorption in the triculture when elacridar, a potent Pgp inhibitor, was incubated in the triculture prior to the addition of digoxin (n=6, at 95% CI = 0 ± 0.009).....98

Figure 4.3. A comparison of hydrophilic transcellular permeability coefficients across mono- and tri-culture models. There was no significant difference in the permeability of hydrophilic transcellular permeants across mono- and tri-culture models of the human BBB. Urea seem to have a higher permeability across the triculture than across the monoculture (the 95% CI = 0.15 ± 0.073). On the contrary L-histidine exhibited a lower permeability in the triculture (the 95% CI = 0.36 ± 0.121). Thiamine showed similar permeability across the mono- and triculture models of the BBB in this study with a 95% CI of (0.03 ± 0.094).....99

Figure 4.4. A comparison of lipophilic permeability coefficients for propranolol and verapamil. There was no significant difference in the permeability of lipophilic transcellular permeants (propranolol and verapamil) under the mono- and tri-culture models. The 95% CI for the difference in the mean Papp values were 1.16 ± 1.734 for propranolol and 0.05 ± 0.802 for verapamil. However, the permeability value of verapamil, a Pgp-marker compound, was significantly lower than that of propranolol, a marker of fast transcellular permeation, both in the mono- and triculture settings (the 95% CI intervals for the differences in the mean Papp values were 3.52 ± 1.792 under the monoculture settings, and 2.41 ± 0.634 under the triculture settings.....100

Figure 4.5. A basic permeability scale for a small set of transcellular BBB-permeants. Blue and Green compounds represent high BBB permeant-markers, yellow compounds are indicative intermediate permeability markers, and the red compound indicates lower permeability. The triculture model is capable of ranking different permeants in different permeability categories (a one-way ANOVA test indicated the difference where $n = 3$ in each category, with a p -value < 0.001). A post hoc Tukey's Honestly Significant Difference value of 0.036 indicated that propranolol and paclitaxel had similar apparent permeability values with a non-significant difference ($HSD > 0.009$) in the mean values 103

Figure 5.1. Conceptual designs on how to mimic a preclinical BBB-glia unit system in a neuronal environment. Panel (A) shows a direct-contact model of the BBB in a neuronal environment on the apical chamber of a Transwell™. Panel (B) illustrates a direct-contact model maintained in a neuronal environment on the basolateral chamber of a *Transwell™*..... 117

Figure 5.2. A framework for the application of BBB cell culture methods in the development of IVIVC models. The ultimate goal is to generate robust IVIVC models capable of predicting pre-

clinical or clinical pharmacokinetic and pharmacodynamic parameters of interest in CNS-drug development. For example, data sets from pre-clinical models such as a mouse could be used to assist in the development of IVIVC models for predicting drugs/drug delivery systems that would lead to optimal drug exposure to the brain parenchyma. IVIVC models may be continually refined as more data from in vivo and in vitro studies become available from various researchers. 118

Supplemental Figure 1. Pericytes cultured alone on the surface of a *Transwell*TM filter support. Pericytes did not grow to cover the surface completely even at the end of day 7. The bar represents 100 μm 121

Supplemental Figure 2. Pericytes grown on a basal culture of astrocytes multiplied to cover the underneath astrocytes completely at the end of day 7. The bar represents 100 μm 122

Supplemental Figure 3. Astrocytes cultured on a basal layer of pericytes for 7 days. Astrocytes on the top layer multiplied to cover most of the underneath pericytes. The characteristic needle-like projections, which are unique features to the astrocytes, were clearly visible on the astrocytes. The bar scale represents 100 μm122

Supplemental Figure 4. Thin cross-sectional TEM micrographs of a BBB triculture. Panel A shows a section where three layers (L1, L2, and L3 formed). Panel B shows a section where two cell layers are formed (L1, and L2). It is hoped that a non-ambiguous identification of the cell layers of the BBB triculture will be made using cell-specific staining antibodies as a continuation of the research presented in the current dissertation. The bar scale represents 0.5 μm 123

LIST OF ABBREVIATIONS

CNS	Central Nervous System
BBB	Blood-Brain Barrier
BMECs	Brain Microvessel Endothelial Cells
hCMEC/D3	Human Cerebral Microvessel Endothelial Cells /D3
PEG-4000	Polyethylene Glycol 4000
FDA	Food and Drug Administration
Pgp	P-glycoprotein 1
IVIVC	In Vitro In Vivo Correlation
CSF	Cerebral Spinal Fluid
MDR1	Multi-Drug Resistance gene 1
mRNA	Messenger Ribonucleic Acid
MDCKII	Mardin-Darby Canine Kidney II
OCT1	Organic Cation Transporter 1
JAMs	Junctional Adhesion Molecules
VE-cadherin	Vascular Endothelial Cadherin
ZO-1, 2, 3	Zonula Occludens-1, 2 and 3
TEER	Trans-Endothelial Electrical Resistance
METH	Methamphetamine
BCRP	Breast Cancer Resistance Protein
OATP	Organic Anion-Transporting Polypeptide
EVOM2	Epithelial Volt-Meter 2
HEPES	4-(2-hydroxyethyl)-1-piperazineethanesulfonic acid
HBVP	Human Brain Vascular Pericytes
FBS	Fetal Bovine Serum
PBS	Phosphate Buffered Saline
PGS	Pericytes Growth Supplement
HBSS	Hank's Balanced Salt Solution
ANOVA	Analysis Of Variance

SEM	Standard Error of the Mean
VVOs	Vesiculo-Vacuolar Organelles
CCD	Charge-Coupled Device
IPPH	Industrial and Physical Pharmacy
HPLC	High-Performance Liquid Chromatography
ATP	Adenosine Tri-Phosphate
SLC	Solute Carrier Superfamily
ABC	ATP-Binding Cassette
MRP	Multidrug Resistance-associated Protein
EBM2	Endothelial Basal Medium-2
DMSO	Dimethyl sulfoxide
LAT 1	L-type Amino acid Transporter 1
HTS	High Throughput Screening
TEM	Transmission Electron Microscopy

ABSTRACT

Author: Ngendahimana, Aimable PhD

Institution: Purdue University

Degree Received: December 2017

Title: Development of a Direct-Contact Triculture Model of the Human Blood-Brain Barrier and Potential Applications as a Preclinical Drug Screening Tool

Committee Chair: Gregory T. Knipp

Given the high cost and emerging ethical and public concerns associated with the use of animal models, the use of *in vitro* techniques is gaining considerable attention in research programs related to CNS drug discovery and development. More specifically, various *in vitro* cell culture models for studying and predicting drug transport across the Blood-Brain Barrier (BBB) were developed as preclinical research tools for neurological drug discovery and development. The main goal of the present studies has been to improve conventional *in vitro* methods used in mimicking the BBB physiology and functions by allowing physiologically complex interactions of the human BBB cells (astrocytes, pericytes, and Brain Microvessel Endothelial cells or the BMECs) to occur *in vitro*. This goal was achieved by carrying out a systematic seeding of layers corresponding to all the principal cellular components of a human BBB, such that a confluent and continuous layer of BMECs would form on a basement of human brain astrocytes and pericytes.

Therefore, it was hypothesized that if complex interactions among these BBB cells were allowed to occur *in vitro*, then this would lead to an improved multicellular culture model of the BBB system, showing better paracellular tightening in comparison to the conventional BBB monoculture models. Results presented in this dissertation indicate that a confluent and continuous layer of hCMEC/D3 cells (an immortalized BBB cell line) was formed directly on a basal coculture made of astrocytes and pericytes layers to make a physiological configuration resembling that of the human BBB *in vivo*. The resulting direct-contact triculture model was more restrictive to the permeation of various paracellular markers (mannitol, sucrose, PEG-4000 and inulin) than its corresponding monoculture of hCMEC/D3 cells.

In order to compare the transcellular absorption between mono- and tri-culture models, digoxin (an FDA recommended probe substrate for efflux transporters) and elacridar (an FDA recommended potent inhibitor of efflux transporters) were used to compare efflux activity between the mono- and tri-culture models. While, a statistically significant effect of elacridar on the

absorption of digoxin was observed in the hCMEC/D3 monocultures, there was no statistically significant effect of elacridar on the absorption of digoxin in the triculture model. The observed difficulty to increase the absorption of digoxin using a potent Pgp inhibitor (elacridar) in the triculture model is in agreement with previously published research showing that it is difficult to improve brain drug exposure even when efflux transporters at the human BBB are inhibited. In addition, the triculture model showed a valid ranking order of transcellular BBB permeants; L-histidine (a non-Pgp substrate) showed higher apparent permeability, followed by thiamine (a Pgp-substrate, but essential for brain function), followed by propranolol (a weak Pgp substrate), then paclitaxel, and the lowest permeability corresponded to verapamil which is a strong Pgp substrate.

The final chapter of this dissertation provides possible strategies on how the triculture methodology can be further improved and applied in an industrial setting as a screening tool for studying the effect of pharmaceutical drugs and drug products on the BBB physiology and functions. Ultimately, it is hoped that the triculture will be useful in the creation of *IVVC* models to predict clinical pharmacokinetic and pharmacodynamic parameters.

CHAPTER 1. JUSTIFICATION FOR THE DEVELOPMENT OF A LAYERED DIRECT-CONTACT TRICULTURE MODEL OF THE BLOOD-BRAIN BARRIER

1.1 Summary

Objectives: To explain the BBB-concept and to propose a physiologically representative methodology for mimicking the BBB-glia unit on a *Transwell*TM membrane.

Findings: The role of three CNS-barriers (the BBB, the blood-CSF, and the arachnoid barrier) in limiting neurological drug delivery is described. The BBB-glia unit is considered the most relevant barrier in neurological drug delivery. Under normal physiological conditions, brain capillaries (or the BBB) deliver nutrients, energy molecules and other important molecules to the neurons. However, the BBB is a selective conduit system that allows delivery of certain molecules such as nutrients to the neurons but prevents neurological drug delivery. Strategies to deliver neuronal drugs through the BBB are highly needed in order to halt the high attrition rates in CNS-drug development.

Research problem: It is a Herculean task to study drug transport across a BBB-glia unit *in vivo*. One of the current approaches to address this challenge involves mimicking the BBB-physiology on a *Transwell*TM in order to study BBB-drug transport mechanisms and permeation rates. However, conventional methods are not optimized to allow the formation of physiologically relevant cell-cell junctions and vesicular exchange as it occurs between cellular constituents of the BBB-glia unit *in vivo*. While it is known that astrocytes, pericytes and endothelial cells of the BBB-system do exchange cell organelles, mRNAs, ions and small molecules through direct cell-cell connections, conventional *Transwell*TM methods separate astrocytes and pericytes from the BBB-endothelial cells by plating them on different sides of a thick membranous filter support. Thus, conventional methods need to be optimized to allow for the formation of direct cell-cell channels (gap junctions or peg-socket junctions). Cell-cell junctions/channels that form among BBB cells (i.e., astrocytes, pericytes and BMECs) offer an alternative route through which neuroactive drugs may circumvent rapid clearance by a circulating brain-CSF in the CNS compartments.

A novel methodology for mimicking the BBB on a Transwell™ support: A novel methodology in which astrocytes, pericytes, and BMECs are seeded in direct layers on a transwell membrane would form a more representative model of the BBB *in vitro*. Chapters 2, 3, & 4 describe the development of a direct-contact triculture model of the human Blood-Brain Barrier. Variants of the direct-contact triculture model of the BBB are described here in chapter 1.

Keywords: CNS barriers, BBB-glia unit, CNS-drug delivery, neuronal drug delivery, gap-junctions, peg-socket junctions, *Transwell™*.

1.2 Introduction

Paul Ehrlich discovered the BBB more than 100 years ago, when he noticed that hydrophilic dyes injected into blood circulation could not be absorbed into the brain region [Ribatti et al., 2006]. Since then, much knowledge has been gained about the role of CNS barriers in limiting drug delivery into brain parenchyma [Pardridge, 2011 & 2016]. The process of CNS-drug absorption is regulated by a system of CNS-barriers including the BBB, the brain arachnoid epithelia and the blood-CSF barrier [Pardridge, 2011 & 2016]. A successful strategy for CNS drug delivery would have to consider a delicate transport system controlled by these three main CNS-barriers [Pardridge, 2011 & 2016].

Even though transport of CNS drugs may occur at all three major CNS barriers, experts consider the BBB to be the most difficult drug delivery barrier in CNS drug development [Pardridge, 2011 & 2016]. CNS-drug absorption via epithelial cells of the choroid plexus is much higher than the absorption through the BBB-microvascular unit [Pardridge, 2011 & 2016]. However, drug delivery through the blood-CSF barrier is not feasible; drug diffusion from CSF into the brain tissue/neurons is limited due to a rapid clearance by the efflux pumps back into the blood circulation system [Pardridge, 2011 & 2016].

The arachnoid epithelial barrier may contribute to the absorption of drugs into the CSF circulating in the brain ventricles [Yasuda et al., 2013]. However, drugs absorbed this way would still be highly cleared in the same way as drugs absorbed through the blood-CSF barrier. Thus, more efforts are focused on understanding drug absorption through the BBB-capillaries. A successful absorption of a CNS-drug/drug delivery system, through the BBB-cell layers, would increase its concentration levels at neuronal sites. The close association and direct connections

formed between neurons and cells of the BBB-glia vascular unit makes the BBB a formidable interface through which a potential CNS-drug would be delivered directly to the neurons while avoiding CSF dilution and clearance back into blood circulation.

Therefore, a perplexing challenge in CNS drug development is not how to get the drug into the brain-CSF, but rather, how to deliver CNS-therapeutics through the BBB-cell layers to achieve effective concentrations at neuronal sites, while avoiding CSF dilution and clearance back into the blood circulatory system. Preclinical methods for understanding drug absorption through layers of the BBB-cells would be useful in predicting which CNS-drug candidates/delivery strategies would work successfully in a clinical setting. A major purpose of the research reported here is to develop a novel methodology in which a CNS-drug candidate would be exposed to a directly stacked layer of BBB-cells, in order to predict if it would be well absorbed through the glial vascular unit/the BBB *in vivo*.

1.3 Blood-brain barrier glial unit

Brain endothelial microvessels together with the associated pericytes and astrocytes form a multicellular control unit that regulates molecular trafficking between blood in the lumen of brain microvessels and the brain parenchyma [Obermeier et al., 2013]. The BBB unit may be regarded as a smart and complex physiological barrier that uses multiple mechanisms to accomplish multiple tasks at the interface of brain and blood circulatory system [Pardridge, 2002]. The principal cellular components of the BBB are the brain microvessel endothelial cells (BMECs), pericytes and astrocytes [Persidsky et al., 2006]. The BBB-capillary is continuous and completely covered by a combination of pericytes and astrocytes [Mathiisen et al., 2010]. Together, these cells form a formidable control unit that protects the CNS environment from peripheral fluctuations [Weiss et al., 2009].

The large surface area (15-25 m²) of the brain microvasculature/the BBB would be ideal for CNS-drug absorption; however, most small molecule drugs are not able to cross these capillaries [Wong, 2013]. Though the BBB plays a neuroprotective role, stopping neurotoxic drugs from getting into the CNS region, it also prevents most neurotherapeutics from gaining access to the brain neurons [Pardridge, 2005]. Consequently, many neurological diseases may not be cured, largely due to the inability of scientists to develop drug delivery systems that would circumvent

the BBB protective mechanisms [Pardridge, 2005]. Thus, *in vitro* methods for mimicking specific BBB-functions are needed for applications in CNS-drug delivery research [Mangas-Sanjuan et al., 2013].

It is highly important to understand relevant BBB-properties prior to developing methods for mimicking specific aspects of the BBB-physiology *in vitro*. It is also improbable that a single cell-line based technique would capture all the relevant features of the BBB-system. Different cell lines may be used to obtain specific information regarding the BBB transport [Morrissey et al., 2012]. For example, the potential for a BBB drug-drug interaction due to Pgp efflux activity has been traditionally evaluated in the MDCKII-MDR1 cell line that overexpresses Pgp. The potential for a drug to cross the BBB using an uptake transporter may employ a cell line overexpressing the transporter of interest, e.g., KCL22 cell line overexpressing OCT1 would be used to predict the potential for a novel CNS-drug to be delivered through an OCT1 carrier [Morrissey et al., 2012].

It should be noted that most BBB-transport properties are evaluated using animal cell lines. Such cell lines may present significant species differences and hence undermine their predictive capability [Deo et al, 2013]. Therefore, there is a need to develop more human cell lines for application in CNS- drug permeability and transporter assays. Although an immortalized human cell line, the hCMEC/D3, is gaining popular application in BBB research, additional human cell lines representing specific BBB states may be more informative in specific CNS-drug delivery studies. For example, the hCMEC/D3 cell line would perhaps be relevant in studies related to a cancerous BBB since it is transfected with oncogenes to allow it to proliferate over many passages. However, it may not be useful for application in studies related to a healthy BBB.

1.4 BBB transport properties

The BBB is a multipurpose physiological barrier, allowing the uptake of select molecules from blood circulating in the lumen of brain microvessels, but also restricting the entry of potential therapeutic molecules for neurological diseases [Takeshita et al., 2015]. The ability for the BBB to carry out such multiple functions is due to its unique physiological properties involving complex interactions between the BBB-endothelia, BBB-pericytes, BBB-astrocytes and the extracellular matrix secreted by all these BBB-cells. Furthermore, the BBB functions concertedly with the CSF circulating in the brain ventricles in order to clear drugs (or metabolites) that enter into brain

ventricles through the blood-CSF barrier further limiting CNS-drug diffusion and distribution into the brain parenchyma [Wolak and Thorne, 2013]. A **summary** of key structural and physiological properties used by the BBB-system to regulate movement of molecules in and out of cerebral region is provided in the next subsections.

1.4.1 Cell-cell junctions

Cell junctions at the BBB-cells limit free diffusion of most large and small molecules (assuming no carrier-mediated transport) in and out of the brain-CSF [Stamatovic et al., 2008]. The BBB cell-cell junctions are manifested in different forms including junctional complexes, peg-socket junctions, gap junctions and adhesion plaques [Haddad-Tóvulli et al., 2017]. These types of cell junctions may be expressed between the same kind of cells, e.g., between two endothelial cells, or between different kinds of cells, e.g., between a BBB-endothelium and a pericyte [Limmer et al., 2014].

An *in vitro* methodology that allows for optimal contacts among cellular constituents of the BBB-glia unit would allow pharmaceutical scientists to understand the role of all the BBB cell-cell junctions, and not only the endothelial tight junctions, in CNS-drug disposition. Specific cell-cell junctions at the BBB glial vascular unit are described briefly in the next subsections.

1.4.1.1 Junctional protein complexes

The BBB-endothelium expresses two main categories of junctional proteins, namely the tight and the adherent junctions [Tietz & Engelhard, 2015]. Tight junctions are formed by the overlapping membrane-protein loops between two adjacent BBB-endothelia [Tietz & Engelhard, 2015]. Transmembrane proteins that form tight junctions include the occludin, various isoforms of claudins, and JAMs [Tietz & Engelhard, 2015]. Details on the molecular biology of junctional protein complexes is beyond the scope of this study (detailed information can be found in *current neuropharmacology, 2008, vol 6 No.3.*).

In summary, a complex network involving adherent junctional complexes such as VE-cadherin, and the cytoplasmic junctions such as ZO-1, 2, and 3, further control the integrity of BBB-endothelial tight junctions [Tietz and Engelhard, 2015]. A high expression of the aforementioned protein complexes in the BBB cell models correlates with a more restricted paracellular permeation indicated by a low paracellular permeability or high TEER values [Helms

[et al., 2010](#)]. A major endeavor in the development of BBB-cell models has been to obtain a highly restrictive cell line manifesting high TEER values in excess of $1000 \Omega\text{-cm}^2$ [[Thomson et al., 2015](#)].

1.4.1.2 Peg & socket junctions

The BBB-endothelium interacts with pericytes by forming membrane interdigitations known as peg-socket junctions (pericytes form pegs and endothelial cells form sockets) [[Armulik et al., 2005](#)]. Adherent and gap junctions further stabilize peg-socket junctions and prevent membrane mixing of pericytes and BBB-endothelia [[Winkler et al., 2011](#)]. In addition, peg-socket junctions are stabilized by membrane integrins that anchor pericytes and endothelial cells in a thick extracellular matrix [[Winkler et al., 2011](#)].

Direct contacts formed between pericytes and endothelial cells are prerequisites for various signaling events that lead to the control of many properties of the BBB-endothelia [[Winkler et al., 2011](#)]. Peg-socket junctions may play an important role in regulating the permeation of neurological drugs or CNS-drug delivery systems. An *in vitro* method that allows the formation of peg-socket junctions between BBB-cell models could be useful in cases where a CNS-drug or drug delivery system is designed to use peg-socket junctions as a delivery channel to reach cerebral neurons.

1.4.1.3 Gap junctions

There exist direct connections between all the BBB cells formed through cell-cell contacts known as gap junctions [[Brink et al., 2012](#)]. Gap junctions consist of intercellular hemi channels that connect two adjacent cells to allow the transfer of small molecules, ions or signaling molecules between cells [[Zong et al., 2016](#)]. Given that free drug molecules circulating in the brain CSF can hardly diffuse in the brain tissue to reach neurons, the alternative passage of neurological drugs from the BBB-endothelium to the neurons may be achieved through a series of channeling junctions that connect the BBB-endothelium to the astrocytes and pericytes and eventually to the neurons in the brain parenchyma. In addition, a neurological drug delivered via gap junctions may avoid dilution and clearance by the CSF circulating through brain ventricles or extracellular spaces [[Brink et al., 2012](#)]

There is a gap-junctional protein, connexin-43, which connects the BBB-endothelium to the astrocytes, and the astrocytes to a neuron [[De Bock et al., 2014](#)]. Thus, it is possible for a

therapeutic molecule/drug delivery system to escape brain-CSF dilution or clearance by traveling through an intracellular pathway established through gap junctions in order to reach the intracellular lumen of a diseased neuron. The interactions of BBB-cells through gap junctions may be achieved by mimicking their physiological configuration *in vitro* whereby layers of astrocytes and other BBB-cell models are seeded directly onto one another. The purpose of this research is to propose a novel *in vitro* methodology that would allow the formation of gap junctions among BBB endothelia, pericytes and astrocytes.

1.4.2 Cell transmigration

Under certain pathological conditions such as Multiple Sclerosis, the BBB allows leukocytes to cross from CNS-periphery into the brain parenchyma [Genaro et al., 2014]. Leukocyte trafficking across the BBB is believed to involve four steps: tethering and rolling; activation; adhesion; and diapedesis [Lopes-Pinheiro et al., 2016]. In the first step (attachment on the endothelial), a leukocyte adheres on the BBB-endothelia through a biochemical interaction involving carbohydrate ligands expressed on leukocytes, and also selectins and chemokines expressed on the BBB-endothelial cells [Lopes-Pinheiro et al., 2016]. A leukocyte bound on the BBB-endothelial wall triggers an intracellular signaling cascade that causes endothelial junctions to open for a leukocyte to pass through the BBB-glia unit. Once a leukocyte has migrated, the BBB-junctions close again [Lopes-Pinheiro et al., 2016].

There is interest in understanding mechanisms by which cells undergo diapedesis at the BBB; in the future, CNS-drugs may be delivered across the BBB to diseased neurons via mechanisms involving diapedesis [Ali IU et al., 2015]. *In vitro* cell culture methods for mimicking the BBB-glia unit may be applied in understanding cell transmigration across the BBB [Sreekanthreddy P et al., 2016].

1.4.3 Vesicular transport

Drugs of abuse such as *METH* may induce/ enhance vesicular transport at the BBB and hence compromise the neuroprotective function of the BBB [Martins et al., 2013]. Vesicular transport of macromolecules such as insulin or transferrin at the BBB may involve transcytosis or endocytosis [Jones and Shusta, 2007]. Disease causing agents such as viruses or bacteria may infiltrate through the BBB using phagocytes or leukocytes as Trojan horses [Dando et al., 2014]. Thus, the BBB-

system can be a pharmacological target for halting the entry of microbial or viral agents into the brain parenchyma.

Although macromolecules such as insulin or transferrin cross the BBB using transcytosis, efforts to deliver promising neurotherapeutics via transcytosis have not yielded positive results [Mager et al, 2017]. There is a need to understand the molecular basis of transcytosis in order to develop successful CNS-drug delivery strategies that exploit receptor mediated transcytosis [Mager et al, 2017]. Although research in the molecular basis of drug transcytosis is still in its nascent stage, it may require the availability of *in vitro* BBB models that would capture all the relevant aspects of transcytosis at the BBB. Specifically, *in vitro* BBB models containing BMECs, pericytes, and astrocytes in direct configuration would be more informative since pericytes are known to control transcytosis at the BBB [Dohgu and Banks, 2013]. Astrocytes are also known to be mediators in the transcytosis of nutrients across the BBB and to deliver them to a neuronal environment [Seneff et al., 2011].

Therefore, an *in vitro* BBB model containing BMECs, pericytes and astrocytes would be the most physiologically relevant for application in studies related to nutrient/drug transcytosis across the BBB-system.

1.4.4 Membrane transporters

Drug transporters at the human BBB may affect CNS-drug concentration levels in the brain CSF and brain cells. The membrane bound drug transporters found at the BBB fall into two broad categories: uptake and efflux transporters [Uchida et al, 2011]. Therefore, precautions have to be taken in preclinical drug development to ensure that a novel CNS or non-CNS drug would not be a substrate for select BBB-regulatory transporters [Zhang et al., 2006].

If a novel CNS-drug candidate is a substrate for key uptake transporters (OAT3 or OCT2), or key efflux transporters (Pgp or BCRP), then it may lead to clinical drug-drug interactions and/or neurotoxicity [Zhang et al., 2006]. In some cases, a novel CNS-drug candidate may interact with a peripheral drug such as digoxin (a substrate for OATP and Pgp) at the efflux pumps of the BBB-cells to increase their concentration in the brain parenchyma and hence cause neurotoxicity [Mayer et al., 1996; Taska et al., 2017]. Thus, *in vitro* prediction of drug-drug interaction and potential neurotoxicity is of paramount significance in preclinical drug development.

Efflux pumps at the BBB are expressed at the endothelial and astroglial levels [Decleves et al., 2000]. However, efflux assays for potential CNS-drug candidates are rarely performed in the astroglial cell cultures, perhaps because efflux assays in the BBB-endothelial cells would be sufficient to predict the potential for drug-drug interactions. However, if a comparison in the fraction of CNS-drug absorbed through the BBB-layers is required, then it may be relevant to use *in vitro* methods that contain not only the BBB-endothelia but also astrocytes and pericytes.

1.4.5 Lipophilic diffusion

Cell membranes at the BBB allow passive diffusion of certain lipophilic drugs. The optimal molecular properties for lipophilic CNS drugs include a log P value ranging from 1.5 – 2.7; a molecular weight ranging between 400 – 600Da; the number of (O+N) ≤ 5 ; a polar surface area between 60\AA^2 - 90\AA^2 ; and a positive charge in the pH range between 7 and 8 [Pajouhesh and Lenz, 2005]. There are additional non-BBB factors that may hinder neuronal bioavailability. For example, a lipophilic drug circulating in the lumen of a brain capillary may bind to red-blood cells, or serum proteins and may become unavailable for BBB permeation [Tanaka and Mizojir et al., 1999].

In addition, the fraction of drug molecules not bound to the serum proteins may diffuse through the cell membranes to interact with membrane bound proteins that would, in turn, reduce their effective permeability through the BBB-cells [Mateus et al., 2013]. Lipophilic drugs that bind membrane-bound proteins may be effluxed back into the lumen of a blood capillary, or, may simply accumulate in the BBB-cell membranes when efflux pumps are inhibited [Mankhetkorn and Garnier-Suillero, 1998].

Lipophilic drugs that escape membrane-bound proteins may bind to cytoplasmic proteins or to metabolic enzymes that may further reduce their bioavailability across the cell membranes [Molinari et al., 2002; Yamagishi et al., 2013; Mateus et al., 2017]. However, intracellular protein binding may also assist in cytoplasmic trafficking of CNS-drugs/nutrients from the apical side of a cell membrane to the basolateral side towards neurons [McArthur et al., 1999].

A lipophilic drug molecule that has escaped protein binding at various levels may still be hindered from diffusing freely through brain interstitial fluids to get to the target neuronal receptors due to non-specific tissue binding [Maure et al., 2005]. Thus, lipophilic drug delivery through cell

membranes of the BBB-glia unit would be highly limited by non-specific protein binding at various locations in and out of the cell milieu. A physiologically representative *in vitro* methodology for estimating and comparing the free fraction of a lipophilic drug escaping most of the BBB protective mechanisms may help in the selection of drugs with optimal physico-chemical properties for lipophilic diffusion.

1.5 Mimicking the BBB function in a *Transwell*TM

As described in the preceding sections, the BBB is a smart, multicellular barrier at the interface between blood and brain parenchyma. The BBB accomplishes its neuroprotective role through complex cellular and biochemical networks that may be complicated to mimic using simple cell culture models in *Transwell*TM chambers. It should be noted that the BBB problem is even more complex as its physiology is very dynamic, manifesting different physiological states under different pathological conditions [Guérin et al., 2001]. However, a good starting point in mimicking the BBB *in vitro* would be to form a multicellular culture of the principal cellular constituents of the BBB in a configuration resembling that of the BBB *in vivo*.

Conventional methods for modeling the BBB on a *Transwell*TM may not allow for the formation of optimal contacts and biochemical networks that exist at the BBB-system *in vivo* (see **Figure 1.1**). The problem is that usually, BMECs are seeded on the apical surface of a *Transwell*TM membrane while the astrocytes and pericytes are seeded on the basolateral surfaces, separated from endothelial cells by a physical wall of the filter support of varying thickness (120µm, 50µm, and 10µm thickness; see **Figure 1.2** for comparisons with the cell thickness). In such a *Transwell*TM setting, pericytes and astrocytes may not be able to form optimal junctions with endothelial cells, and the diffusional or transport pathway of a drug or drug delivery system may not be elucidated *in vitro*, if the BBB configuration is misrepresented in *in vitro* transport studies.

For example, a novel drug or drug delivery system *in vivo* may be exchanged from endothelial cells into pericytes and astrocytes, then to the neurons by mechanisms that involve either gap junctions or peg-socket junctions, or vesicular exchange, or uptake transporters in series. Of equal importance would be drug clearance from brain CSF. A novel drug or drug delivery system delivered in the brain parenchyma through non-BBB routes, such as nasal or direct injection in the spinal cord may be conversely cleared into the blood circulatory system by a combination of

transport mechanisms that exist between the BBB-endothelia, astrocytes and pericytes [Deane et al., 2009]. *In vitro* cell culture methods may be equally useful in investigating clearance of molecules from brain parenchyma into the lumen of brain capillaries. More specifically, the role of astrocytes and pericytes in cerebral drug clearance could be investigated using a directly layered multicellular model of the BBB that closely mimics the actual BBB physiology and function *in vivo*.

Therefore, cell culture methods used in mimicking the BBB function could be more informative if the BBB-endothelia were free to form direct interactions/connections with astrocytes and pericytes by seeding direct layers of these BBB cells on the same side of a *Transwell*TM chamber (apical or basolateral). The new approach proposed in here would allow the BBB-endothelia, pericytes and astrocytes to interact freely on either the apical or the basolateral surface of a *Transwell*TM membrane. This approach would allow for more spatial freedom to add other cellular components that are closely associated with the human BBB (i.e., neurons and microglia). The proposed direct-contact methodology could be suitable for application in studies related to CNS-drug delivery strategies and mechanisms.

1.6 Specific research aims

- I. To develop a direct-contact method for mimicking BBB-physiology on a *Transwell*TM support using the methodology described in **Figure 1.3**. The proposed method is expected to allow direct contacts (**cell-cell junctions**) between BBB-endothelia, pericytes and astrocytes to allow free cell-cell interactions similar to the contacts formed between BBB cells at the glial-vascular unit *in vivo*.
- II. To compare cross-sectional configuration of a directly layered tricellular culture model of the human BBB to that of the human BBB *in vivo*
- III. To evaluate potential application of a direct triculture model of the BBB glial vascular unit in predicting potential clinical drug-drug interactions using digoxin as a Pgp probe substrate and elacridar as a potent non-competitive inhibitor of efflux transporters

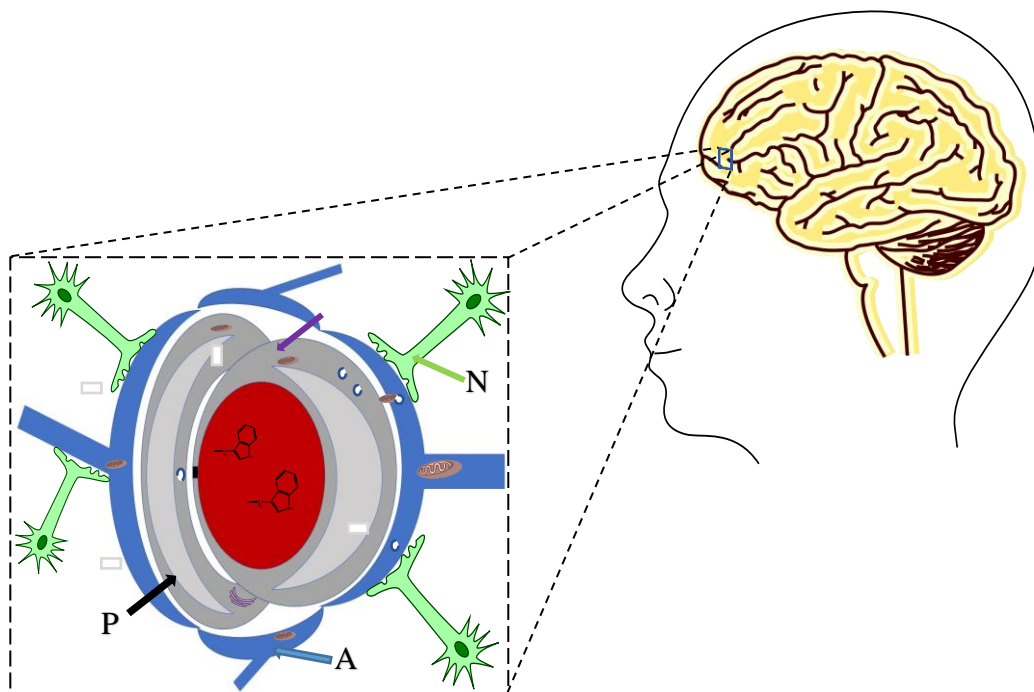


Figure 1.1. A neuroprotective BBB. The bright green arrow shows a neuron (**N**), the light blue arrow shows an astrocyte (**A**), the black arrow shows a pericytes (**P**) and the purple arrow shows a BBB-endothelium. Note that for a neuronal drug delivery to be attained, a drug molecule would have to be transported past the BBB-endothelium, the extracellular matrix, and pericytes or astrocytes. Cell-cell junctions (molecular channels) that connect neurons, astrocytes, pericytes and the BBB-endothelium may provide an alternative transport pathway to circumvent tight junctions, extracellular enzymes, and CFS clearance in neuronal drug delivery. An *in vitro*-multicellular model of the BBB that allows for unlimited and direct interactions between the cellular constituents of the BBB-glia unit would be useful in preclinical CNS-drug delivery studies.

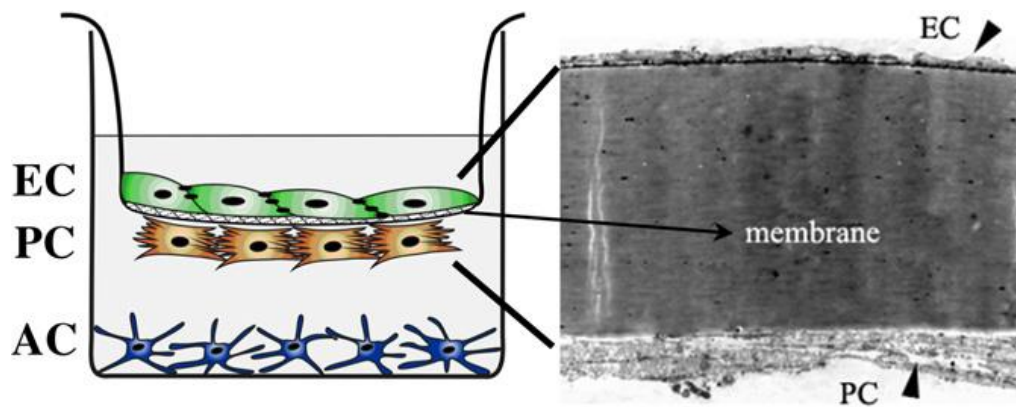


Figure 1.2. Lack of optimal cell-cell interactions in the conventional methodology when modeling the BBB-glia unit on a *Transwell™* support. EC stands for Endothelial Cells, PC for pericytes, and AC for astrocytes. A thick membrane filter support limits the formation of cell-cell junctions between ECs and PCs. In addition, ACs are seeded at the bottom surface where they are largely separated from ECs and PCs. Therefore, optimal cell-cell channels such as gap junctions, peg-socket junctions may not be formed between ACs, PCs and ECs. Figure 1.2 was reproduced with permission from Elsevier [Cerruti et al. 2011].

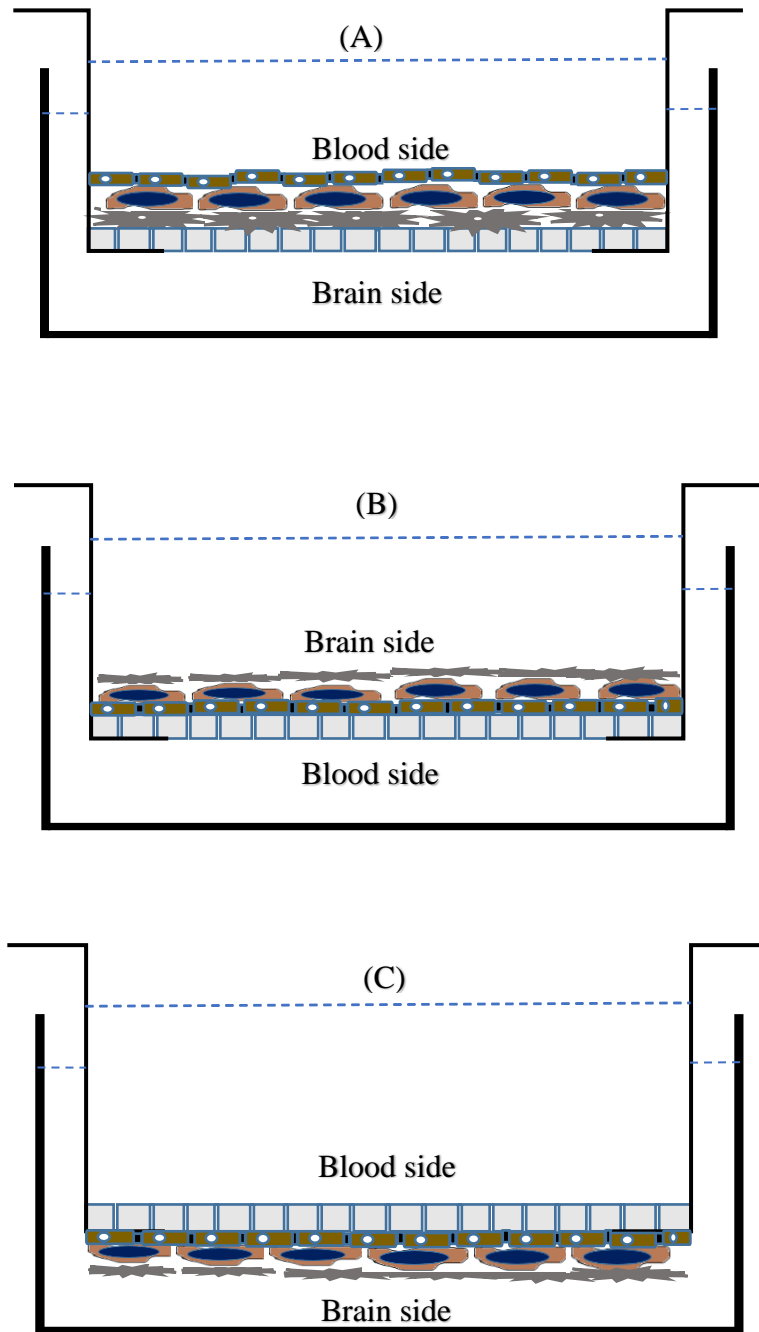


Figure 1.3. A direct-contact triculture methodology for mimicking the BBB-glia unit on a *TranswellTM* support. Configuration (A) involves seeding the triculture on the apical surface, (B) is an inversed configuration of (A), and (C) is configuration (A) seeded on the basolateral surface of a transwell membrane. The proposed methodology leads to a spatial arrangement that would allow for additional cellular components of the neurovascular unit to be added in the model.

1.7 Concluding remarks

The role of CNS-barriers is highly diversified. CNS barriers have multiple functions including neuroprotection, molecular delivery of nutrients to the neurons, clearance of neurotoxic compounds and metabolites. A distinction between CNS-drug delivery and neuronal drug delivery ought to be clarified before justifying the need to develop a directly layered triculture model of the human BBB. While many small and large molecules may gain access into CNS-ventricles through the blood-CSF barrier, or, through direct injection into the spinal cord, the circulating CSF would rapidly clear drugs delivered through these non-BBB routes via paravenous drainage pathway and hence limit their bioavailability to the target diseased neurons [Tachikawa et al., 2008; Iliff et al., 2012].

Of all the three CNS-barriers/conduits, the BBB location and distribution in the brain parenchyma make it a better conduit for optimal neuronal drug delivery. The distance between a BBB-capillary and a brain neuron (8-20 μm) is optimized to allow a fast transfer of select nutrients and oxygen from the lumen of a BBB-capillary to the neurons [Spencer and Verma, 2007]. It is approximated that each neuron in the brain parenchyma is associated with at least one BBB-glia unit [Spencer and Verma, 2007]. Thus, a neuronal drug delivered through the BBB would escape rapid clearance by the interstitial fluid flow and would be well distributed in the cerebral region where target diseased neurons are extremely difficult for most therapeutic molecules to get access [Spencer and Verma, 2007]. The main challenge in neuronal drug delivery is not how to circumvent the BBB to gain access to various CNS compartments but rather how to use the BBB as a conduit for delivering promising neurological drugs.

Neuronal drug delivery through the BBB glial-vascular system could be investigated during preclinical stages by using the proposed multicellular culture models that closely mimic the BBB physiology and function in an *in vitro* setting. Conventional cell culture methods for mimicking the BBB function/physiology are not optimized to allow for the formation of intracellular channels (e.g., gap junctions and peg-socket junctions that form between BBB-endothelia and astrocytes or pericytes) that may act as additional conduits for trafficking drug molecules from the apical/luminal side of the BBB to the basolateral/abluminal side. A novel direct-contact methodology that involve direct layers of BBB-endothelia, pericytes and astrocytes would better mimic the BBB physiology and function than conventional methods that involve separation of the

three principal cellular components of the BBB glial vascular system. A detailed description on the development and testing of a direct-contact triculture model of a human BBB as a potential CNS-drug research tool is given in the proceeding chapters.

1.8 References

- Ali, I. U., & Chen, X. (2015). Penetrating the Blood–Brain Barrier: Promise of Novel Nanoplatfoms and Delivery Vehicles. *ACS Nano*, 9(10), 9470-9474. doi:10.1021/acsnano.5b05341
- Armulik, A. (2005). Endothelial/Pericyte Interactions. *Circulation Research*, 97(6), 512-523. doi:10.1161/01.res.0000182903.16652.d7
- Berk, P. D., & Stump, D. D. (1999). Mechanisms of cellular uptake of long chain free fatty acids. *Lipid Binding Proteins within Molecular and Cellular Biochemistry*, 17-31. doi:10.1007/978-1-4615-4929-1_3
- Brink, P. R., Valiunas, V., Gordon, C., Rosen, M. R., & Cohen, I. S. (2012). Can gap junctions deliver? *Biochimica et Biophysica Acta (BBA) - Biomembranes*, 1818(8), 2076-2081. doi:10.1016/j.bbmem.2011.09.025
- Cory Kalvass, J., & Maurer, T. S. (2002). Influence of nonspecific brain and plasma binding on CNS exposure: implications for rational drug discovery. *Biopharmaceutics & Drug Disposition*, 23(8), 327-338. doi:10.1002/bdd.325
- Dando, S. J., Mackay-Sim, A., Norton, R., Currie, B. J., St. John, J. A., Ekberg, J. A., ... Beacham, I. R. (2014). Pathogens Penetrating the Central Nervous System: Infection Pathways and the Cellular and Molecular Mechanisms of Invasion. *Clinical Microbiology Reviews*, 27(4), 691-726. doi:10.1128/cmr.00118-13
- De Bock, M., Vandenbroucke, R. E., Decrock, E., Culot, M., Cecchelli, R., & Leybaert, L. (2014). A new angle on blood-CNS interfaces: A role for connexins? *FEBS Letters*, 588(8), 1259-1270. doi:10.1016/j.febslet.2014.02.060
- Decleves, X., Regina, A., Laplanche, J., Roux, F., Boval, B., Launay, J., & Scherrmann, J. (2000). Functional expression of p-glycoprotein and multidrug resistance-associated protein (mrp1) in primary cultures of rat astrocytes. *Journal of Neuroscience Research*, 60(5), 594-601. doi:10.1002/(sici)1097-4547(20000601)60:53.0.co;2-6
- Deo, A. K., Borson, S., Link, J. M., Domino, K., Eary, J. F., Ke, B., ... Unadkat, J. D. (2014). Activity of P-Glycoprotein, a -Amyloid Transporter at the Blood-Brain Barrier, Is Compromised in Patients with Mild Alzheimer Disease. *Journal of Nuclear Medicine*, 55(7), 1106-1111. doi:10.2967/jnumed.113.130161
- Dohgu, S., & Banks, W. A. (2013). Brain pericytes increase the lipopolysaccharide-enhanced transcytosis of HIV-1 free virus across the in vitro blood–brain barrier: evidence for cytokine-mediated pericyte-endothelial cell crosstalk. *Fluids and Barriers of the CNS*, 10(1), 23. doi:10.1186/2045-8118-10-23

- Galasko, D. (2012). Faculty of 1000 evaluation for A Paravascular Pathway Facilitates CSF Flow Through the Brain Parenchyma and the Clearance of Interstitial Solutes, Including Amyloid β . F1000 - Post-publication peer review of the biomedical literature. doi:10.3410/f.717953972.793459499
- Guérin, C., Nolan, C., Mavroudis, G., Lister, T., Davidson, G., Holton, J., & Ray, D. (2001). The dynamics of blood–brain barrier breakdown in an experimental model of glial cell degeneration. *Neuroscience*, 103(4), 873-883. doi:10.1016/s0306-4522(01)00015-x
- Haddad-Tóvolli, R., Dragano, N. R., Ramalho, A. F., & Velloso, L. A. (2017). Development and Function of the Blood-Brain Barrier in the Context of Metabolic Control. *Frontiers in Neuroscience*, 11. doi:10.3389/fnins.2017.00224
- Helms, H. C., Waagepetersen, H. S., Nielsen, C. U., & Brodin, B. (2010). Paracellular Tightness and Claudin-5 Expression is Increased in the BCEC/Astrocyte Blood–Brain Barrier Model by Increasing Media Buffer Capacity During Growth. *The AAPS Journal*, 12(4), 759-770. doi:10.1208/s12248-010-9237-6
- Ilf, J. J., Wang, M., Liao, Y., Plogg, B. A., Peng, W., Gundersen, G. A., ... Nedergaard, M. (2012). A Paravascular Pathway Facilitates CSF Flow Through the Brain Parenchyma and the Clearance of Interstitial Solutes, Including Amyloid. *Science Translational Medicine*, 4(147), 147ra111-147ra111. doi:10.1126/scitranslmed.3003748
- Jones, A. R., & Shusta, E. V. (2007). Blood–Brain Barrier Transport of Therapeutics via Receptor-Mediation. *Pharmaceutical Research*, 24(9), 1759-1771. doi:10.1007/s11095-007-9379-0
- Limmer, S., Weiler, A., Volkenhoff, A., Babatz, F., & Klämbt, C. (2014). The Drosophila blood-brain barrier: development and function of a glial endothelium. *Frontiers in Neuroscience*, 8. doi:10.3389/fnins.2014.00365
- Lopes Pinheiro, M. A., Kooij, G., Mizee, M. R., Kamermans, A., Enzmann, G., Lyck, R., ... De Vries, H. E. (2016). Immune cell trafficking across the barriers of the central nervous system in multiple sclerosis and stroke. *Biochimica et Biophysica Acta (BBA) - Molecular Basis of Disease*, 1862(3), 461-471. doi:10.1016/j.bbadis.2015.10.018
- Mäger, I., Meyer, A. H., Li, J., Lenter, M., Hildebrandt, T., Lepar, G., & Wood, M. J. (2017). Targeting blood-brain-barrier transcytosis – perspectives for drug delivery. *Neuropharmacology*, 120, 4-7. doi:10.1016/j.neuropharm.2016.08.025
- Mangas-Sanjuan, V., González-Álvarez, I., González-Álvarez, M., Casabó, V. G., & Bermejo, M. (2013). Innovative in Vitro Method To Predict Rate and Extent of Drug Delivery to the Brain across the Blood–Brain Barrier. *Molecular Pharmaceutics*, 10(10), 3822-3831. doi:10.1021/mp400294x
- Mankhetkorn, S., & Garnier-Suillerot, A. (1998). The ability of verapamil to restore intracellular accumulation of anthracyclines in multidrug resistant cells depends on the kinetics of their uptake. *European Journal of Pharmacology*, 343(2-3), 313-321. doi:10.1016/s0014-2999(97)01548-3

- Martins, T., Burgoyne, T., Kenny, B., Hudson, N., Futter, C. E., Ambrósio, A. F., ... Turowski, P. (2013). Methamphetamine-induced nitric oxide promotes vesicular transport in blood–brain barrier endothelial cells. *Neuropharmacology*, 65, 74-82. doi:10.1016/j.neuropharm.2012.08.021
- Mateus, A., Matsson, P., & Artursson, P. (2013). Rapid Measurement of Intracellular Unbound Drug Concentrations. *Molecular Pharmaceutics*, 10(6), 2467-2478. doi:10.1021/mp4000822
- Mateus, A., Treyer, A., Wegler, C., Karlgren, M., Matsson, P., & Artursson, P. (2017). Intracellular drug bioavailability: a new predictor of system dependent drug disposition. *Scientific Reports*, 7, 43047. doi:10.1038/srep43047
- Mathiisen, T. M., Lehre, K. P., Danbolt, N. C., & Ottersen, O. P. (2010). The perivascular astroglial sheath provides a complete covering of the brain microvessels: An electron microscopic 3D reconstruction. *Glia*, 58(9), 1094-1103. doi:10.1002/glia.20990
- Maurer, T. S. (2004). RELATIONSHIP BETWEEN EXPOSURE AND NONSPECIFIC BINDING OF THIRTY-THREE CENTRAL NERVOUS SYSTEM DRUGS IN MICE. *Drug Metabolism and Disposition*, 33(1), 175-181. doi:10.1124/dmd.104.001222
- Mayer, U., Wagenaar, E., Beijnen, J. H., Smit, J. W., Meijer, D. K., Asperen, J., ... Schinkel, A. H. (1996). Substantial excretion of digoxin via the intestinal mucosa and prevention of long-term digoxin accumulation in the brain by the mdrla P-glycoprotein. *British Journal of Pharmacology*, 119(5), 1038-1044. doi:10.1111/j.1476-5381.1996.tb15775.x
- Mitragotri, S., Burke, P. A., & Langer, R. (2014). Overcoming the challenges in administering biopharmaceuticals: formulation and delivery strategies. *Nature Reviews Drug Discovery*, 13(9), 655-672. doi:10.1038/nrd4363
- Molinari, A., Calcabrini, A., Meschini, S., Stringaro, A., Crateri, P., Toccaceli, L., ... Arancia, G. (2002). Subcellular Detection and Localization of the Drug Transporter P-Glycoprotein in Cultured Tumor Cells. *Current Protein & Peptide Science*, 3(6), 653-670. doi:10.2174/1389203023380413
- Morrissey, K. M., Wen, C. C., Johns, S. J., Zhang, L., Huang, S., & Giacomini, K. M. (2012). The UCSF-FDA TransPortal: A Public Drug Transporter Database. *Clinical Pharmacology & Therapeutics*, 92(5), 545-546. doi:10.1038/clpt.2012.44
- Obermeier, B., Daneman, R., & Ransohoff, R. M. (2013). Development, maintenance and disruption of the blood-brain barrier. *Nature Medicine*, 19(12), 1584-1596. doi:10.1038/nm.3407
- Pardridge, W. M. (2002). DRUG AND GENE TARGETING TO THE BRAIN WITH MOLECULAR TROJAN HORSES. *Nature Reviews Drug Discovery*, 1(2), 131-139. doi:10.1038/nrd725
- Pardridge, W. M. (2005). The blood-brain barrier and neurotherapeutics. *Neurotherapeutics*, 2(1), 1-2. doi:10.1007/bf03206637
- Pardridge, W. M. (2005). The blood-brain barrier: Bottleneck in brain drug development. *Neurotherapeutics*, 2(1), 3-14. doi:10.1007/bf03206638
- Pardridge, W. M. (2011). Drug transport in brain via the cerebrospinal fluid. *Fluids and Barriers of the CNS*, 8(1), 7. doi:10.1186/2045-8118-8-7

- Pardridge, W. M. (2016). CSF, blood-brain barrier, and brain drug delivery. *Expert Opinion on Drug Delivery*, 13(7), 963-975. doi:10.1517/17425247.2016.1171315
- Persidsky, Y., Ramirez, S. H., Haorah, J., & Kanmogne, G. D. (2006). Blood–brain Barrier: Structural Components and Function Under Physiologic and Pathologic Conditions. *Journal of Neuroimmune Pharmacology*, 1(3), 223-236. doi:10.1007/s11481-006-9025-3
- Ribatti, D., Nico, B., Crivellato, E., & Artico, M. (2006). Development of the blood-brain barrier: A historical point of view. *The Anatomical Record Part B: The New Anatomist*, 289B(1), 3-8. doi:10.1002/ar.b.20087
- Rizk, M., Zou, L., Savic, R., & Dooley, K. (2017). Importance of Drug Pharmacokinetics at the Site of Action. *Clinical and Translational Science*, 10(3), 133-142. doi:10.1111/cts.12448
- Seneff, S., Wainwright, G., & Mascitelli, L. (2011). Nutrition and Alzheimer's disease: The detrimental role of a high carbohydrate diet. *European Journal of Internal Medicine*, 22(2), 134-140. doi:10.1016/j.ejim.2010.12.017
- Spencer, B. J., & Verma, I. M. (2007). Targeted delivery of proteins across the blood-brain barrier. *Proceedings of the National Academy of Sciences*, 104(18), 7594-7599. doi:10.1073/pnas.0702170104
- Sreekanthreddy, P., Gromnicova, R., Davies, H., Phillips, J., Romero, I. A., & Male, D. (2016). A three-dimensional model of the human blood-brain barrier to analyse the transport of nanoparticles and astrocyte/endothelial interactions. *F1000Research*. doi:10.12688/f1000research.7142.2
- Stamatovic, S., Keep, R., & Andjelkovic, A. (2008). Brain Endothelial Cell-Cell Junctions: How to “Open” the Blood Brain Barrier. *Current Neuropharmacology*, 6(3), 179-192. doi:10.2174/157015908785777210
- Taberero, A., Velasco, A., Granda, B., Lavado, E. M., & Medina, J. M. (2001). Transcytosis of Albumin in Astrocytes Activates the Sterol Regulatory Element-binding Protein-1, Which Promotes the Synthesis of the Neurotrophic Factor Oleic Acid. *Journal of Biological Chemistry*, 277(6), 4240-4246. doi:10.1074/jbc.m108760200
- Tachikawa, M., Kasai, Y., Takahashi, M., Fujinawa, J., Kitaichi, K., Terasaki, T., & Hosoya, K. (2008). The blood-cerebrospinal fluid barrier is a major pathway of cerebral creatinine clearance: involvement of transporter-mediated process. *Journal of Neurochemistry*, 107(2), 432-442. doi:10.1111/j.1471-4159.2008.05641.x
- Takeshita, Y., & Ransohoff, R. M. (2015). Blood-brain barrier and neurological diseases. *Clinical and Experimental Neuroimmunology*, 6(4), 351-361. doi:10.1111/cen3.12229
- Taskar, K. S., Mariappan, T. T., Kurawattimath, V., Singh Gautam, S., Radhakrishna Mullapudi, T., Sridhar, S. K., ... Mandlekar, S. (2017). Unmasking the Role of Uptake Transporters for Digoxin Uptake Across the Barriers of the Central Nervous System in Rat. *Journal of Central Nervous System Disease*, 9, 117957351769359. doi:10.1177/1179573517693596
- Thomsen, L. B., Burkhart, A., & Moos, T. (2015). A Triple Culture Model of the Blood-Brain Barrier Using Porcine Brain Endothelial cells, Astrocytes and Pericytes. *PLOS ONE*, 10(8), e0134765. doi:10.1371/journal.pone.0134765

- Tietz, S., & Engelhardt, B. (2015). Brain barriers: Crosstalk between complex tight junctions and adherens junctions. *The Journal of Cell Biology*, 209(4), 493-506. doi:10.1083/jcb.201412147
- Uchida, Y., Ohtsuki, S., Katsukura, Y., Ikeda, C., Suzuki, T., Kamiie, J., & Terasaki, T. (2011). Quantitative targeted absolute proteomics of human blood-brain barrier transporters and receptors. *Journal of Neurochemistry*, 117(2), 333-345. doi:10.1111/j.1471-4159.2011.07208.x
- Weiss, N., Miller, F., Cazaubon, S., & Couraud, P. (2009). The blood-brain barrier in brain homeostasis and neurological diseases. *Biochimica et Biophysica Acta (BBA) - Biomembranes*, 1788(4), 842-857. doi:10.1016/j.bbamem.2008.10.022
- Winkler, E. A., Bell, R. D., & Zlokovic, B. V. (2011). Central nervous system pericytes in health and disease. *Nature Neuroscience*, 14(11), 1398-1405. doi:10.1038/nn.2946
- Wolak, D. J. (2013). Diffusion of Macromolecules in the Brain: Implications for Drug Delivery. *Molecular Pharmaceutics*, 10(5), 1492-1504. doi:10.1021/mp300495e
- Wong, A. D., Ye, M., Levy, A. F., Rothstein, J. D., Bergles, D. E., & Searson, P. C. (2013). The blood-brain barrier: an engineering perspective. *Frontiers in Neuroengineering*, 6. doi:10.3389/fneng.2013.00007
- Yamagishi, T., Sahni, S., Sharp, D. M., Arvind, A., Jansson, P. J., & Richardson, D. R. (2013). P-glycoprotein Mediates Drug Resistance via a Novel Mechanism Involving Lysosomal Sequestration. *Journal of Biological Chemistry*, 288(44), 31761-31771. doi:10.1074/jbc.m113.514091
- Yasuda, K., Cline, C., Vogel, P., Onciu, M., Fatima, S., Sorrentino, B. P., ... Schuetz, E. G. (2013). Drug Transporters on Arachnoid Barrier Cells Contribute to the Blood-Cerebrospinal Fluid Barrier. *Drug Metabolism and Disposition*, 41(4), 923-931. doi:10.1124/dmd.112.050344
- Zhang, L. (2014). Epstein Barr Virus and Blood Brain Barrier in Multiple Sclerosis. doi:10.21236/ada596844
- Zhang, L., Strong, J. M., Qiu, W., Lesko, L. J., & Huang, S. (2006). Scientific Perspectives on Drug Transporters and Their Role in Drug Interactions†. *Molecular Pharmaceutics*, 3(1), 62-69. doi:10.1021/mp050095h
- Zong, L., Zhu, Y., Liang, R., & Zhao, H. (2016). Gap junction mediated miRNA intercellular transfer and gene regulation: A novel mechanism for intercellular genetic communication. *Scientific Reports*, 6(1). doi:10.1038/srep19884

CHAPTER 2. IMPROVED PARACELLULAR TIGHTNESS IN THE DIRECT-CONTACT TRICULTURE MODEL OF THE BLOOD-BRAIN BARRIER

2.1 Summary

Background: The human blood-brain barrier (BBB) has traditionally been mimicked in preclinical drug development using cell-culture methods prepared from animal or human cells. However, many of the conventional cell-culture methods have not been optimized to allow direct cell-cell contacts or proximal associations between human brain astrocytes and/or pericytes with brain microvessel endothelial cells (BMECs) to form a physiological configuration similar to that of the human BBB *in vivo*. A novel cell-culture method in which human primary brain astrocytes, pericytes and BMECs are cultured in direct contact on the apical surface of a *Transwell*TM to form a direct –contact triculture model of a human BBB is described in this chapter. The contribution of astrocytes and pericytes in the resulting layered triculture model is delineated in order to understand the role of these non-endothelial cells in reinforcing the paracellular tightness of the BBB system. The permeability values of various established paracellular marker molecules are used to compare paracellular tightness in the mono-, co- and tri-cultures that are used for partial or full mimicking of the BBB-system.

Methods: TEER (Trans-Endothelial Electrical Resistance) values were used as a guide to establish when stable, optimal tightening of paracellular permeation route occurs post culturing of the hCMEC/D3 cells on a pre-attached coculture of pericytes on astrocytes. Upon reaching stable TEER values, permeability coefficients of sucrose and mannitol (smaller paracellular marker compounds), were then obtained from monocultures of hCMEC/D3 cells, cocultures of hCMEC/D3 cells with astrocytes or pericytes, and tricultures containing layers of all the three types of BBB cells. In addition, permeability coefficients of mannitol through cocultures of pericytes that were directly seed onto pre-attached astrocytes were determined and compared to the values obtained under the hCMEC/D3 monoculture and tricultures. Evaluation of this novel triculture model of the BBB followed standard methodology needed to characterize new cell culture methods for mimicking the BBB *in vitro*.

Results: A co-culture of astrocytes and pericytes, directly over-layered, showed a normalized TEER value of $43 \pm 9 \Omega\text{-cm}^2$ when both the astrocytes and pericytes layers were seeded at a density of 4×10^4 cells/cm². A direct seeding of hCMEC/D3 cells at 8×10^4 cells/cm² on the basal coculture of astrocytes and pericytes led to a 46% gain in normalized TEER-values with a maximum value observed in the resulting triculture at $81 \pm 6 \Omega\text{-cm}^2$. The permeability co-efficient of mannitol was similar between cocultures of pericytes grown on a layer of astrocytes versus monocultures of hCMEC/D3 cells, i.e., $(6.9 \pm 0.16) \times 10^{-5}$ cm/s, across the cocultures, and $(6.3 \pm 0.34) \times 10^{-5}$ cm/s in the monoculture of hCMEC/D3 cells. The tricultures developed by seeding hCMEC/D3 cells directly on a basal coculture of astrocytes and pericytes was more restrictive to the permeation of smaller (mannitol and sucrose) and larger paracellular permeants (PEG-4000 and inulin-5000) when compared to the monoculture of hCMEC/D3 cells alone.

Conclusions: A direct co-culture of astrocytes and pericytes exhibited a resistance to the flux of mannitol, a small paracellular permeant, in a similar magnitude to that experienced by mannitol through a monoculture of hCMEC/D3 cells. When hCMEC/D3 cells were seeded directly onto a layered coculture of astrocytes and pericytes, the resulting triculture became a system of barriers that help provide a more physiologically relevant configuration in support of the hCMEC/D3 barrier cultured at the top section of a BBB triculture model. The Permeability coefficients of various paracellular permeants indicated that the triculture model of a human BBB is significantly tighter than the corresponding monoculture model containing only the hCMEC/D3 cells. Thus, a direct-contact *in vitro* triculture methodology described in this chapter may better mimic paracellular barrier function of a human BBB than a monoculture methodology, which is only a partial representation of the BBB system.

Key words: Blood-Brain Barrier, tight junctions, Trans-Endothelial Electrical Resistance (TEER), and paracellular permeation

2.2 Introduction

The transport phenomena of small or large molecules, in and out of the brain parenchyma, is controlled by the Blood-Brain Barrier [McAllister et al., 2001; Pardridge, 2005]. The human BBB is a multi-cellular barrier consisting of an endothelium capillary surrounded by pericytes and astrocytes that are widely believed to be very important in mass transfer resistance to most xenobiotics [Zlokovic BV, 2008, see **Figure 2.1**].

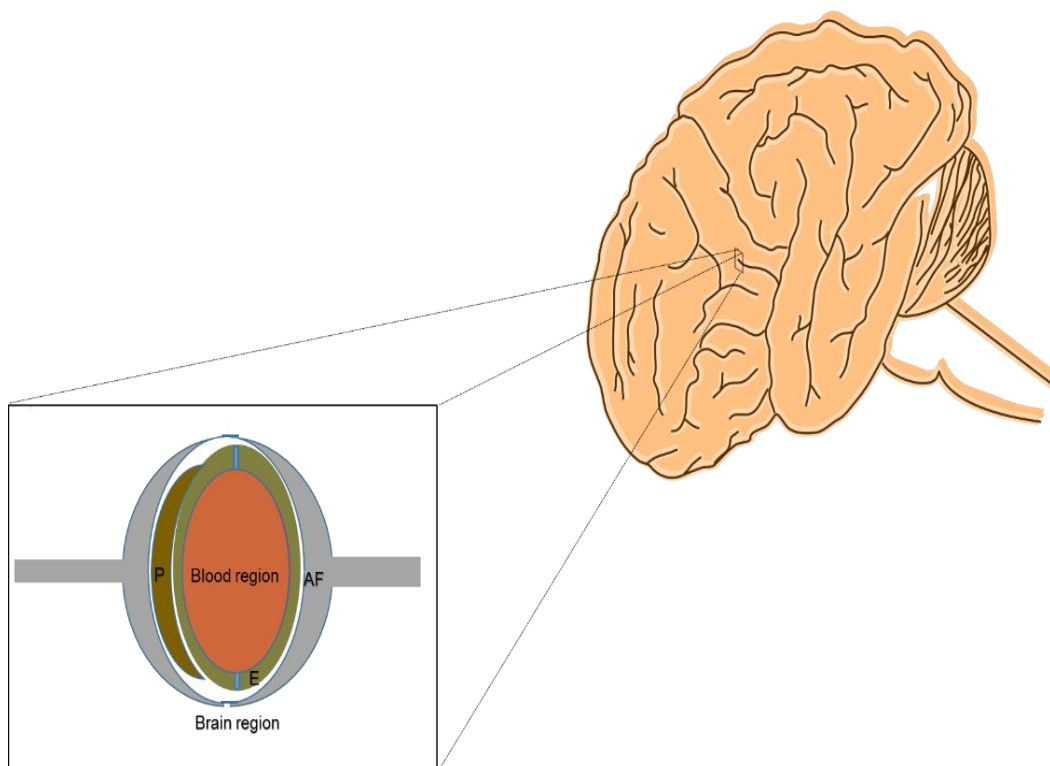


Figure 2.1. BBB-glia vascular unit. **AF** stands for Astrocytic-Foot process, **E** stands for endothelial cell, and **P** stands for pericyte. Note that blood in inside the endothelial capillary lumen does not cross the paracellular space of the endothelial cells. The junctional space of the endothelial cells (blue region) is filled with tight junctions that restrict free passage of cells, serum proteins and molecules circulating in the capillary lumen from accessing the brain parenchyma.

The direct interactions between brain endothelial capillaries and the supporting pericytes and astrocytes have been implicated in the regulation of properties that are unique to the BBB. For example, pericytes form direct connections with endothelial cells through peg socket-like junctions or gap junctions that allow for the transfer of small molecules or ions from endothelium into the

brain parenchyma through direct physical connections that they form with other BBB cells [Armulik et al., 2011; Kloc et al., 2015]. While gap junctions are commonly formed between cells of the BBB system, conventional methodologies for mimicking the BBB function *in vitro* are not optimized to allow direct physical configuration between astrocytes, pericytes and the BMECs [Trosko et al., 2000, Dere and Zlomuzica, 2012].

While astrocytes do not form continuous physical connections with the BBB-endothelium, they form a close association for paracrine signaling with BMECs and pericytes in regions of the brain capillaries that lack direct physical contacts with astrocytes [Abbott, 2002]. For example, it is well known that astrocytes are involved in paracrine signaling with pericytes and the BBB-endothelium in order to control the passage of substances from the lumen of blood capillaries into the brain parenchyma [Cleaver & Melton, 2003; Argaw et al., 2012; Prasad and Cucullo, 2013; Shindo et al., 2016]. Conventional *in vitro* methods employed in mimicking the human BBB lack the optimal configuration to allow such close interactions between astrocytes, pericytes and endothelial cells [Ye et al., 2015]. Therefore, a more physiologically relevant method for mimicking the BBB-physiology is warranted for applications in pharmaceutical drug discovery and development research [Booth et al., 2012; Wang et al., 2013; He et al., 2014; Wang et al., 2017].

While some of the recent methods reported in the literature involved plating BMECs directly on a culture of astrocytes or pericytes, **currently no *Transwell*TM method has been reported in which astrocytes, pericytes and BMECs are all layered directly on the same side of a filter support** [Srekanthreddy et al., 2016; Herland et al., 2016]. Instead, methodologies in which BMECs are cultured on the apical surface of a *Transwell*TM chamber and astrocytes or pericytes seeded on the basolateral or bottom surface of a *Transwell*TM membrane have gained popularity in BBB research. In fact, BBB co-culture models where either pericytes or astrocytes are cultured at the basolateral or bottom surface of a *Transwell*TM chamber are prevalent in BBB research, even though they form a partial representation of the BBB cells. However, the lack of optimal direct-contacts (as observed *in vivo*), and the laborious efforts that would be needed to establish such a triculture configuration may render indirect approach more difficult for larger scale applications in preclinical neurotherapeutic screening. Thus, a novel methodology described in this chapter is an attempt to improve previous methodologies for mimicking the BBB *in vitro*, including a

recently published *direct contact* co-culture method from our laboratory (see work done by Kulczar et al., 2017).

There are three key steps involved in developing a direct triculture methodology. First, a monoculture of primary human brain astrocytes is seeded on the apical surface of a filter support of a *Transwell*TM to grow and spread on the surface for two days. Pericytes are then seeded (layered) directly on a pre-formed lawn culture of astrocytes to grow and establish connections with astrocytes for two additional days. In a third step, a layer of human BMECs is grown on top of the astrocytes-pericytes co-culture to form a representation of the human BBB configuration *in vitro*. In the present study, restrictive properties of the resulting triculture model are compared to the cocultures containing hCMEC/D3 cells with pericytes/astrocytes or monocultures containing just the hCMEC/D3 cells alone (see details in **Figure 2.2**).

The fact that astrocytes surround most CNS-barriers such as the BBB-capillary, the arachnoid membranes and meningeal tissue, suggests that they may play an important role in limiting free permeation of molecules across the BBB towards the brain parenchyma [Sofroniew et al., 2015]. For example astrocytes exhibit a protective mechanism that limits the entry of toxic substances into the brain parenchyma when CNS-barriers breakdown [Sofroniew and Vinters, 2010]. Thus, a direct inclusion of astrocytes in the cell culture methods for mimicking CNS-barriers may form a more physiologically representative model for studying the role of astrocytes in neuroprotection or neuro-inflammation.

Even though pericytes are not present at all major CNS-barriers, their localization between astrocytes and the BBB-endothelial wall suggests that they may support BBB-endothelium and/or the BBB-astrocytes in regulating molecular trafficking at the BBB [Bonkowski et al., 2011; Bai et al., 2015]. Therefore, the combined role of astrocytes and pericytes in reinforcing the endothelial barrier function at the BBB is examined in this chapter. It is worth noting that numerous studies reported an increase in the functional expression of tight junctional proteins in the BBB-cell models when they were cocultured indirectly with astrocytes or pericytes [Li et al., 2010; Thomsen et al., 2015; Appelt-Menzel et al., 2017]. The role of astrocytes and pericytes in minimizing paracellular permeation across a direct-contact triculture model of the BBB may therefore be due

to upregulation of tight junctions in the BBB cell models such as the hCMEC/D3 used in the present study.

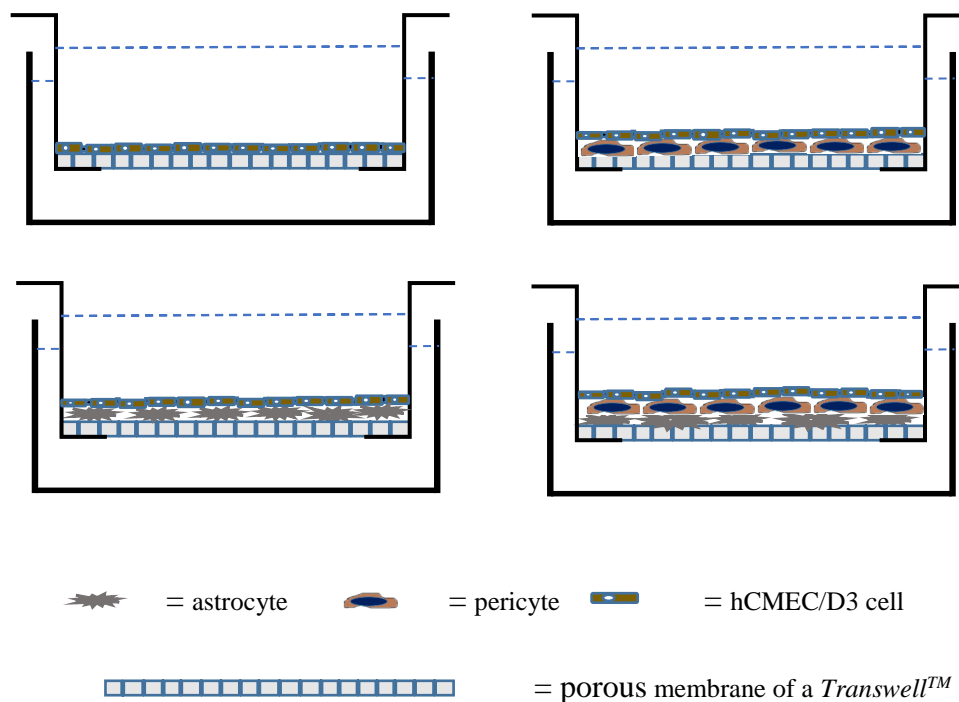


Figure 2.2. BBB-culture models employed in the study: (1) is the hCMEC/D3 monoculture representing a section of the BBB-glia vascular unit (2), the hCMEC/D3 co-culture with pericytes; a partial representation of the BBB-glia vascular unit and (3) the hCMEC/D3-triculture, which fully mimics the BBB-glia unit as it contains all physiologically relevant cell layers formed by endothelial, pericytes and astrocytes.

2.3 Hypothesis

Astrocytes and pericytes, together, form a distinct barrier to the permeation of small ions or molecules in an in vitro BBB triculture model; inclusion of astrocytes and pericytes with the hCMEC/D3 cells in a direct-contact triculture model of the BBB would lead to enhanced resistance to the paracellular permeation of hydrophilic molecules.

2.4 Test Parameters

Two types of parameters were used to compare paracellular permeability in the direct-contact triculture model of the BBB to the paracellular permeability in the mono- or direct-contact co-culture models. Two kinds of paracellular permeation were examined; the first kind involved the

permeability of ion fluxes (Trans-Endothelial Electrical Resistance, TEER), and the second involved the permeability of hydrophilic molecular permeants that rely on the paracellular diffusion to cross the layered cultures of BBB cells (astrocytes, pericytes, and BMECs). These parameters are described in detail in the following sub-sections.

2.4.1 Trans-Endothelial Electrical Resistance (TEER)

There are numerous commercial ohmmeters for use in evaluating the tightness/leakiness of BBB cell culture models; the Evom2 ohmmeter is one of the most commonly used system to measure TEER values in cell-cultures [Srinivasan et al., 2015]. For this study, a sharp increase in TEER values served as a good indicator in the paracellular tightening of BBB-culture models. However, many factors may affect the reproducibility of TEER values, especially when using conventional human BBB-cell models [Srinivasan et al., 2015]. Therefore, numerous precautions should be taken when determining TEER values. First, it is advisable to take TEER measurements at constant temperature, preferably at 37° C [Matter and Balda, 2003]. Otherwise, cell-cultures should be equilibrated at room temperature for a period of 20 minutes to avoid temperature fluctuations when TEER values are recorded. TEER-values at 37°C may then be predicted from TEER values obtained at room temperature using Blume's equations [Blume et al., 2010].

Secondly, it is important to use cells at similar passage numbers, preferably low passage numbers as TEER values start to become highly variable if high cell passage numbers are used in flux studies [Briske-Anderson et al., 1997]. Thirdly, it is recommended to use same media-buffers when TEER values are measured; different media buffers have different solute compositions and may therefore have different electrical properties that would lead to variations in TEER measurements [Ferruzza et al., 2012]. Therefore, caution needs to be taken when using TEER values as a guide to inform the analyst when a paracellular tightening occurs in cell culture models of the BBB system. It is prudent to validate the observed paracellular tightening with permeability coefficients of small hydrophilic molecules such as sucrose and mannitol.

2.4.2 Permeability coefficients

Small hydrophilic drugs such as cisplatin may diffuse across the BBB through paracellular tight junctions to cause neurotoxicity [Minami et al., 1996]. It is therefore important to gain insight on the paracellular tightness of a cell-culture model of the BBB before its application in predicting

potential neurotoxicity associated with paracellular permeants through cell junctions of the BBB system. Characterization of paracellular tightness associated with a given BBB-cell culture model may be estimated using permeability coefficients of small hydrophilic molecule whose molecular size is similar to that of a typical non-CNS drug like atenolol [McAinsh et al., 1990]. Therefore, permeability coefficients of small paracellular permeants such as sucrose and mannitol are useful in probing properties of tight junctions in BBB-cell culture models [Preston et al., 1995; Miah et al., 2017].

Several precautions ought to be taken when performing paracellular permeability assay. First, it is important to use media buffers that provide a physiologically representative pH; this would be a pH of 7.3 for the BBB [Youdim et al., 2003]. Second, the effects of unstirred water layer on the diffusion of a paracellular permeant should be minimized by using a rocking stage set between 25 to 150 rpms [Youdim et al., 2003]. Third, mass balance should be above 90% at the end of a paracellular permeability assay to ensure minimal retention of the paracellular marker compound by the cells [Youdim et al., 2003].

2.5 Materials and methods

2.5.1 Cells and cell growth materials

The hCMEC/D3, human cerebral astrocytes, and the human brain vascular pericytes were utilized in the development and comparison of a directly layered hCMEC/D3 triculture to the hCMEC/D3 monocultures and the hCMEC/D3 cocultures with astrocytes or pericytes. The hCMEC/D3 cell line was donated from Dr. Pierre-Olivier Couraud (Institut Cochin, Paris-France), human cerebral astrocytes were purchased from *ScienceCell* (Catalog # 1800), and the human brain vascular pericytes from *ScienceCell* as well (Catalog # 1200). The use of hCMEC/D3 cells is recommended between passage numbers 30 and 40; the hCMEC/D3 are known not differentiate at this passage interval [Hatherell et Al., 2011]. Therefore, the hCMEC/D3 cells used in the present study were between passage 33 and 40.

The hCMEC/D3 cells, cultured in collagen-coated T-75 flasks, were grown in EBM-2 media supplied from Lonza (Catalog # CC 3156 or 19860) and supplemented with 2% fetal bovine serum, 0.03% VEGF, 0.01% hydrocortisone, 5ug/L bFGF, 10 mM HEPES, and 1% penicillin-

streptomycin. The hCMEC/D3 culture flasks were kept in a sterile incubator set at 95% atmospheric air, 5% CO₂, and at 37°C. Primary astrocytes utilized in the study were at passage numbers between 5 and 10. All astrocytes monocultures were cultivated in Poly-L-Lysine-coated T-75 flasks, and grown in astrocytes media supplemented with 5mL P/S, 10 mL FBS, and 5mL AGS solutions, supplied from *ScienceCell*, per 500mL bottle of astrocyte media. Similarly, the HBVP (at passage number between 4 and 10 were cultivated in T-75 flasks. Pericytes media were supplemented with solutions supplied from *ScienceCell* as follows: 5mL P/S, 10mL FBS, and 5mL PGS per 500mL of pericytes media. T-75 flasks containing cultures of pericytes or astrocytes were kept inside a sterile incubator at 95% atmospheric air, 5% CO₂, and at 37°C for the cells to grow. Each cell type was passaged upon reaching confluency.

2.5.2 Cell seeding

Cell plating densities were first determined in the triculture using various iterations in the seeding density ratios between astrocytes, pericytes, and the hCMEC/D3 cells. Seeding density ratios analyzed were [(5 x 10³A): (5 x 10³P): (1 x 10⁵E)]/cm², [(1 x 10⁴A): (1 x 10⁴P): (1 x 10⁵E)]/cm², [(4 x 10⁴A): (4 x 10⁴P): (1 x 10⁵E)]/cm², [(5 x 10⁴A): (5 x 10⁴P): (1 x 10⁵E)]/cm², [(5 x 10⁴A): (5 x 10⁴P): (8 x 10⁴E)]/cm², [(1 x 10⁴A): (1 x 10⁴P): (1 x 10⁵E)]/cm², [(4 x 10⁴A): (4 x 10⁴P): (8 x 10⁴E)]/cm² where **A** stands for the astrocytes, **P** stands for pericytes, and **E** stands for the hCMEC/D3 cells. Astrocytes were seeded first for two days; then pericytes were layered over the resulting culture of astrocytes, and allowed to grow for two days; then hCMEC/D3 cells were seeded over the resulting lawn coculture of astrocytes and pericytes for 6 to 7 days to form a triculture model of a human BBB.

Note that *Transwell*TM filter supports were pre-coated overnight with 10ug/mL of poly-L-lysine before seeding astrocytes to promote the attachment of astrocytes on the surface of a *Transwell*TM membrane support. Additionally, 10ug/mL of poly-L-Lysine was applied onto astrocytes culture before seeding pericytes, and 100ug/mL of type I rat-tail collagen was applied onto the coculture of astrocytes and pericytes before seeding the hCMEC/D3 cells to promote their attachment on the lawn coculture of astrocytes and pericytes. Cells were fed with supplemented EBM-2 media on the apical chamber and alternate astrocytes or pericytes media on the basolateral chamber.

2.5.3 TEER measurement

TEER values were measured first across filter supports of a free *Transwell*TM, followed by monocultures of hCMEC/D3 cells, cocultures of hCMEC/D3 cells directly seeded on pre-attached astrocytes and lastly across tricultures of hCMEC/D3 cells directly layered over cocultures of astrocytes and pericytes to form a triculture. TEER-values across filter supports of a free *Transwell*TM containing HBSS buffers, were used to correct values obtained from cell cultures grown on the apical surface of the *Transwell*TM membranes. Cell media were replaced with HBSS buffer, followed by equilibration at room temperature before recording TEER values in cell cultures that were evaluated in this study.

2.5.4 Test compounds

A set of compounds that represents small and large paracellular permeants was selected to evaluate and compare the paracellular permeation across mono-, co- and tri-culture methods for mimicking the BBB *in vitro*. This set consisted of [¹⁴C]-sucrose purchased from *PerkinElmer*, [¹⁴C]-mannitol purchased from *Moravek Biochemicals*, [¹⁴C]-PEG-4000 purchased from *American Radiolabeled Chemicals Inc.*, and [¹⁴C]-inulin purchased from *PerkinElmer*.

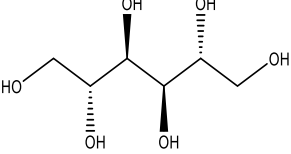
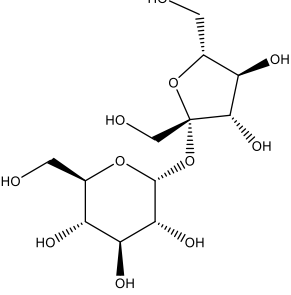
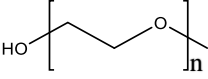
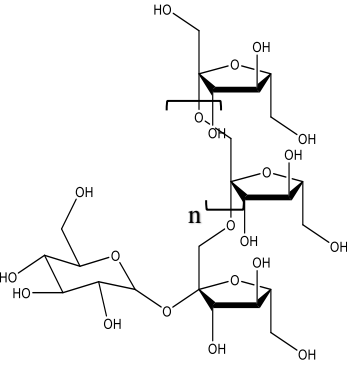
Sucrose was initially used in making permeability comparisons involving monocultures of hCMEC/D3 cells, cocultures of hCMEC/D3 cells with pericytes or astrocytes, and the tricultures of hCMEC/D3 cells layered over cocultures of astrocytes and pericytes. Mannitol was used to compare paracellular tightness in the monocultures of astrocytes, pericytes, with tightness in the cocultures of astrocytes and pericytes. PEG-4000 and Inulin-5000 were used to confirm the observed paracellular tightening in the direct contact triculture model relative to the monoculture. A comparison of the physicochemical properties for the paracellular permeants used in this study are listed in **Table 4.1**.

2.5.5 Permeability assays under monocultures of the hCMEC/D3 cells

Immortalized hCMEC/D3 cells (frozen at passage 32) were re-grown in a vented T-75 flask in an incubator set at 37°C and 5% CO₂. The hCMEC/D3 cells were used after three or more passages in a T-75 flask pre-coated with 100ug/mL collagen. Upon 90% confluency, the hCMEC/D3 cells were detached from T-75 flask using a solution of a trypsin solution. Calculation of permeability values was achieved using equations 2.1 and 2.2, where P_{apparent} stands for the apparent permeability of a molecular permeant across the BBB cell culture layers including the porous membranes of the filter support, P_{Layers} stand for the effective permeability across the BBB cell culture layers, and P_{Filter} stands for the permeability value across an empty filter support of a *Transwell*TM, V_R is the volume of the receiver chamber, C_R is the concentration of the BBB permeant in the receiver chamber at time t , A is the area of the transwell surface onto which BBB cells layers are attached, and C_{D0} is the concentration of the BBB permeant in the donor chamber of a transwell at time $t = 0$.

$$\frac{1}{P_{\text{apparent}}} = \frac{1}{P_{\text{Layers}}} + \frac{1}{P_{\text{Filter}}} \quad (\text{Equation 2.1}), \quad \& \quad P_{\text{apparent}} = \frac{V_R \times dC_R}{dt \times A \times C_{D0}} \quad (\text{Equation 2.2})$$

Table 2.1. The Physicochemical properties for the tested paracellular permeants.MW = Molecular weight, r_H = hydrodynamic radius

Compound	Physicochemical properties	Radiolabel
 <p>^{14}C-Mannitol</p>	<p>MW = 182.172 g/mol Aqu. solubility= 16mg/mL $r_H = 3.8\text{\AA}$</p>	<p>^{14}C</p>
 <p>^{14}C-Sucrose</p>	<p>MW = 342.297 Aqu. solubility = 210mg/mL $r_H = 4.4\text{\AA}$</p>	<p>^{14}C</p>
 <p>PEG-4000</p>	<p>MW =4000g/mol Aqu.solubility= 630 mg/mL $r_H = 16\text{\AA}$</p>	<p>^{14}C</p>
 <p>Inulin-5000</p>	<p>MW =5000 Aqu. solubility = NA, $r_H = 15\text{\AA}$</p>	<p>^{14}C</p>

Trypsin was then removed by centrifugation at 1500 rpm and the re-suspended hCMEC/D3 cells were seeded in triplicates at 8×10^4 cells/cm² on the collagen-coated apical surface of filter inserts of a *Transwell*TM (0.4 μ m pore size). The hCMEC/D3 monocultures were placed in a sterile incubator for 7 days and their cell media was changed every 48 hours.

Before performing permeability assays, the hCMEC/D3 monocultures were washed three times in PBS followed by incubation with HBSS (Hank's Balanced Salt Solution containing 25 mM HEPES buffer, pH ~ 7.4) for 15 minutes before carrying out transport studies. At the start of paracellular permeability experiments, 1.5mL of fresh HBSS buffer was placed in the receiver chamber of a *Transwell*TM and 0.5mL of fresh HBSS containing a test radio labelled marker compound were added at the donor chamber. Paracellular marker concentrations used in this study were 0.25uCi/mL for mannitol, 0.25 uCi/mL for sucrose, 1uCi/mL for PEG-4000 and 1 uCi/mL for inulin-5000. Samples from the receiver chamber were collected at 15, 30, 45, 60, 90 minutes intervals. Transport assays were carried out on rocking plate at 40 rpm. Radioactivity in the donor samples was detected using a liquid scintillation counter. The rates of mass transfer from the donor chamber to the receiver chamber were used to calculate permeability coefficients using Equations 2.1 and 2.2.

2.5.6 Permeability assays under cocultures of the hCMEC/D3 cells with pericytes

A direct coculture of hCMEC/D3 cells on pericytes was achieved on the apical surface of a filter insert as follows: Primary human brain vascular pericytes (HBVP frozen at passage 3) were re-grown up to passage 5 in a vented T-75 flask positioned inside a sterile incubator set at 37°C and 5% CO₂ atmosphere. Upon 90% confluency, pericytes were detached from T-75 flask using a trypsin solution. The trypsin solution was separated from pericytes by centrifugation of the suspended cells at 1500 rpm.

The resulting pellet of pericytes was re-suspended in media, and subsequently the suspended cells were plated in triplicates at seeding density of 4×10^4 cells/cm² on the apical surface of filter inserts that were pre-coated with 10 μ g/mL Poly-L-lysine. At the end of 48 hours, cultures of pericytes were rinsed with HBSS, followed by incubation for 10 minutes with 0.5mL of 100 μ g/mL rat-tail collagen type I, at 37°C and 5% CO₂. This collagen solution was then removed before

plating the hCMEC/D3 cells directly on top of the pericytes layer at a density of 8×10^4 cells/cm². The permeability assay was performed on day 7 using sucrose in section 2.4.5.

2.5.7 Permeability assays under cocultures of the hCMEC/D3 cells with Astrocytes

A direct co-cultivation of hCMEC/D3 cells on top of astrocytes that were pre-attached on the surface of a filter membrane of a *Transwell*TM was carried out using a similar protocol for the hCMEC/D3 coculture with pericytes as explained in section 2.4.6. The permeability of sucrose across the direct coculture of hCMEC/D3 cells with astrocytes, was performed in a similar way to the hCMEC/D3 monoculture as described in section 2.4.5.

2.5.8 Permeability assays under tricultures of the hCMEC/D3 cells with pericytes and astrocytes

Direct tri-cultivation of layers of astrocytes, pericytes and hCMEC/D3 were set up on the apical surface of a *Transwell*TM filter support as follows. Astrocytes are first plated at 4×10^4 cells/cm² on filter inserts that had been pre-coated with 10ug/mL poly-L-lysine overnight. At the end of 48 hours, astrocytes were incubated with 0.5mL of 10ug/mL poly-lysine on the apical side for 10 minutes at 37°C and 5% CO₂ atmosphere. Once poly-L-lysine solution was removed, pericytes were plated on top of astrocytic-layer at a seeding density of 4×10^4 cells/cm². At the end of 48 hours, the co-culture of astrocytes and pericytes layers was rinsed using HBSS and incubated (on the apical side) with 0.5mL, 100ug/mL of rat-tail collagen type I for 10 minutes at 37°C and 5% CO₂. At the end of 10 minutes, the collagen solution was removed and the hCMEC/D3 cells are plated on top of the co-culture layers at a density of 8×10^4 cells/cm² to form a full tri-culture model of the BBB-glia vascular unit. Permeability assays for mannitol, sucrose, PEG-4000 and Inulin-5000 were performed as described in section 2.4.5.

2.5.9 Statistical Analysis

Results were reported as the means \pm SEM and a p-value < 0.05 (*) indicated a significant difference. Data comparisons were conducted using one tailed student's T-tests or one-way ANOVA tests followed by a post hoc Tukey-multiple comparison test to identify specific differences in the mean values of experimental parameters being compared. In addition, a non-overlapping 95% confidence interval (CI) was used to establish significant differences in the mean values where parameters under comparisons were closely spaced.

2.6 Results and discussion

2.6.1 Selection of the cell-seeding density ratio for the triculture model

Cell seeding densities can have a significant effect on the integrity of a BBB cell-culture model [Wilson et al., 2015]. The first task in the present study was to select an optimal seeding density ratio for the direct-contact triculture model of the BBB (see **Table 2**). Initially, a seeding density ratio of [(5 x 10³**A**): (5 x 10³**P**): (1 x 10⁵**E**)] cells/cm² was selected as a slight modification in the seeding density ratio first reported in methods involving indirect tri-cultivation of hCMEC/D3 cells with pericytes and pericytes where these cells were separated by a thick filter membrane [Hatherell et al., 2011]. The seeding densities for astrocytes and pericytes were increased gradually to obtain an optimal coverage of the filter membrane, which would result in the optimal lawn of cells onto which the hCMEC/D3 cell layer would form. When the astrocytes and pericytes seeding density-ratio was increased upto [(4 x 10⁴**A**): (4 x 10⁴**P**)] cells/cm², the resulting co-culture was well attached on the surface of a *Transwell*TM filter support. The seeding density for the hCMEC/D3 cells was reduced gradually from 1 x 10⁵ cells/cm² to 8 x 10⁴ cells/cm² to avoid overgrowth in the hCMEC/D3 layer in the triculture model of the BBB system. Ultimately, a seeding density ratio of [(4 x 10⁴**A**): (4 x 10⁴**P**): (8 x 10⁴**E**)] cells/cm² was selected due to its good stability and early increase in TEER values showing a better range of days in which the resulting triculture would be useful for permeability studies (refer to **Table 2.2** for the TEER values).

Table 2.2. Selection of a seeding density ratio. **A** = astrocytes, **P** = pericytes, **E** = hCMEC/D3 cells

Seeding density ratio x 1000 cells/cm ²	TEER-Max(Ω -cm ²), AP co- culture	TEER-Max (Ω -cm ²), triculture
(5A: 5P: 100E)	47 \pm 14	73 \pm 7
(10A: 10P: 100E)	51 \pm 10	72 \pm 10
(40A: 40P: 100E)	25 \pm 2	81 \pm 3
(50A: 50A: 100E)	41 \pm 6	77 \pm 5
(50A: 50P: 80E)	41 \pm 4	73 \pm 3
(40A: 40P: 80E)	43 \pm 9	81 \pm 6

TEER values in the coculture of astrocytes and pericytes had similar magnitudes to those observed in the monocultures of primary hBMECs or the hCMEC/D3 cells ($\sim 40 \Omega$ -cm²). This was an intriguing observation suggesting that astrocytes or pericytes may be forming an additional paracellular barrier in series with the endothelial barrier in the triculture model. The observation of an electrical resistance in the coculture of astrocytes and pericytes also supports previous studies by other researchers, which demonstrated the existence of a glial or pericytic barrier in species that lack a functional endothelial barrier [Frey et al., 1991; Alvarez et al., 2013; Limmer et al., 2014]. The restrictive property in the paracellular permeation was investigated further in this study using mannitol, (a small paracellular permeant).

There was approximately a two-fold increase in TEER values on day 7 after seeding the hCMEC/D3 cells on the coculture of astrocytes and pericytes. The observed resistance conformed to a system of two barriers in a serial configuration; the first electrical resistance experienced in the hCMEC/D3 layer, and the second experienced in the coculture section made of astrocytes and pericytes. Surprisingly, the maximum TEER values determined in the direct-contact triculture ($\sim 80 \Omega$ -cm²) were similar in magnitude to those reported using indirect-methods where the hCMEC/D3 cells are cultured separately together with astrocytes and pericytes to form a triculture

model of the BBB system [Daniels et al., 2013]. However, the proposed triculture model presents a novel configuration containing all the principal cellular components of the BBB in direct-contact. In addition, the proposed configuration would provide space for additional BBB-components such as neurons or microglia.

2.6.2 Selection of the day for performing permeability assays

A monoculture of hCMEC/D3 layer was prepared at a seeding density of 8×10^5 cells/cm² as described in **section 2.4.5**. Permeability coefficients of mannitol were determined in the period between 24 hours and 244 hours after seeding the hCMEC/D3 cells in a *Transwell*TM. The resulting trend indicated a sharp reduction in the permeability of mannitol ($\sim 2.1 \times 10^{-4}$ cm/s to $\sim 5.2 \times 10^{-5}$ cm/s), a 4-fold reduction on day 7. The sharp decrease in the paracellular permeation was used as an indicator for the formation of tight junctions between adjacent hCMEC/D3 cells in the monoculture. Furthermore, additional permeability coefficients of mannitol were determined on day 7, 9 and 10 to confirm that tight junctions remained intact once they formed.

Though the hCMEC/D3 was more restrictive on day 10, permeability assays were run between day 6 and 9 to avoid the possibility of cell overgrowth of the hCMEC/D3 cell layer. Furthermore, TEER measurements obtained in the triculture showed maxima on day 7 and a downward trend after day 9. Thus, again, it was preferred to perform permeability assays on day 7 as both TEER and mannitol permeability indicated the formation of tight paracellular junctions between hCMEC/D3 cells around day 7.

Table 2.3. The formation of tight cell-cell junctions in a monoculture of hCMEC/D3 cells. A sudden reduction in the mannitol permeability across the hCMEC/D3 culture at the end of 144 hours indicated a reduced cell-cell junctional space

Time post-hCMEC/D3 seeding (hours)	Mannitol Permeability (P _L) (cm/s)
24	3.0 x 10 ⁻⁴
72	1.4 x 10 ⁻⁴
120	2.1 x 10 ⁻⁴
144	6.3 x 10 ⁻⁵
168	5.2 x 10 ⁻⁵
216	6.0 x 10 ⁻⁵
240	4.0 x 10 ⁻⁵

2.6.3 Microscopic examination in triculture seeding

Step 1: Seeding astrocytes

The microscopic examination was carried out during triculture preparation to ensure that astrocytes were attached and dispersed well on the surface of a *Transwell*TM membrane to promote the formation of a stable basal culture of astrocytes onto which pericytes and hCMEC/D3 cells would be grown in layers. Astrocytes seeded at a density of 4 x 10⁴ cells/cm² settled on the surface of a *Transwell*TM membrane with good dispersion distances (see **Figure 2.3.**). At the end of 48 hours, the astrocytes had multiplied to cover a large portion of the *Transwell*TM membrane. They also changed their original round morphology to a new morphology that showing sharply pointed peripheries. However, it was difficult to establish if astrocytes covered the filter membrane completely. A phase contrast microscope was required for better visualization of the confluency level on the membrane surface.

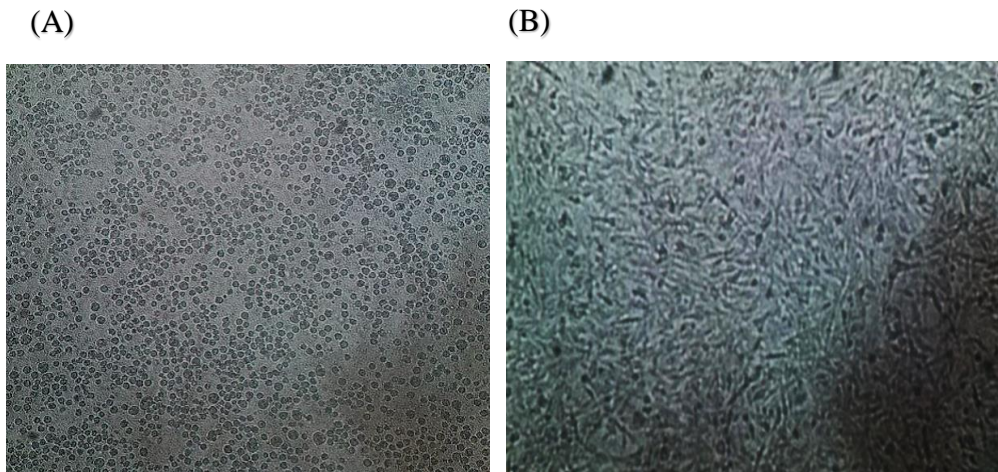


Figure 2.3. Step I: Preparation of a layer of astrocytes in the course of seeding a direct-contact triculture. Prior to seeding, the suspended astrocytes were sheared up and down using a Pasteur pipette to ensure that no cell clumps were seeded on the transwell membrane. Initially a seeding volume of .250mL was used to seed astrocytes at a density of 4×10^4 cells/cm² (**panel A**). Cells were left in the sterile hood for 30 minutes in order to settle down on the surface of the membrane. An additional .250mL of astrocytes media was then added on the apical chamber where the astrocytes were seeded. The basolateral chamber was filled with 1.5 mL of astrocytes media. The astrocytes culture was then set in a sterile incubator. The astrocytes culture expanded and changed the morphology from round circular cells to a sharp-ended morphology at the end of 48 hours (**panel B**).

Step 2: Seeding pericytes on a basal culture of astrocytes

Pericytes were seeded directly on the attached culture of astrocytes at a density of 4×10^4 cells/cm². **Figure 2.4** shows pericytes settling on a basal culture of astrocytes; the sharp-ended morphology of astrocytes is clearly visible underneath the round dispersed pericytes. Pericytes multiplied to form a layer that covered the astrocytes layer at the end of 48 hours.

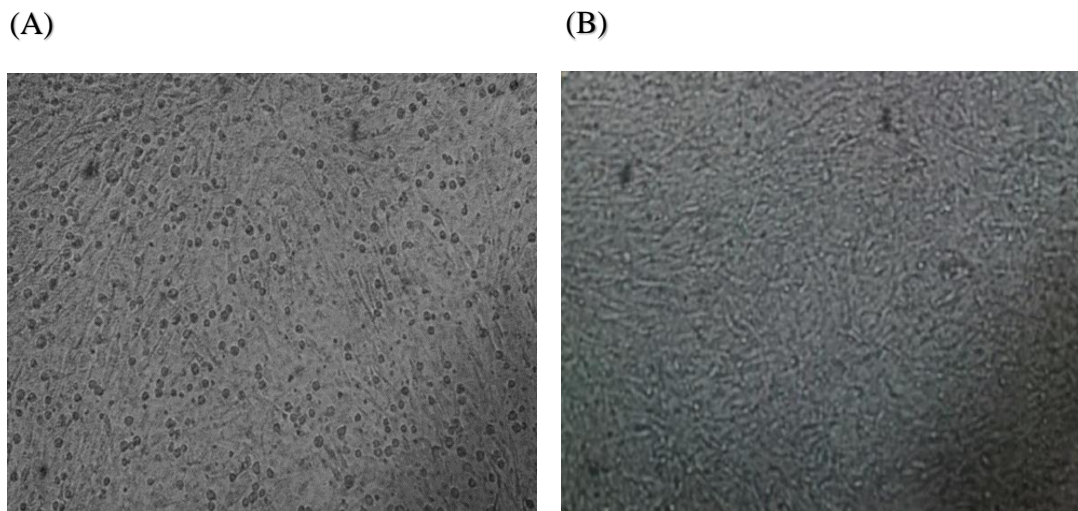


Figure 2.4. Step II: Culturing a layer of pericytes on top of the astrocytes prepared in step I. Pericytes were prepared in the same way as astrocytes in step I. **Panel A** shows pericytes settling on a base-culture of astrocytes. Pericytes were dispersed well to avoid formation of multiple layers or overgrowth. **Panel B** shows pericytes growing in the co-culture at the end of 48 hours. Though the new culture looks distinct from the astrocytes culture, it was difficult to visualize a distinct layer of pericytes due to poor phase contrast in an inverted light microscope.

The original morphology of pericytes changed at the end of two days; the resulting confluent culture did not reveal cell morphologies associated with astrocytes. Therefore, it was difficult to obtain focal regions specific to each cell layer regions. A phase contrast microscope was required for further characterization of superimposed cell cultures prepared in this study.

Step 3: Seeding the hCMEC/D3 on a basal coculture of pericytes and astrocytes

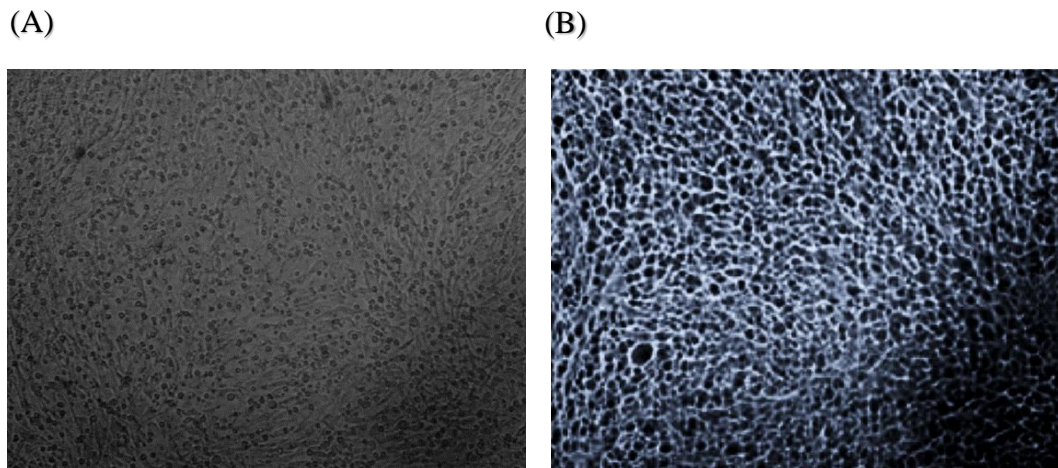


Figure 2.5. Step III: Culturing a layer of hCMEC/D3 cells after step II. Panel A is a micrograph showing the hCMEC/D3 cells seeded at 8×10^4 cells/cm², on top of a co-culture of pericytes & astrocytes prepared in step II. The hCMEC/D3 cells were left to grow on a base of astrocytes and pericytes for 6 days. The resulting triculture was stained on day 7 using hematoxylin. A light micrograph of the triculture after staining is shown in panel B

The coculture of astrocytes and pericytes in steps 1 and 2 formed a base onto which the hCMEC/D3 cells were seeded at $\sim 8 \times 10^4$ cells/cm² to form the target triculture model of the BBB. **Figure 2.5** shows that the hCMEC/D3 cells settled and dispersed well on a basal co-culture of pericytes seeded on top of astrocytes. The hCMEC/D3 cells multiplied to form a cobblestoned layer on day 7 post seeding. The resulting hCMEC/D3 layer was stained with **hematoxylin**, and was subsequently photographed under an inverted light microscope. The resulting micrograph in step 3 shows a characteristic arrangement of BMECs at 100% confluency level [Lim et al., 2011].

2.6.4 Relative paracellular tightness in the BBB triculture

TEER values and permeability coefficients of sucrose were used to compare paracellular tightness of the mono-, co- and triculture models of the BBB where hCMEC/D3 cells represented human BBB-endothelial cells. The average TEER values measured in the monoculture of hCMEC/D3 on day 7 post seeding were lower than values measured in the coculture of hCMEC/D3 cells with astrocytes and triculture with astrocytes and pericytes (35 ± 5 Ω -cm², 43 ± 9 Ω -cm², and 81 ± 6 Ω -cm² respectively, see **Figure 2.6**). The higher TEER values in the triculture

may be due to the inductive effects from astrocytes and/or pericytes. Alternatively, astrocytes and pericytes may be forming another barrier in series with the hCMEC/D3 barrier juxtaposed on the underneath coculture of astrocytes and pericytes.

A comparison of the permeability of sucrose across the mono-, co- and tricultures showed a concomitant decrease in the paracellular permeation from higher values of sucrose permeability in the hCMEC/D3 monoculture to lower values in the co- and tricultures. A direct coculture of hCMEC/D3 cells with pericytes led to a decrease in the permeability of sucrose by a factor of 2.5 from $(8.7 \pm 0.10) \times 10^{-5}$ cm/s in the hCMEC/D3 monoculture, to $(3.5 \pm 0.25) \times 10^{-5}$ cm/s in the coculture with pericytes. Similarly, there was a decrease in the permeability of sucrose in the coculture of hCMEC/D3 cells with astrocytes, i.e., from a value of $(8.7 \pm 0.10) \times 10^{-5}$ cm/s, in the hCMEC/D3 monoculture, to $(3.1 \pm 0.13) \times 10^{-5}$ cm/s in the coculture with astrocytes; this decrease was similar in magnitude to the decrease observed under coculture of hCMEC/D3 cells with pericytes.

Though tricultures were expected to show higher paracellular tightness than hCMEC/D3 monocultures or cocultures, sucrose permeability in the triculture was not relatively lower in the cocultures with astrocytes nor pericytes. Sucrose permeability was $(3.0 \pm 0.20) \times 10^{-5}$ cm/s in the triculture versus $(3.5 \pm 0.25) \times 10^{-5}$ cm/s in the coculture with pericytes and $(3.1 \pm 0.13) \times 10^{-5}$ cm/s in the coculture with astrocytes. Therefore, it seems that paracellular tightening in the hCMEC/D3 barrier may only be increased upto a certain extent; further inclusion of astrocytes or pericytes may not lead to a further decrease in the permeability of sucrose.

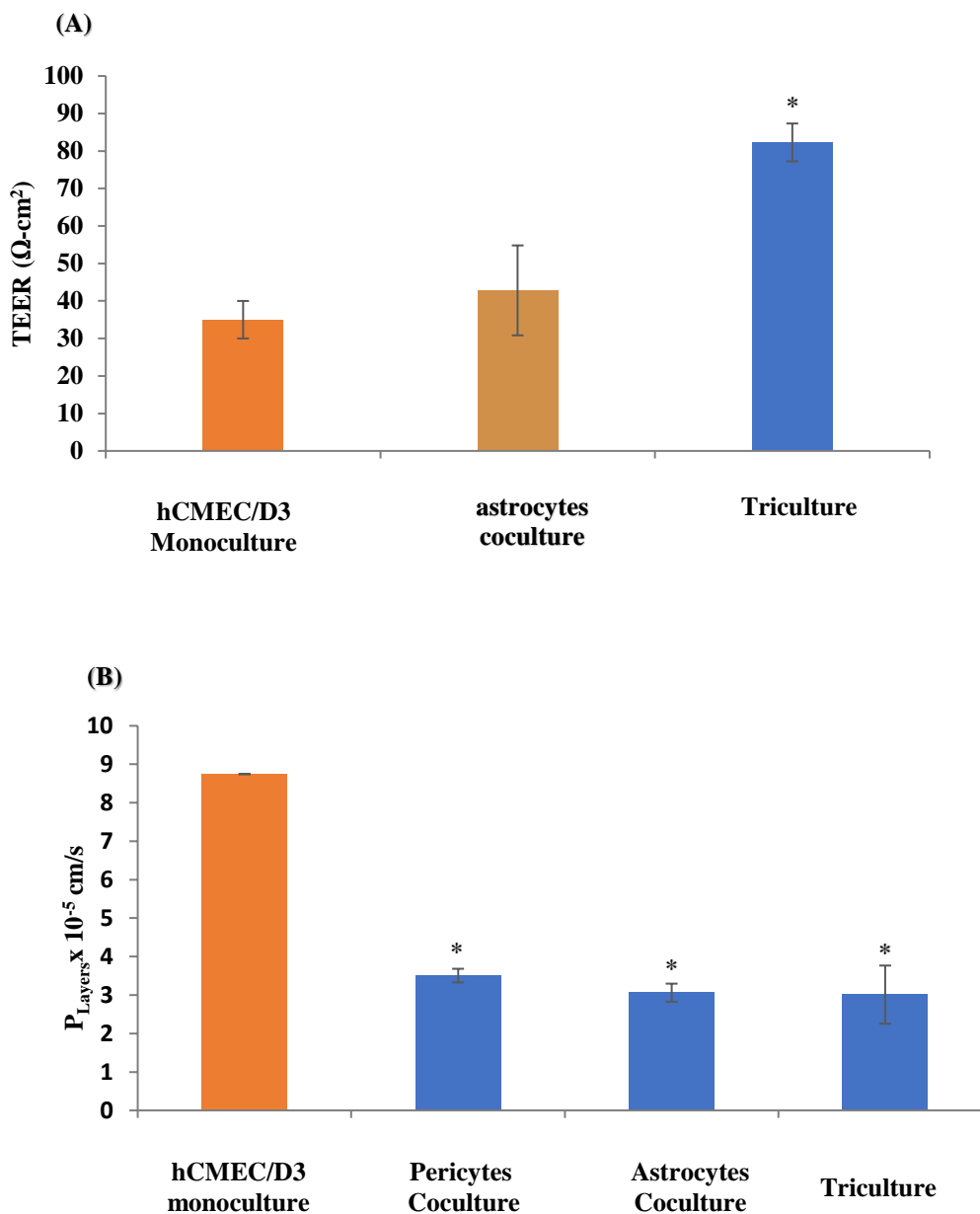


Figure 2.6. A comparison of paracellular tightness in the mono-, co- and triculture models of the BBB. TEER values (**Panel A**) indicated that the direct-contact triculture shows more resistance to the flux of conducting ions in comparison to the mono- or cocultures (one-way ANOVA; $n = 12$, p -values were 0.001 and 0.004 respectively). The higher resistance in the triculture was confirmed using the permeability of sucrose. The hCMEC/D3 monoculture was less restrictive to sucrose permeation in comparison to the co-cultures of hCMEC/D3 with pericytes or with astrocytes and the triculture as shown in **Panel B** (one way ANOVA; $n=6$, p -values were < 0.001 in each comparison where the hCMEC/D3 monoculture was used in the control experiment). A Turkey's post hoc test showed that a significant difference in the mean permeability values existed only between the hCMEC/D3 monoculture control versus co- and tricultures examined in this study.

2.6.5 Relative permeability of mannitol in the coculture of astrocytes with pericytes

The permeability of mannitol was tested in the monoculture of astrocytes and cocultures of pericytes that were directly seeded on top of astrocytes culture to determine whether non-endothelial components of the BBB of any significant paracellular resistance to the flux of small molecular permeants across the glial vascular unit. Monocultures of astrocytes were used to represent the astrocytic portion of the BBB system, pericytes monocultures represented the pericytic component, and the coculture of pericytes and astrocytes were used to test if there was a synergistic effect in resistance to the permeation of mannitol across non-endothelial cellular regions of the BBB system.

The apparent permeability of mannitol was higher in the monoculture of pericytes than in the monoculture of astrocytes or the astrocytes-pericytes coculture. Mannitol permeability was $(3.5 \pm 0.29) \times 10^{-5}$ cm/s in the monoculture of pericytes versus $(2.7 \pm 0.13) \times 10^{-5}$ cm/s in the astrocytes monoculture, and versus $(2.3 \pm 0.35) \times 10^{-5}$ cm/s in the coculture of pericytes on astrocytes. The permeability of mannitol in the monoculture of pericytes was similar in magnitude to the permeability of mannitol through a free filter membrane of a *Transwell*TM. Therefore, pericytes seem not to have offered any effective resistance to the flux of mannitol. Pericytes may be inducing the formation of a more effective barrier in the astrocytes in a similar way they do in the hCMEC/D3 cells. The average effective permeability of mannitol across a coculture of pericytes layered on astrocytes was 6.9×10^{-5} cm/s, (See **Figure 2.7** for more discussion of results). Therefore, future studies are required to establish whether pericytes induce paracellular junctions (gap or tight junctions) in the astrocytes.

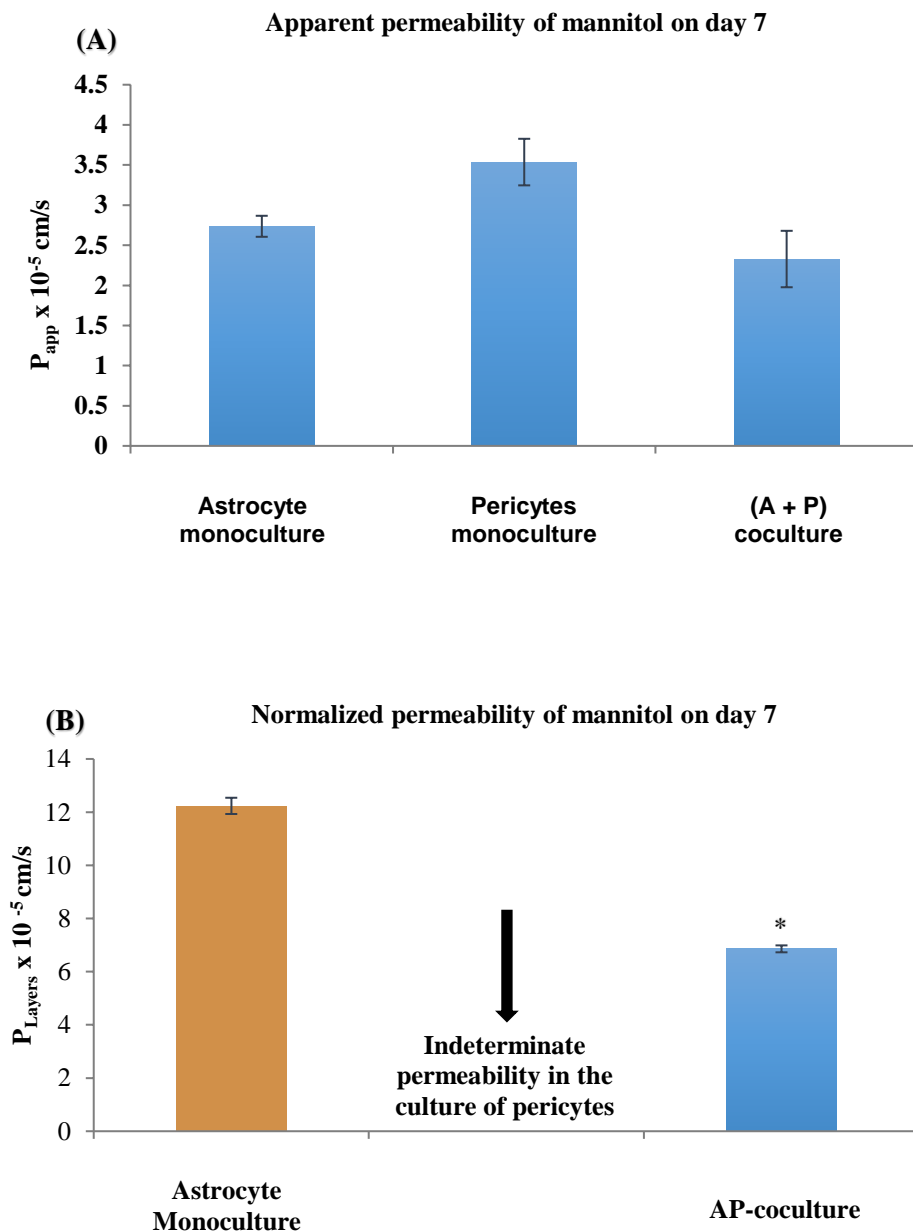


Figure 2.7. Permeability of mannitol across mono- or co-cultures of astrocytes and pericytes. The apparent permeability of mannitol is lower in the co-culture of astrocytes and pericytes in comparison to the astrocytes or pericytes alone (**Panel A**). The effective permeability of mannitol (**Panel B**) in the culture of pericytes could not be determined since it was equal to that of a free filter membrane containing no cell layers. The effective permeability of mannitol across layers pericytes and astrocytes in a coculture, was significantly lower in comparison to monoculture of astrocytes alone as shown in Panel B (T-test: $n = 6$, $p\text{-value} = 0.002$)

2.6.6 Size-dependent permeability of paracellular marker compounds

The BBB shows a size-selective paracellular transport whereby small hydrophilic molecular permeants may diffuse through paracellular junctions more easily in comparison to the larger ones [Nitta et al., 2003; Yanagida et al., 2017]. In the present study, permeability coefficients of hydrophilic permeants with varying hydrodynamic radii were determined under the monoculture and triculture methods for mimicking the BBB in a *Transwell*TM. Two categories of molecules representing either small or large hydrophilic molecules were used to compare the effect of molecular size on the paracellular permeation rates through a monoculture of hCMEC/D3 cells and through the triculture of hCMEC/D3 on a lawn of pericytes and astrocytes.

Mannitol and sucrose that were used in the first category of paracellular permeants, representing small hydrophilic drugs such as atenolol and nadolol that may cross a leaky human BBB via paracellular routes to cause neurotoxicity. PEG-4000 and inulin-5000 used in the second category, representing large-sized pharmaceutical excipients that should not diffuse through tight-junctions of the BBB-endothelium. **Figure 2.8** shows that the triculture model of the BBB is more restrictive than the monoculture for the two categories of compounds examined in this study.

The permeability of mannitol in the triculture model was reduced by a factor of 1.5; sucrose permeability was reduced by a factor of 2.4; PEG-4000 permeability by a factor of 4.5 and Inulin-5000 by a factor of 8. Note that, unlike the hCMEC/D3 monoculture, the triculture model showed a size-dependent sieving property. Mannitol and sucrose had similar permeability values (i.e., 3.8×10^{-6} cm/s, and 3.6×10^{-6} cm/s) respectively in the triculture, perhaps because they have similar hydrodynamic radii (3.8Å and 4.4Å respectively). PEG-4000 had a slightly higher permeability value than inulin-5000 under the triculture model (2.1×10^{-6} cm/s and 2.6×10^{-6} cm/s respectively) even though PEG-4000 has a slightly larger hydrodynamic radius than inulin-5000. This observation indicates that there may be additional physicochemical factors, other than hydrophilicity and hydrodynamic radii that determine selectivity in the paracellular permeation of hydrophilic molecules across cellular barriers of the BBB system.

Overall, the triculture model was more restrictive against permeation of the tested hydrophilic permeants than the monoculture model that offer a partial representation of the BBB system. Both small and large molecules were more restricted in the triculture model in comparison to the

monoculture. On the scale of 100% permeation, sucrose is at 83%, mannitol at 63% in the monoculture.

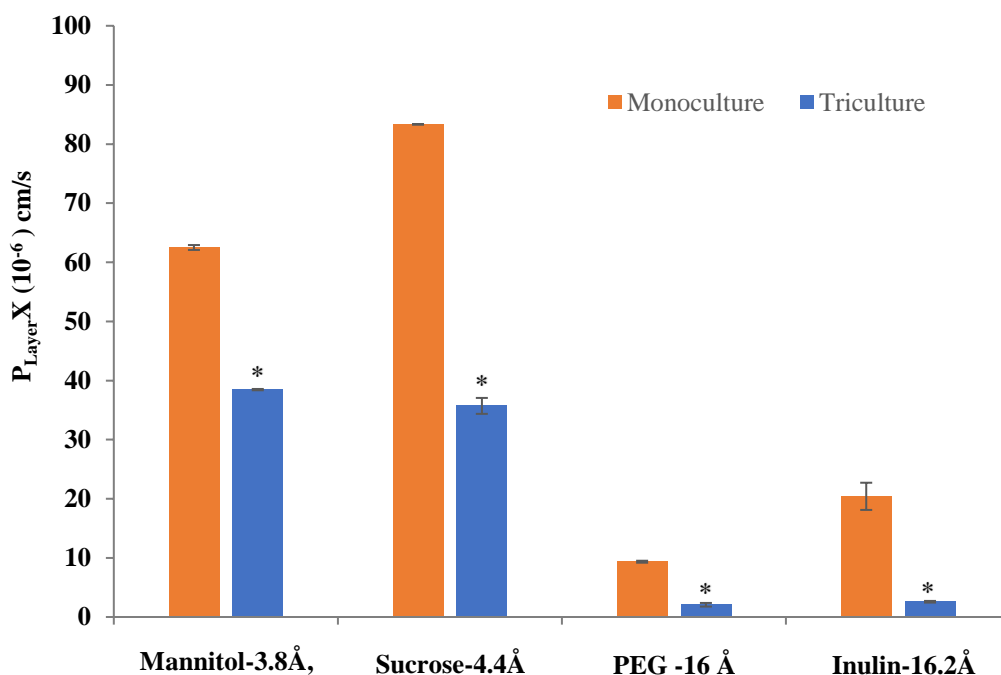


Figure 2.8. Size-dependent reduction of paracellular permeability through the triculture. In comparing mono- and tri-cultures, the decrease in permeability was **1.5-fold** for mannitol, **2.4-fold** for sucrose, **4.5-fold** for PEG-4000, and **8-fold** for Inulin-5000. The larger compounds would be much more restricted in the triculture than in the monoculture models of the BBB system. T-tests indicated a higher paracellular tightening in the triculture model for all four marker compounds employed in this study (n = 5, p-values were less than 0.05 in all the cases)

In the triculture, sucrose permeated at 38.5% level, while mannitol permeated at 36% level. Therefore, the triculture model may be more physiologically representative of the human BBB *in vivo* since it exhibited higher resistance to the flux of small hydrophilic molecules, sucrose and mannitol, which are on the size scale of small hydrophilic drugs that may traverse paracellular junctions of the human BBB to cause neurotoxicity. PEG-4000 and inulin-5000 would be classified as non-permeants under the triculture method, due to their low levels in permeation rates (2.1 % permeation rate for PEG-4000 and 2.6 % rate for inulin-5000).

2.7 Conclusions

The study presented in this chapter showed that, contrary to the popular belief that astrocytes and pericytes only play a supporting role for the BBB-endothelium, together these non-endothelial cells might also form a physiological barrier to the flux of a small paracellular permeant such as mannitol and sucrose that are on the size scale of small hydrophilic drugs. A triculture model of the human BBB prepared by seeding a layer of hCMEC/D3 cells on a pre-established base coculture of astrocytes and pericytes leads to the formation of a more physiologically representative model of the human BBB in *Transwell*TM chambers. If the triculture is used in permeability screens of hydrophilic drugs, sucrose and mannitol permeability values should be used as references to identify hydrophilic compounds with high potential for good permeability across the human BBB, while permeability values of PEG-4000 and inulin-5000 should be used to identify hydrophilic compounds with low permeability through the human BBB.

2.8 Acknowledgements

I wish to express gratitude to the department of industrial and physical pharmacy at Purdue University, for supporting my graduate research through various scholarships including Dollens and Flemming's graduate scholarships.

2.9 References

- Abbott, N. J. (2002). Astrocyte-endothelial interactions and blood-brain barrier permeability*. *Journal of Anatomy*, 200(6), 629-638. doi:10.1046/j.1469-7580.2002.00064.x
- Alvarez, J. I., Katayama, T., & Prat, A. (2013). Glial influence on the blood brain barrier. *Glia*, 61(12), 1939-1958. doi:10.1002/glia.22575
- Appelt-Menzel, A., Cubukova, A., Günther, K., Edenhofer, F., Piontek, J., Krause, G., ... Metzger, M. (2017). Establishment of a Human Blood-Brain Barrier Co-culture Model Mimicking the Neurovascular Unit Using Induced Pluri- and Multipotent Stem Cells. *Stem Cell Reports*, 8(4), 894-906. doi:10.1016/j.stemcr.2017.02.021
- Argaw, A. T., Asp, L., Zhang, J., Navrazhina, K., Pham, T., Mariani, J. N., ... John, G. R. (2012). Astrocyte-derived VEGF-A drives blood-brain barrier disruption in CNS inflammatory disease. *Journal of Clinical Investigation*, 122(7), 2454-2468. doi:10.1172/jci60842

Armulik, A., Genové, G., & Betsholtz, C. (2011). Pericytes: Developmental, Physiological, and Pathological Perspectives, Problems, and Promises. *Developmental Cell*, 21(2), 193-215. doi:10.1016/j.devcel.2011.07.001

Bai, Y., Zhu, X., Chao, J., Zhang, Y., Qian, C., Li, P., ... Yao, H. (2015). Pericytes Contribute to the Disruption of the Cerebral Endothelial Barrier via Increasing VEGF Expression: Implications for Stroke. *PLOS ONE*, 10(4), e0124362. doi:10.1371/journal.pone.0124362

Blume, L.F., Denker, M., Gieseler, F., Kunze T. (2010). Temperature corrected transepithelial electrical resistance (TEER) measurement to quantify rapid changes in paracellular permeability. *Pharmazie*, 65(1):19-24.

Bonkowski, D., Katyshev, V., Balabanov, R. D., Borisov, A., & Dore-Duffy, P. (2011). The CNS microvascular pericyte: pericyte-astrocyte crosstalk in the regulation of tissue survival. *Fluids and Barriers of the CNS*, 8(1), 8. doi:10.1186/2045-8118-8-8

Booth, R., & Kim, H. (2012). Characterization of a microfluidic in vitro model of the blood-brain barrier (μ BBB). *Lab on a Chip*, 12(10), 1784. doi:10.1039/c2lc40094d

Briske-Anderson, M. J., Finley, J. W., & Newman, S. M. (1997). The Influence of Culture Time and Passage Number on the Morphological and Physiological Development of Caco-2 Cells. *Experimental Biology and Medicine*, 214(3), 248-257. doi:10.3181/00379727-214-44093

Cleaver, O., & Melton, D. A. (2003). Endothelial signaling during development. *Nature Medicine*, 9(6), 661-668. doi:10.1038/nm0603-661

Daniels, B. P., Cruz-Orengo, L., Pasiaka, T. J., Couraud, P., Romero, I. A., Weksler, B., ... Klein, R. S. (2013). Immortalized human cerebral microvascular endothelial cells maintain the properties of primary cells in an in vitro model of immune migration across the blood brain barrier. *Journal of Neuroscience Methods*, 212(1), 173-179. doi:10.1016/j.jneumeth.2012.10.001

Dere, E., & Zlomuzica, A. (2012). The role of gap junctions in the brain in health and disease. *Neurosci Biobehav Rev*. 36(1):206-17. doi: 10.1016/j.neubiorev.2011.05.01

Ferruzza, S. (2013). Serum-reduced and serum-free media for differentiation of Caco-2 cells. *ALTEX*, 30(2), 159-168. doi:10.14573/altex.2013.2.159

FREY, A., MECKELEIN, B., WEILER-GUTTLER, H., MOCKEL, B., FLACH, R., & GASSEN, H. G. (1991). Pericytes of the brain microvasculature express gamma-glutamyl transpeptidase. *European Journal of Biochemistry*, 202(2), 421-429. doi:10.1111/j.1432-1033.1991.tb16391.x

Hatherell, K., Couraud, P., Romero, I. A., Weksler, B., & Pilkington, G. J. (2011). Development of a three-dimensional, all-human in vitro model of the blood-brain barrier using mono-, co-, and tri-cultivation Transwell models. *Journal of Neuroscience Methods*, 199(2), 223-229. doi:10.1016/j.jneumeth.2011.05.012

He, J., Hsueh, H., He, Y., Kastin, A. J., Wang, Y., & Pan, W. (2014). Sleep Restriction Impairs Blood-Brain Barrier Function. *Journal of Neuroscience*, 34(44), 14697-14706. doi:10.1523/jneurosci.2111-14.2014

He, Y., Yao, Y., Tsirka, S. E., & Cao, Y. (2014). Cell-Culture Models of the Blood-Brain Barrier. *Stroke*, 45(8), 2514-2526. doi:10.1161/strokeaha.114.005427

Herland, A., Van der Meer, A. D., FitzGerald, E. A., Park, T., Sleeboom, J. J., & Ingber, D. E. (2016). Distinct Contributions of Astrocytes and Pericytes to Neuroinflammation Identified in a 3D Human Blood-Brain Barrier on a Chip. *PLOS ONE*, 11(3), e0150360. doi:10.1371/journal.pone.0150360

Kloc, M., Kubiak, J. Z., Li, X. C., & Ghobrial, R. M. (2015). Pericytes, Microvascular Dysfunction, and Chronic Rejection. *Transplantation*, 99(4), 658-667. doi:10.1097/tp.0000000000000648

Li, G., Simon, M. J., Cancel, L. M., Shi, Z., Ji, X., Tarbell, J. M., ... Fu, B. M. (2010). Permeability of Endothelial and Astrocyte Cocultures: In Vitro Blood-Brain Barrier Models for Drug Delivery Studies. *Annals of Biomedical Engineering*, 38(8), 2499-2511. doi:10.1007/s10439-010-0023-5

Lim, W., Seo, W., Choe, W., Kang, C., Park, J., Cho, H., ... Kim, H. (2011). Stent Coated With Antibody Against Vascular Endothelial-Cadherin Captures Endothelial Progenitor Cells, Accelerates Re-Endothelialization, and Reduces Neointimal Formation. *Arteriosclerosis, Thrombosis, and Vascular Biology*, 31(12), 2798-2805. doi:10.1161/atvbaha.111.226134

Limmer, S., Weiler, A., Volkenhoff, A., Babatz, F., & KlÄmbt, C. (2014). The Drosophila blood-brain barrier: development and function of a glial endothelium. *Frontiers in Neuroscience*, 8. doi:10.3389/fnins.2014.00365

Matter, K., & Balda, M. S. (2003). Functional analysis of tight junctions. *Methods*, 30(3), 228-234. doi:10.1016/s1046-2023(03)00029-x

McAinsh, J., & Cruickshank, J. M. (1990). Beta-blockers and central nervous system side effects. *Pharmacology & Therapeutics*, 46(2), 163-197. doi:10.1016/0163-7258(90)90092-g

McAllister, M. S., Krizanac-Bengez, L., Macchia, F., Naftalin, R. J., Pedley, K. C., Mayberg, M. R., ... Janigro, D. (2001). Mechanisms of glucose transport at the blood-brain barrier: an in vitro study. *Brain Research*, 904(1), 20-30. doi:10.1016/s0006-8993(01)02418-0

Miah, M. K., Bickel, U., & Mehvar, R. (2017). Effects of hepatic ischemia-reperfusion injury on the blood-brain barrier permeability to [14C] and [13C]sucrose. *Metabolic Brain Disease*, 32(6), 1903-1912. doi:10.1007/s11011-017-0069-2

Minami, T., Ichii, M., & Okazaki, Y. (1996). Detection of Platinum in the Brain of Mice Treated with Cisplatin and Subjected to Short-term Hypoxia. *Journal of Pharmacy and Pharmacology*, 48(5), 505-509. doi:10.1111/j.2042-7158.1996.tb05962.x

- Nitta, T., Hata, M., Gotoh, S., Seo, Y., Sasaki, H., Hashimoto, N., ... Tsukita, S. (2003). Size-selective loosening of the blood-brain barrier in claudin-5-deficient mice. *The Journal of Cell Biology*, 161(3), 653-660. doi:10.1083/jcb.200302070
- Pardridge, W. M. (2005). The blood-brain barrier: Bottleneck in brain drug development. *Neurotherapeutics*, 2(1), 3-14. doi:10.1007/bf03206638
- Prasad, S., Sajja, R. K., Park, J. H., Naik, P., Kaisar, M. A., & Cucullo, L. (2015). Impact of cigarette smoke extract and hyperglycemic conditions on blood-brain barrier endothelial cells. *Fluids and Barriers of the CNS*, 12(1). doi:10.1186/s12987-015-0014-x
- Preston, J. E., Al-Sarraf, H., & Segal, M. B. (1995). Permeability of the developing blood-brain barrier to ¹⁴C-mannitol using the rat in situ brain perfusion technique. *Developmental Brain Research*, 87(1), 69-76. doi:10.1016/0165-3806(95)00060-q
- Shindo, A., Maki, T., Mandeville, E. T., Liang, A. C., Egawa, N., Itoh, K., ... Arai, K. (2016). Astrocyte-Derived Pentraxin 3 Supports Blood-Brain Barrier Integrity Under Acute Phase of Stroke. *Stroke*, 47(4), 1094-1100. doi:10.1161/strokeaha.115.012133
- Sofroniew, M. V., & Vinters, H. V. (2009). Astrocytes: biology and pathology. *Acta Neuropathologica*, 119(1), 7-35. doi:10.1007/s00401-009-0619-8
- Sofroniew, M. V. (2015). Astrocyte barriers to neurotoxic inflammation. *Nature Reviews Neuroscience*, 16(6), 372-372. doi:10.1038/nrn3966
- Soriani, M. (2017). Faculty of 1000 evaluation for Microfluidic blood-brain barrier model provides in vivo-like barrier properties for drug permeability screening. *F1000 - Post-publication peer review of the biomedical literature*. doi:10.3410/f.726494757.793534155
- Sreekanthreddy, P., Gromnicova, R., Davies, H., Phillips, J., Romero, I. A., & Male, D. (2016). A three-dimensional model of the human blood-brain barrier to analyse the transport of nanoparticles and astrocyte/endothelial interactions. *F1000Research*. doi:10.12688/f1000research.7142.2
- Srinivasan, B., Kolli, A. R., Esch, M. B., Abaci, H. E., Shuler, M. L., & Hickman, J. J. (2015). TEER Measurement Techniques for In Vitro Barrier Model Systems. *Journal of Laboratory Automation*, 20(2), 107-126. doi:10.1177/2211068214561025
- Thomsen, L. B., Burkhart, A., & Moos, T. (2015). A Triple Culture Model of the Blood-Brain Barrier Using Porcine Brain Endothelial cells, Astrocytes and Pericytes. *PLOS ONE*, 10(8), e0134765. doi:10.1371/journal.pone.0134765
- Trosko, J. E., Chang, C., Wilson, M. R., Upham, B., Hayashi, T., & Wade, M. (2000). Gap Junctions and the Regulation of Cellular Functions of Stem Cells during Development and Differentiation. *Methods*, 20(2), 245-264. doi:10.1006/meth.1999.0941
- Wang, L., Cao, Y., Tang, Q., & Liang, G. (2013). Role of the blood-brain barrier in rabies virus infection and protection. *Protein & Cell*, 4(12), 901-903. doi:10.1007/s13238-013-3918-8

Wang, Y. I., Abaci, H. E., & Shuler, M. L. (2016). Microfluidic blood-brain barrier model provides in vivo-like barrier properties for drug permeability screening. *Biotechnology and Bioengineering*, 114(1), 184-194. doi:10.1002/bit.26045

Wilson, H. K., Canfield, S. G., Hjortness, M. K., Palecek, S. P., & Shusta, E. V. (2015). Exploring the effects of cell seeding density on the differentiation of human pluripotent stem cells to brain microvascular endothelial cells. *Fluids and Barriers of the CNS*, 12(1). doi:10.1186/s12987-015-0007-9

Wong, A. D., Ye, M., Levy, A. F., Rothstein, J. D., Bergles, D. E., & Searson, P. C. (2013). The blood-brain barrier: an engineering perspective. *Frontiers in Neuroengineering*, 6. doi:10.3389/fneng.2013.00007

Ye, D., Dawson, K. A., & Lynch, I. (2015). A TEM protocol for quality assurance of in vitro cellular barrier models and its application to the assessment of nanoparticle transport mechanisms across barriers. *The Analyst*, 140(1), 83-97. doi:10.1039/c4an01276c

Youdim, K. A., Avdeef, A., & Abbott, N. (2003). In vitro trans-monolayer permeability calculations: often forgotten assumptions. *Drug Discovery Today*, 8(21), 997-1003. doi:10.1016/s1359-6446(03)02873-3

Zlokovic, B. V. (2008). The Blood-Brain Barrier in Health and Chronic Neurodegenerative Disorders. *Neuron*, 57(2), 178-201. doi:10.1016/j.neuron.2008.01.003

CHAPTER 3. ANALYSIS OF THE MULTILAYERED CONFIGURATION OF THE TRICULTURE MODEL OF A HUMAN BLOOD-BRAIN BARRIER

3.1 Summary

Background and objective: Current *in vitro* methods for mimicking the Blood-Brain Barrier (BBB) are often not physiologically representative of the *in vivo* neurovascular unit; thus, they do not allow optimal interactions between principle cellular components (astrocytes, pericytes, and the brain microvessel endothelium) that are layered *in vivo*. Conventional models do not enable physical contacts and proximal association between the BBB endothelium, pericytes and astrocytes, which combined play a synergistic role in the regulation of the restrictive barrier properties. The objective of this study was to examine the cellular configuration of a directly layered triculture model of the human BBB and make a comparison to the cellular configuration from a reference TEM micrograph of a human BBB as presented in the literature.

Methods: The overlay of cell layers, as described in Chapter 2, was examined using a phase contrast microscope during different stages of preparation of a triculture by imaging cellular morphology of the first seeded layer corresponding to astrocytes, then the second layer of pericytes, and finally the third seeded layer of hCMEC/D3 cells. Cross-sectional features of the BBB cell layers were examined using a Transmission Electron Microscopy (TEM) and were compared to the reference cross-sectional images of a human glial BBB unit. Lastly, the formation of distinct optical sections in the triculture was examined using a confocal microscope.

Results: There was an overlay of distinct cell layers in the course of seeding the triculture. The first layer showed characteristic features corresponding to the astrocytes, the second layer showed mixed features corresponding to pericytes and astrocytes, the third layer showed features corresponding to the hCMEC/D3 cells. Cross-sectional TEM micrographs of the triculture showed localization of the hCMEC/D3 cells at the top layer, a mix of pericytes and astrocytes in the middle layer, and a distinct localization of astrocytes at the bottom layer. A Z-scan using confocal microscopy revealed the existence of two distinct optical sections in the triculture model; the first optical sections showed features of hCMEC/D3 cells, and the second showed mixed features of astrocytes and pericytes.

Conclusion: The present triculture model of the BBB contains three layers of cells. The first top layer consisted of the hCMEC/D3 cells, the second layer showed a mix of astrocytes and pericytes, and the base-layer corresponded to the astrocytes.

Keywords: Blood-Brain Barrier, Phase-Contrast Microscopy, Bright-Field Transmission Electron Microscopy, Confocal Fluorescence Microscopy, Optical Sectioning

3.2 Introduction

The Blood-Brain Barrier (BBB) refers to a set of mechanisms used by the brain endothelial capillaries and the surrounding glial barrier (i.e., mainly the astrocytes) to regulate the exchange of molecules from capillary lumen to the brain parenchyma and vice versa [Hawkins and Davis, 2005; Banerjee and Bhat, 2007]. Pericytes form direct connections with the BBB endothelium while astrocytes mostly form proximal associations with the BBB endothelium [Banerjee and Bhat, 2007]. Both pericytes and astrocytes have an influence on the expression and function of tight junctions at the BBB endothelium [Daneman et al., 2010; Cabezas et al., 2014]. Furthermore, direct connections and channels formed between pericytes and BBB endothelium facilitate a bidirectional transfer of ions and small molecules from the BBB endothelium into pericytes, thereby mediating a selective exchange between BBB endothelia and pericytes or astrocytes [Larson et al., 1987; Winkler et al., 2011]. Such exchanges suggest that small drug molecules or drug delivery systems may also be selectively exchanged from BBB endothelia into pericytes and astrocytes before reaching brain parenchyma. The BBB endothelium is almost completely covered by a layer of astrocytes that wrap pericytes around the endothelial capillary [Hawkins et al., 2006; Herland et al., 2016]. This complex configuration may be responsible for the formation of a highly selective barrier to the permeation of novel CNS drugs/drug delivery systems into the brain parenchyma.

In vitro cell culture models of the BBB system are often used in studies related to the permeation properties of drug molecules across the human BBB [Naik et al., 2012; The International Transporter Consortium, 2010]. In conventional methods, BMECs are cultured on *Transwell*TM support or a lab-chip to form a monoculture that represents only the endothelium portion of the BBB, while the important direct physical arrangements and connections that exist between the BBB endothelia and the BBB astrocytes or pericytes are omitted or not fully

optimized. The astrocytes and pericytes cultured on the basolateral surface are largely separated from the endothelial cells by a thick filter support that limit physical association between all the three types of BBB cells, i.e., BMECs, astrocytes and pericytes [Hatherell et al., 2011; Brown et al., 2015]. Thus, a novel method involving direct seeding of all the principal cellular components of the BBB system on the same side of a filter support would be more physiologically representative of the *in vivo*-BBB. However, a challenging task would be in establishing if a direct overlay of all the principal BBB cells would result in a multicellular configuration similar to that of the glial-vascular unit at the BBB *in vivo*.

One of the goals in the present study was to analyze the spatial arrangement of layers corresponding to the different types of the BBB cells overlaid *in vitro* in order to mimic the BBB in a more representative configuration that would allow for free interactions between astrocytes, pericytes and the hCMEC/D3 cells. To achieve this goal, cross-sectional TEM micrographs of a direct contact, layered triculture model of the BBB were compared to a reference micrograph of a human BBB as published in the literature. Note that there is a limited number of TEM micrographs for the human BBB in the literature. In most cases, cross-sectional TEM micrographs correspond to a rat BBB. Since the study described in this chapter used only human-BBB cells, it was rational to rely on a TEM micrograph obtained from a human BBB rather than that of the rat.

There are notable differences between a human BBB specimen and a rat-BBB specimen. The TEM micrographs of a rat BBB (Figure 3.1) shows a layer of small transparent pericytes surrounding a relatively larger capillary-endothelium [Farkas et al., 2001]. In the same micrograph, circumferential, fairly transparent astrocytes are observed covering pericytes and the endothelium capillary completely forming a supporting layer for the capillary to form within. Astrocytes are separated from pericytes and the endothelium by a thin extracellular space [Farkas et al., 2001]. On the contrary, a close look at a reference TEM micrograph of a human BBB (Figure 3.2) shows pericytes that have similar size and morphology to adjacent BBB endothelium [Garbuzova-Davis, 2012].

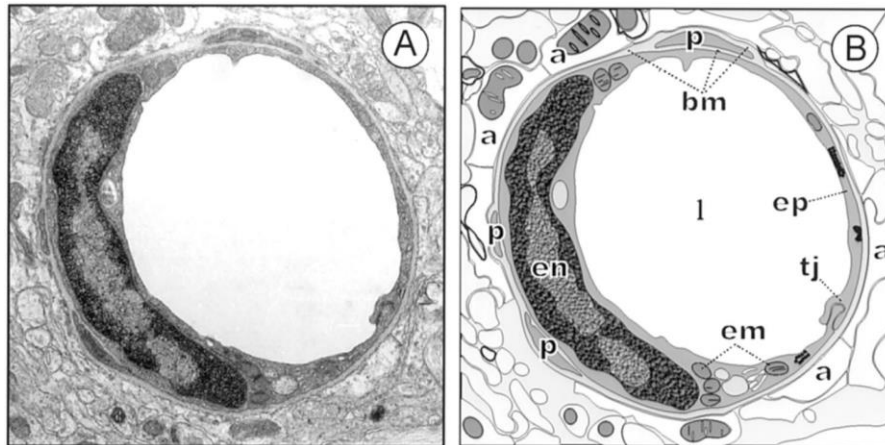


Figure 3.1. A reference TEM micrograph of a Blood-Brain Barrier specimen from the rat. Panel A represents the actual micrograph and Panel B is a pictorial representation of the micrograph in panel A. The cross-sectional BBB micrograph of a rat, as presented in the micrograph, consists of a single endothelium that forms a lumen of the blood capillary. The BBB endothelium locks its peripheral ends by forming tight-junctions. The BBB endothelium shows prominent cell organelles in the cytoplasm including mitochondria, vacuoles, nucleus, and the nucleolus. Numerous regions of the capillary lumen seem to be budding off the endothelial surface. Pericytes that surround the BBB capillary seem to be relatively smaller than endothelium. The surrounding astrocytes are more transparent to the beam of electrons, and they have a heterogeneous morphology that lack prominent nuclei and other cell organelles [Farkas et al., 2001, image reproduced with permission from Elsevier]

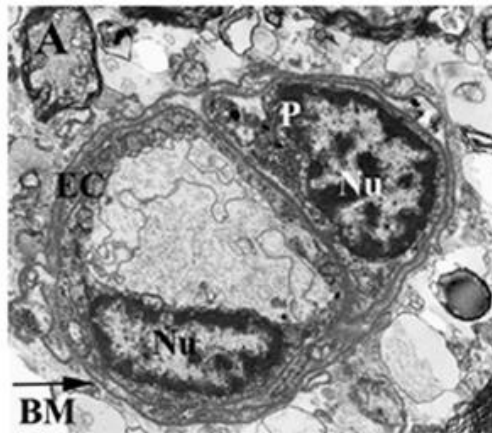


Figure 3.2. A cross-sectional TEM micrograph of a human BBB. The BBB capillary is associated with a single pericyte. The BBB endothelium forms cytoplasmic extensions that loop to form a capillary lumen stabilized by tight junctions. Pericytes do not form a lumen nor tight junctions similar in a similar way to the BBB endothelium [Garbuzova-Davis et al., 2012, image reproduced with permission from Elsevier].

Thus, a distinction between a human BBB pericyte from a human BBB endothelium may not be achieved in the TEM micrographs of a human BBB triculture model, where pericytes and endothelial cells could be highly similar in size and morphology.

In cases where the distinction between pericytes and endothelium is not so apparent, one may rely on the examination of additional ultrastructural features such as the type of cell-cell junctions between adjacent endothelial cells or differences in the size or structure of select internal cell organelles. For example, a layer of endothelial cells at the top section of a triculture model would be stabilized by tight junctions formed when two adjacent endothelial cells form contacts while similar cell-cell connections/associations would not be consistently observed between pericytes or astrocytes in adjacent positions. The middle layer composed of pericytes would be less stable, and more disordered in space in comparison to the endothelial layer due to lack of stabilizing tight junctions between two adjacent pericytes.

On the contrary, astrocytes would be stabilized on the surface of a filter support by the poly-L-lysine coating that was applied a few hours prior to seeding on the *Transwell*TM filter support. In addition, astrocytes would have a distinct morphology from pericytes and endothelial cells, and therefore would be more easily distinguished from the other cells in the triculture model. A close

examination of a thin cross-sectional specimen from the BBB triculture would reveal characteristic features corresponding to each cell type in the multilayered triculture.

As noted earlier, the distinction between BBB endothelium and the pericytes may be difficult to achieve just based on size or morphological features. In that case, an alternative approach involving fluorescence imaging may be used to establish a difference in the fluorescence properties of pericytes and endothelial cells in a triculture setting. Briefly, the cytoskeleton of each cell type (the hCMEC/D3, pericyte, and astrocyte) would be labeled fluorescently with rhodamine-phalloidin (a fluorescent dye for mapping the F-actin distribution inside a cell) and the triculture would be imaged in a confocal microscope to see if distinct cell features would be visible at discrete optical sections. If each cell layer fluoresces differently, then a confocal microscope would reveal a triculture configuration in which astrocytes form the first layer, pericytes the second and hCMEC/D3 cells the third, in a Z-stacking mode.

3.3 Hypothesis

The triculture model of the BBB shows characteristic features for the hCMEC/D3 cells in the top layer, for pericytes in the middle layer, and for astrocytes in the basal layer to mimic the cellular configuration of the human glial-vascular unit/the BBB.

3.4 Cell specific features

3.4.1 Cell specific morphologies

If there were a difference in the cell morphologies of astrocytes and pericytes or the hCMEC/D3 cells, then, a layer of hCMEC/D3 cells would reveal an arrangement of cells and morphologies that would be distinct from that of pericytes or the astrocytes. However, as mentioned before, pericytes seeded in an in vivo-like environment may exhibit a morphology like that of a BBB endothelium. In this study, the formation of distinct cell layers would be monitored by a phase contrast microscope during preparation of a BBB triculture model, in a LabTek II chamber slide. A further distinction between astrocytes, pericytes and the hCMEC/D3 layers would be achieved by using TEM micrographs of thin cross-sections prepared from the triculture specimen. TEM micrographs of cross-sectional thin specimen developed from monocultures of

astrocytes, pericytes and the hCMEC/D3 cells would be used as control TEM micrographs to identify the relative positions of each type in the triculture model.

3.4.2 Cell-cell junctions

There are distinct types of cell-cell junctions that would form in each cell-layer of the BBB triculture model. The top layer of hCMEC/D3 was expected to form a continuous arrangement of cells with tight junctions that stabilize the endothelial layer spreading on a basement of astrocytes or pericytes. The formation of tight cell-cell junctions would not form among pericytes in the middle section. However, the occasional formation of peg/socket junctions between pericytes and the hCMEC/D3 cells was expected since such junctions form between BBB-endothelia and BBB-pericytes *in vivo*.

While extensive cell-cell connections between astrocytes and the BBB endothelium are not common, it is currently established that astrocytes form extensive gap junctions between themselves in order to propagate chemical signals between neurons and perhaps the BBB endothelium [Anders et al., 2014; Chen et al., 2016]. The formation of such gap-junctions among the BBB astrocytes may cause astrocytes to act as a secondary barrier that supports the protective endothelial part of the BBB system, especially under conditions such as stroke where the endothelial BBB is compromised [Kassner and Merali, 2015].

3.4.3 Internal cell organelles

It was expected that different types of cells that make up the BBB system would manifest differences in size and distribution of their internal organelles (see **Figure 3.3** for details on the structure of cell organelles). The hCMEC/D3 cells were expected to contain characteristic Vesiculo-Vacuolar Organelles (VVOs) that are responsible for trafficking macromolecules across most endothelial barriers [Dvorak et al., 2000]. Unlike the hCMEC/D3 cells, pericytes were not expected to show extensive VVOs. Instead, pericytes were expected to show a swollen nucleus that occupies much of the cytoplasm [Hurtado-Alvarado et al., 2014]. In addition, pericytes would show a characteristic larger nucleolus in comparison to the relative nucleolus in the hCMEC/D3 cells. Additional differences in the size, morphology and distribution of internal cell organelles between pericytes and hCMEC/D3 cells could be established from their monoculture TEM micrographs and used where possible to distinguish the two cell types in a triculture setting.

Cell organelles in the astrocytes are small and sparsely distributed in the cytoplasm; thus, astrocytes are relatively more transparent to the incident beams of light or electrons when imaged under light or electron microscopes [Garcia-Cabezas et al. 2016; Hayakawa et al., 2016]. An alternative visualization for the size and distribution of internal cell organelles, either in the monoculture controls or the triculture, would involve fluorescence imaging. Fluorescent labelling of the F-actin in each cell type would reveal cytoskeletal structures, where differences in the pattern of F-actin expression for each cell type would be used to establish the localization of each cell type in the optical sections of a triculture specimen.

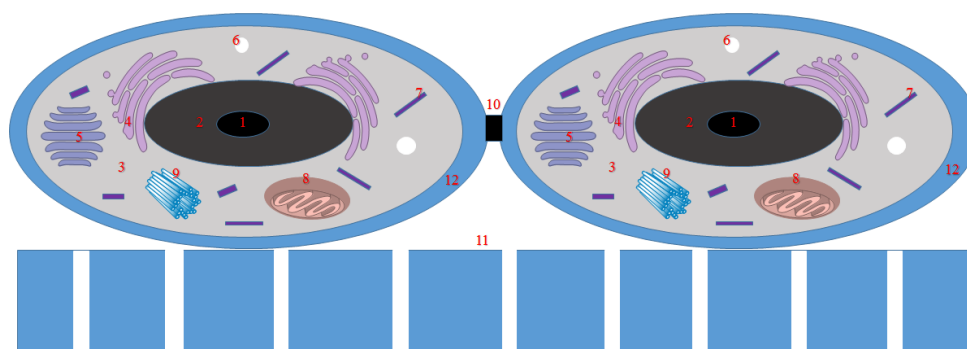


Figure 3.3. A schematic representation for the cross-sectional features of a typical human cell grown on a filter membrane: (1) Nucleolus, (2) Nucleus, (3) Cytosol, (4) Endoplasmic reticulum, (5) Golgi body, (6) Vacuole, (7) Microfilament, (8) Mitochondrion, (9) Microtubules (10) Junctional complex, (11) Filter-support (12) Cell membrane. Sizes and distributions of the cell organelles can vary across different types of cells depending on their functions or environment.

3.5 Materials and imaging techniques

3.5.1 Materials

Astrocytes, pericytes, the hCMEC/D3 cells, *Transwell*TM chambers, poly-L-lysine, collagen, trypsin, PBS, astrocyte growth media, pericytes growth media, P/S solution, Astrocyte growth supplement AGS, pericyte growth supplement PGS, EBM-2 media and supplements, LabTek II slide chambers, 4% paraformaldehyde, acetone, rhodamine phalloidin, bovine serum albumin BSA, and Fetal Bovine Serum FBS, Sorens phosphate buffer, glutaraldehyde, osmium tetroxide, ethanol, epoxy solution, toluidine blue dye-solution, uranyl acetate and lead citrate solutions.

3.5.2 Imaging techniques

3.5.2.1 A brief description of phase contrast microscopy

When a beam of light is focused on a cell, a portion of it follows an unaltered path through the cell, while a different portion of it is absorbed and diffracted by the cell organelles. Intensity of the light following an unaltered path through the cell is slightly higher than that of the light absorbed and diffracted by the cell organelles. A phase contrast microscope is utilized to modify the phase amplitudes of light transmitted through the cell, thereby generating contrast images that have bright and dark regions. The observed brightness would be inversely proportional to the cell density in the light path. Highly dense regions inside the cell, such intracellular region, would appear darker than the peripheral regions that are mainly composed of lipid membranes [Zernike, 1955].

Therefore, phase contrast microscopy was utilized as a density mapping technique in which cell morphologies in confluent or near confluent monocultures could be revealed. Phase contrast micrographs taken from monocultures of astrocytes, pericytes and the hCMEC/D3 cells were compared to the micrographs obtained from the triculture containing layers of all the three types of the BBB cells. A phase contrast micrograph of the triculture specimen was expected to show a highly contrasted optical section corresponding to the confluent layer of hCMEC/D3 cells. The control monoculture of hCMEC/D3 cells would show a cobble stone arrangement similar to the one obtained for the hCMEC/D3 layer in the triculture model of the BBB.

3.5.2.2 Application of phase contrast during preparation of a BBB triculture

Surface morphologies corresponding to each cell-layer formed in the course of preparing a triculture model of the BBB, were detected with a Nikon TiS phase contrast microscope. In the first step, astrocytes were seeded on the surface of a LabTek II slide at a density of 4×10^4 cells/cm². The astrocyte culture was maintained in a sterile incubator (set at 5% CO₂ and 37°C) for 48 hrs. At the end of 48hrs, the culture was rinsed three times with PBS and fixed using 4% formaldehyde in PBS solution for 15 minutes. The culture was washed three times with PBS again to remove the fixative. Phase contrast images of this astrocytes monoculture were collected with a Nikon TiS microscope.

In the second step, pericytes were seeded at 4×10^4 cells/cm² directly on top of pre-cultured astrocytes (at the end of 48hrs) as described in step 1. The resulting coculture was fixed with 4% formaldehyde at the end of 48hrs and imaged under Nikon TiS. In the third step, the hCMEC/D3 cells were seeded (at 8×10^4 cells/cm²) directly on a coculture lawn of the astrocytes and pericytes that was prepared as explained in step 2. The resulting triculture was fixed in 4% formaldehyde on day 7 after seeding hCMEC/D3 cells. The triculture was imaged under Nikon TiS microscope.

3.5.2.3 A brief description of transmission electron microscopy (TEM)

Thin sections of cell-cultures can be imaged in TEM to examine morphological and ultra-structural characteristics of cells [Winey et al., 2014]. Briefly, an incident beam of electrons is focused on a thin cross-sectional specimen of a cell culture, and the scattered electrons are refocused on a detector positioned in the first image focal plane. To visualize various internal features of cells under analysis, a fixed cell-culture specimen is stained with various contrasting agents to allow for a contrasted visualization of specific cell organelles such as nucleus, mitochondria, vacuoles, ribosomes, etc. The stained specimen is embedded in a polymer resin, followed by cutting thin cross-sections that can be mounted on a TEM grid for imaging.

3.5.2.4 Application of TEM in imaging the BBB triculture

Three types of cells that form the BBB system (i.e., astrocytes, pericytes and the hCMEC/D3 cells) were cultured on *Transwell*TM chambers at the seeding densities described in Chapter 2. Briefly, monocultures of the hCMEC/D3 cells (8×10^4 cells/cm²) for seven days, pericytes (4×10^4 cells/cm²) for two days, and astrocytes (4×10^4 cells/cm²) for two days to provide control TEM micrographs for the analysis of cell arrangement in the triculture specimen. For the triculture on a *Transwell*TM chamber, astrocytes were cultured first at a seeding density of (4×10^4 cells/cm²) for two days, followed by pericytes at a density of (4×10^4 cells/cm²) for two additional days, and then by hCMEC/D3 cells at (8×10^4 cells/cm²) for 6 days prior to electron microscopy fixation. All cell-culture samples were fixed with 2.5% glutaraldehyde solution for at least 1 hour. Sorensen phosphate buffer was used to wash the cells three times to remove glutaraldehyde.

A buffer solution containing 1% osmium tetroxide was applied into the samples for 1hr to allow for high contrast images. Sorensen phosphate buffer was used to rinse off excess OsO₄. Samples were then dehydrated with a grades series of ethanol (see publication by Ye et al., 2014

for a detailed protocol). Following dehydration, a solution mixture of epoxy resin and ethanol (1:1, V/V) was added to the apical and basolateral chambers of the *Transwell*TM for 1 hour, using 0.5mL and 1.5mL respectively. At the end of 1 hour, a 100% epoxy solution was added to the prepared specimens followed by incubation at 37°C to ensure a complete evaporation of ethanol. Cell cultures in *Transwell*TM chambers containing the resin solution were then placed in an oven at 65°C for a period of 24 hours to allow for resin polymerization and embedment to take place. At the end of 24 hours, the cell cultures embedded in epoxy resin were used to obtain thin cross-sectional specimen for the TEM analysis.

Briefly, thin cross-sections of the cell culture specimens were prepared using a microtome as described in the methods by Ye et al., 2015. Copper grids of 3.05 mm and 200 square mesh were used for mounting TEM sections. Some of the microtomic sections were stained with toluidine blue and analyzed under a light microscope. Copper grids for TEM-specimen were further stained with 2% uranyl acetate, first for 20 minutes, followed by additional staining with 0.4% lead citrate for an additional 1 hour. TEM images were then acquired using a FEI Tecnai G² T20 electron microscope equipped with a LaB₆ source of electron beam, operating at 100 kV.

3.5.3 A brief description of the fluorescence microscopy

Optical sections of a fluorescent tissues or cell cultures can be visualized using a confocal microscope [Conchello et al., 2005]. The approach allows one to look at different sections of a tissue culture along the Z axis without carrying out actual/physical sectioning. Briefly, specific proteins/protein filaments are stained with a fluorescent antibody which can be excited with a laser light to give visible fluorescent emissions that are detectable with a CCD camera in a confocal microscope. Therefore, cell specific arrangement of proteins or protein filaments may be visualized in a confocal microscope. In this study, the structure and arrangement of the F-actin protein was expected to be different in each of the cell type used in the development of a BBB multicellular model consisting of astrocytes, pericytes, and the hCMEC/D3 cells. The F-actin, a cytoskeleton protein, was stained with rhodamine phalloidin, a commonly used fluorescent dye for visualizing the skeletal structure of cells.

First, the F-actin arrangement in the monocultures of astrocytes, pericytes and the hCMEC/D3 cells would be analyzed and used as controls in the optical sectioning of a multicellular culture containing a superimposed layer of hCMEC/D3 cells (at the top) on the basal

layers of pericytes followed by astrocytes. It was expected that the multicellular culture would show optical sections corresponding to the astrocytes, pericytes and the hCMEC/D3 layers at distinct focal regions. A detailed description of this analysis is described in the proceeding subsection.

3.5.3.1 Application of confocal microscopy in visualizing optical sections of a BBB triculture

Monocultures of hCMEC/D3 cells, pericytes and astrocytes were cultivated in the LabTek slide chambers at a density of 4×10^4 cells/cm² for two days. A triculture of hCMEC/D3 with pericytes and astrocytes was seeded using a density ratio of (4×10^4 **A**: 4×10^4 **P**: 8×10^4 **H**) cells/cm² where **A** stands for the astrocytes, **P** for the pericytes and **H** for the hCMEC/D3 cells. Briefly, astrocytes were seeded for 48 hours; then pericytes were seeded on top of the astrocytes for another period of 48 hours; and hCMEC/D3 cells were then overlaid on the coculture of astrocytes and pericytes for a period of six days. Both mono- and tri-cultures were fixed with 4% formaldehyde. All the cultures (mono- and tri-cultures) were then washed three times with PBS, followed by permeabilization with cold acetone at -20°C for 2 minutes on ice. The cell culture samples were then washed and rinsed with cold PBS at least three times, followed by air-drying at room temperature.

Dried specimens were incubated with 200mL of diluted rhodamine phalloidin solution (150nM). Specimens were wrapped in aluminum foil for a period of 30 minutes at room temperature. Excess rhodamine phalloidin was then washed off three times with PBS. These specimens were dried again in air and wrapped in aluminum foil to reduce exposure to external light. Visualization of the F-actin was achieved by fluorescence excitation at a wavelength of 550nm, and emission detection at a wavelength of 580nm using a confocal microscope (Nikon Eclipse TE200).

3.6 Results

i) Phase contrast images of the cell layers during preparation of a BBB triculture:

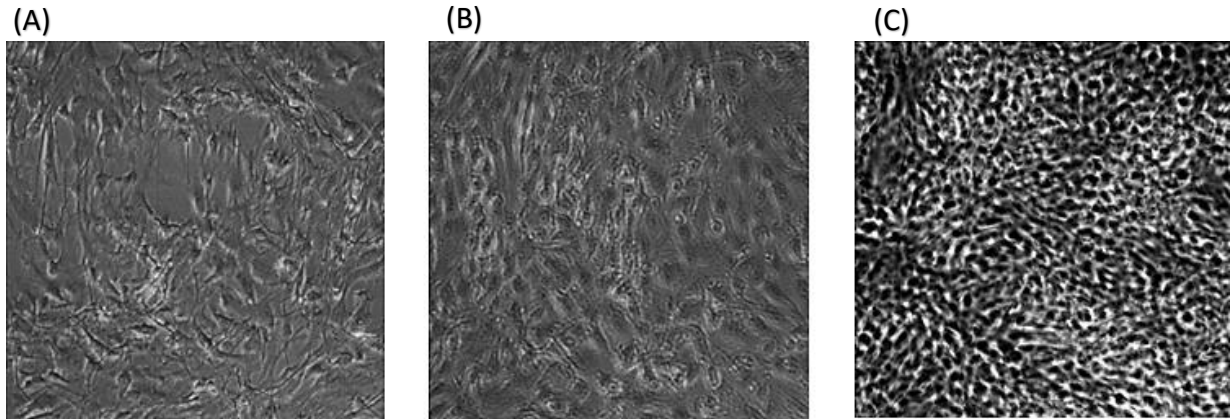


Figure 3.4. Formation of distinct cell-layers during BBB triculture preparation. **(A)** Sub-confluent layer of astrocytes formed after two days (48 hours) shows cells with a characteristic morphology for the astrocytes. **(B)** A sub-confluent layer of pericytes laid over the astrocytes layer at the end of two days (48hrs) post-seeding. **(C)** A confluent-layer of hCMEC/D3 cells laid over the underneath coculture of astrocytes and pericytes (prepared as described in panels **A** and **B**) at the end of six days post-seeding.

ii) TEM micrographs showing ultrastructural features in a monoculture of hCMEC/D3 cells:

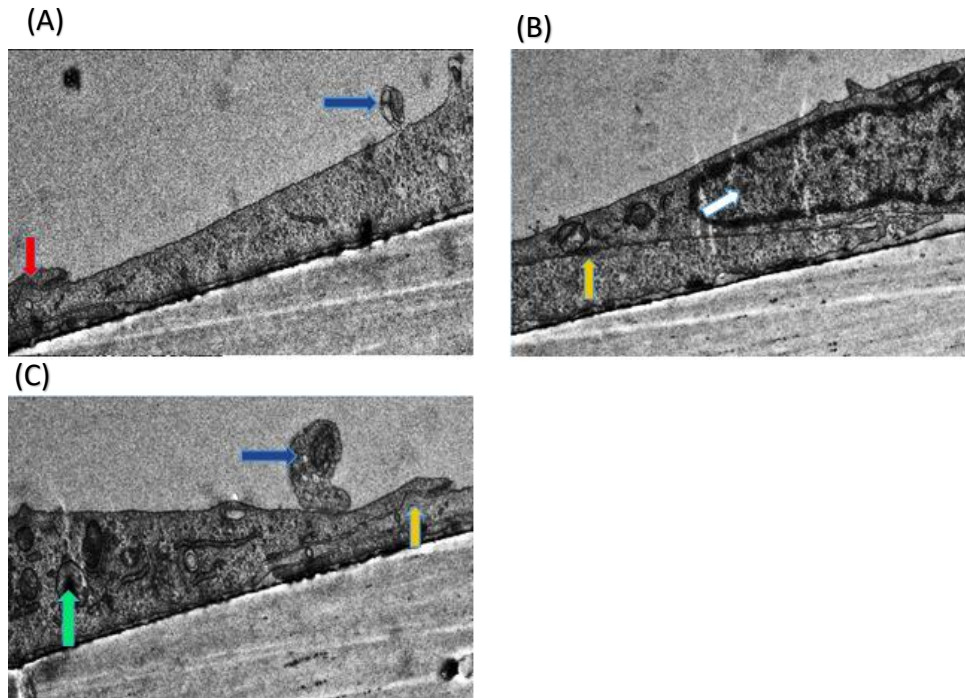


Figure 3.5. Ultrastructural features in the monoculture of hCMEC/D3 cells. **Panel A** shows tight junctions formed between two adjacent hCMEC/D3 cells (**red arrow**) and an exosome budding off the hCMEC/D3 cell (**blue arrow**). **Panel B** shows an overlapping cell-cell junction forming a minute contact points (**orange arrow**) and a larger nucleus occupying most of the cytoplasmic space (**white arrow**). **Panel C** shows the formation of numerous vacuoles (**green arrow**), a large exosome (**blue arrow**) and a fusing cell-cell junction (**orange arrow**).

iv) TEM micrographs showing ultrastructural features in the monoculture of pericytes:

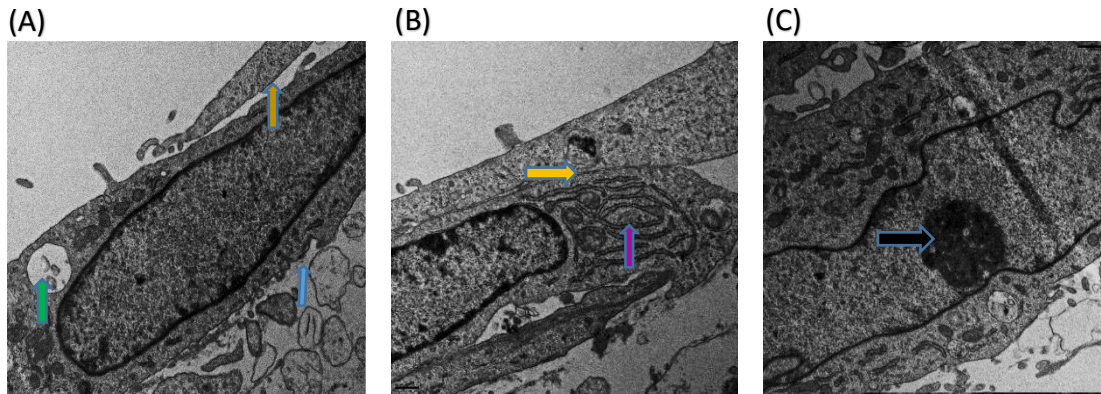


Figure 3.6. Ultrastructural features in the monoculture of pericytes. **Panel A** shows wide cell-cell junctions between two adjacent pericytes (**orange arrow**), and a highly transparent vesicle containing granular materials in its lumen (**green arrow**). **Panel B** shows an overlapping cell-cell junction between two adjacent pericytes (**orange arrow**), a prominent rough endoplasmic reticulum (**red-pink arrow**) and highly transparent exosomes (**blue arrow**). **Panel C** shows a prominent nucleolus structure at the center of a pericyte nucleus (**dark blue arrow**).

v) Ultrastructural features in the monoculture of astrocytes:

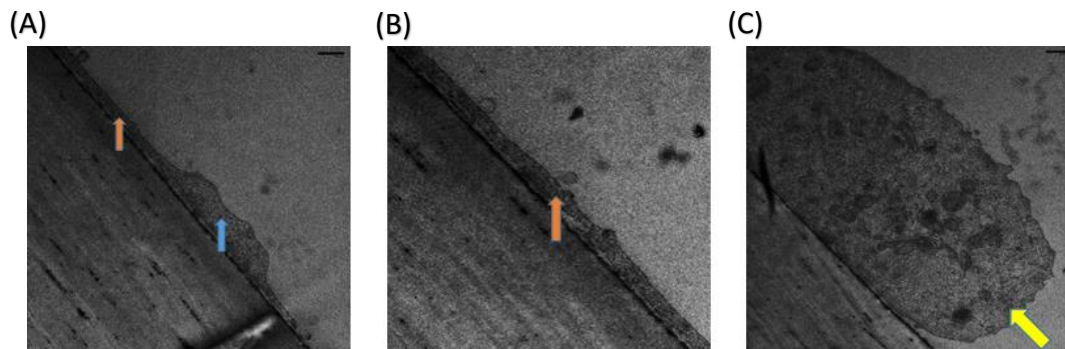


Figure 3.7. Ultrastructural features in the monoculture of astrocytes. **Panel A** shows a stellate projection from the body center of an astrocyte (**orange arrow**) and a swollen body center (**blue arrow**). **Panel B** shows an elongated projection from the body-center of an astrocyte. **Panel C** shows a swollen end-section of an astrocyte (**green-yellow arrow**)

vii) Ultrastructural features in the triculture model of the BBB, Part I:

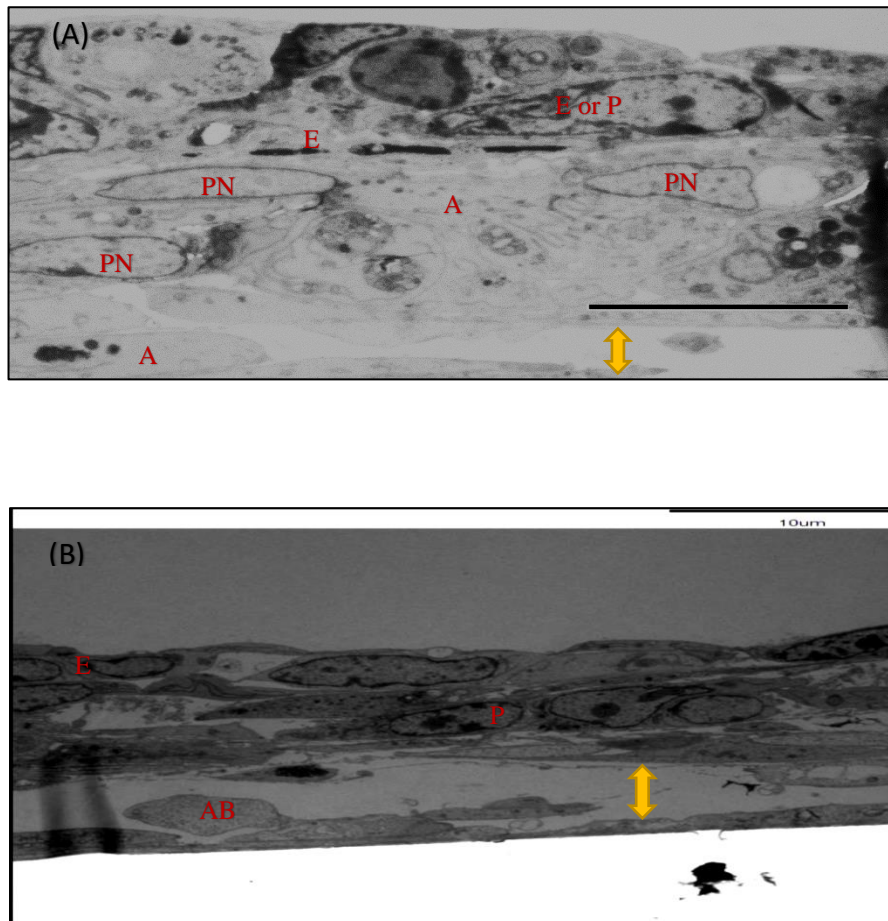


Figure 3.8. Cross-sectional arrangement of cells in the triculture model, part I. **Panel A** shows a multicellular structure composed of closely associated cells at the top layer, which could be endothelial (**E**), or pericytes (**P**). The middle section in **Panel A** contains dispersed cells containing a prominent nucleus (**PN**); these could be disordered pericytes separated by a swollen astrocyte (**A**) between them. The bottom layer in **panel A** consists of cells lacking a prominent nucleus, or formation of vesicles; these could be astrocytes with sharp stellate ends. **Panel B** shows a well-contrasted micrograph of the triculture model. Note that the top layer of cells formed a continuous thin membrane; this is a property of BMECs/BBB endothelium. Also note that though certain cells in the middle section resemble endothelial cells at the top, they do not form a continuous wall; this is a property of pericytes (there is also a large nucleolus in the cells assigned as pericytes). There is a large extracellular space denoted by a **double-headed yellow arrow** in the micrographs. This space could be due to the formation of excess extracellular matrix.

ix) Ultrastructural features in the triculture model of the BBB, Part II:

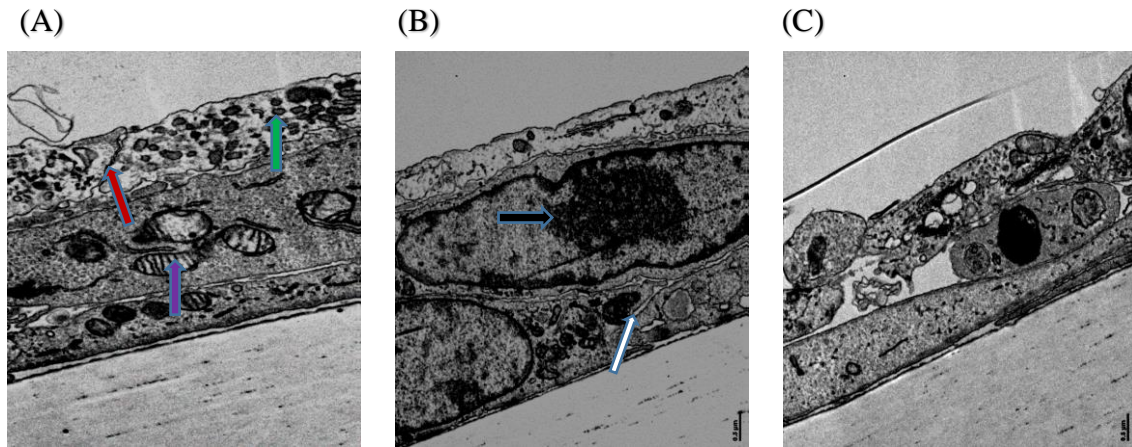


Figure 3.9. Cross-sectional arrangement of the BBB cells in the triculture model, part II. Panel (A) shows junctional contacts between two endothelial cells (**red arrow**), and a high population of vacuoles (**green**) in the two adjacent endothelial cells. The middle and basal layers in panel (A) show prominent mitochondria characteristic of astrocytes at the BBB in vivo (**maroon arrow**). Panel (B) shows middle and basal layers containing cells with prominently large nucleus and nucleolus (**dark blue arrow**). Cells in the basal layer of panel (B) formed widened cell-cell junctions (**white arrow**). Panel (C) shows cells that form a continuous cell layer (characteristic of BMECs, see **red arrow**) at the top layer, a cell in the middle layer that lacks connections with adjacent cells (a characteristic of pericytes) and a basal layer of cells that have long sharp projections, lacking prominent vesicles (a characteristic of astrocytes)

x) The expression pattern of F-actin filaments in the cellular components of the BBB (astrocytes, pericytes and the hCMEC/D3):

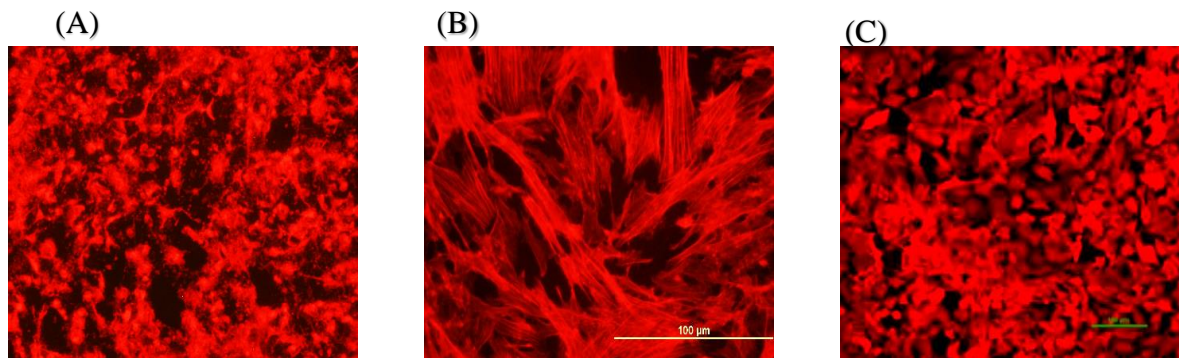


Figure 3.10. Fluorescent patterns of F-actin in the cytoskeletons of astrocytes (**Panel A**), pericytes (**Panel B**) and the hCMEC/D3 cells (**Panel C**). The fluorescence pattern in the astrocytes is more diffuse in a pattern that shows a stellate morphology (**Panel A**). The fluorescence pattern in the pericytes showed a discrete arrangement of the F-actin bundles (**Panel B**). The hCMEC/D3 cells showed a more diffuse fluorescent pattern reflecting their spindle-shaped morphology (**Panel C**)

xi) The expression pattern of F-actin filaments in the assembled triculture

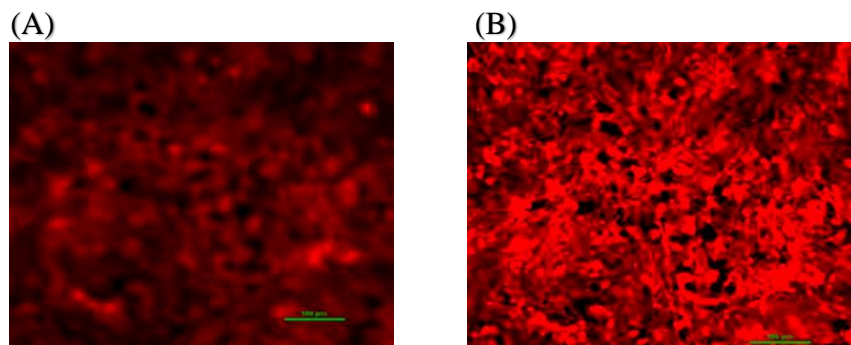


Figure 3.11. Fluorescent optical sections in the BBB triculture. **Panel A** shows a faint optical section showing the expression pattern of F-actin in the hCMEC/D3 section. **Panel B** shows a clearer optical section showing mixed features of astrocytes and hCMEC/D3 cells, all projected in the same plane

3.7 Discussion

In vitro methods for mimicking the BBB physiology are needed in programs related to CNS drug discovery and development [Jeffrey et al., 2010; Aday et al., 2016; Toth et al., 2017]. Many (if not all) conventional *in vitro* static methods lack a direct overlay of the BBB endothelium over astrocytes and pericytes to achieve a physiologically representative configuration. Here we characterize a novel method used to mimic the BBB by culturing a layer of hCMEC/D3 cells directly on a layered coculture composed of pericytes and astrocytes. Various microscopic techniques were utilized in the visualization of cell morphologies, arrangements, internal characteristics, and subsequently, the cross-sectional arrangement of cells in the triculture model of the BBB. The aim of this study was to compare the physical characteristics in the triculture model and those of a BBB specimen obtained in a literature source.

3.7.1 Cell morphologies and arrangements during preparation of a triculture model of the BBB

Three distinct cell morphologies were expected in the course of preparing a triculture composed of a layer of astrocytes in the base, pericytes in the middle and the hCMEC/D3 cells at the top. A sub-confluent layer of astrocytes formed at the end of 48 hours after seeding at 4×10^4 cells/cm² on a LabTek II chamber slide. The astrocytes layer stayed in a sub-confluent state even after culturing for 7 days. Astrocytes had a stellar morphology with long slender terminal projections (see **Figure 3.4-A**). Similar morphologies and growth patterns in the astrocytes monocultures have been reported in other literature reports [Zaheer et al., 2002; Velandia-Romero, 2016]. Pericytes seeded at 4×10^4 cells/cm² directly on the culture of astrocytes, formed a layer of cells that covered the astrocytes culture to form a new distinct layer (see **Figure 3.4-B**). The new layer of pericytes did not show visible foot processes. Instead, pericytes in the new layer were more round with enlarged regions corresponding to the characteristic prominent nuclei of pericytes. In addition, the pattern of the enlarged cells were arranged sparsely in the layer.

The observation of enlarged parts in certain areas of the pericytes layer is consistent with previously published reports on the morphology of pericytes, where a large nucleus occupies much of the cytoplasmic space to show a round “swollen” center [Nakano et al., 2000; Shi et al., 2008; Armulik et al., 2011]. When the hCMEC/D3 cells were plated directly onto the new pericytes layer, at 8×10^4 cells/cm², they formed a distinct layer showing highly contrasted bright and dark

regions at the end of 6 days (see **Figure 3.4-C**). The hCMEC/D3 layer formed in the resulting triculture with characteristics of the confluent endothelial monocultures as reported in numerous publications [Jinga et al., 2000; Lucq et al., 2000]. Cells in a confluent layer of hCMEC/D3 cells in the triculture showed characteristic convex polygonal morphologies associated with epithelial/endothelial cells. Note that several focal regions were observed while imaging the triculture in phase contrast microscopy as well. Each focal region revealed features of either the astrocytes, pericytes or the hCMEC/D3 cells. Thus, the formation of a triculture model of the BBB may be monitored by a phase contrast microscope in a routine application of the method.

3.7.2 Analysis of cell-cell junctions and cell organelles

i) Control 1 (the hCMEC/D3 monoculture)

Cell junctions between hCMEC/D3 cells in a confluent monoculture were examined by bright-field TEM microscopy. Junctions formed at the interface of two hCMEC/D3 cells varied in forms (see **Figure 3.5**). Some of the cell-cell junctions between hCMEC/D3 cells formed a “*key and lock*” configuration (shown by a red arrow in **Figure 3.5.A**) resembling the tight junctions of the BBB endothelium illustrated in reference **Figure 3.1**. In other parts of the hCMEC/D3 monolayer, there were closely overlapping cell-cell junctions (shown by a yellow arrow) showing minute membrane connections **Figure 3.5-B**. Such overlapping junctions are common at the BBB endothelium capillary [Tuma et al., 2003]. Another unique feature in the hCMEC/D3 cells was the formation of numerous vesicles suspended in the cytoplasmic region (shown by the green arrow). Lastly, there were numerous budding sites on the surface of hCMEC/D3 cells (shown by the blue arrow). Such budding cell parts may be associated with the process of cell division. These features in the hCMEC/D3 may be used to distinguish them from other cells in the triculture model of the BBB.

ii) Control 2 (the pericytes monoculture)

Cell features in the monoculture of pericytes were analyzed with a TEM microscope in order to determine what characteristics that would distinguish them from other cells in the triculture model of the BBB. While a prominent nucleus in the cytoplasm of pericytes was observed in the TEM micrographs of pericytes, this feature was also present in the hCMEC/D3 cells, and thus would not be used as a reliable marker characteristic of pericytes in TEM analysis. Instead, the

paracellular gap between adjacent pericytes could be used as a distinguishing characteristic between the hCMEC/D3 layer and the layer of pericytes in TEM micrographs.

The gaps between adjacent pericytes were expected since pericytes do not form tight junctions at the BBB in vivo. However, in some cases, pericytes overlapped each other extensively in a close configuration resembling that formed by the hCMEC/D3 cells. It should be noted that the overlap among pericytes was not consistent. Instead, pericytes were more randomly oriented in space in contrast to the more stable arrangement observed in the monoculture of hCMEC/D3 cells that were stabilized on the surface of a filter support due to the strong tight junctions holding them together (see **Figure 3.6**).

In some of the TEM micrographs, pericytes showed a large rough endoplasmic reticulum; this could be a distinguishing feature between pericytes and astrocytes in the triculture model. Lastly, pericytes formed numerous extracellular vesicles. Such vesicles are known to mediate the exchange between cells [Raposo et al., 2013], consistent with the belief that pericytes play a role in molecular trafficking with the BBB endothelium and potentially to other parts of the brain.

iii) Control 3 (the astrocytes monoculture)

Astrocytes were examined under bright field-TEM to see if they would appear different from pericytes and the hCMEC/D3 cells. Unlike pericytes or the hCMEC/D3 cells, astrocytes lacked prominent cell organelles; they were more transparent to the transmission of electrons than pericytes or the hCMEC/D3 cells. In addition, they showed varied sizes ranging from thin stellate sections to thicker ends (see **Figure 3.7**). In all the cases, they seem not to form tight cell-cell junctions like those observed in the hCMEC/D3 cells. However, in some cases they overlapped with one another, consistent with literature that suggests the coupling behavior in astrocyte cultures is required for the formation of gap junctions between astrocytes or between astrocytes and other CNS-cells [Giaume et al., 1996; Nagy et al., 2000; Goldberg et al., 2010; Le et al., 2014; Hubbard et al., 2016].

iv) The BBB tricultures

The triculture model of the BBB was prepared by overlaying layers of astrocytes, pericytes and the hCMEC/D3 cells on the apical side of a *Transwell*TM filter-support. Various thin sections of the triculture specimen were examined to verify that cross-sectional layers of the triculture would

contain discrete features corresponding to the hCMEC/D3 cells at the top section, pericytes in the middle, and astrocytes in the bottom layer. **Figure 3.8-A** shows the formation of discrete cross-sectional regions containing distinct cell features. The top section contained round and closely arranged cells whose arrangement resemble that of hCMEC/D3 cells in a monoculture; there was a high degree of order in the arrangement of cells at the top layer relative to the underneath layers.

The middle section of the TEM micrograph (see **Figure 3.8-B**) showed a disordered arrangement of heterogeneous cells showing either features of astrocytes or pericytes. In addition, there was a larger extracellular space that separated the bottom section of astrocytes from the heterogeneous middle layer. The bottom layer contained cells with attributes corresponding to those of astrocytes (see **Figure 3.8-B**).

The seeding protocol used in the preparation of “*triculture II*” (see **Figure 3.9.**) was optimized by seeding well suspended cells, using a small seeding volume to allow cells to settle well on the surface of a filter or the basal cell-cultures, and giving cells a little time to settle and attach before transferring the culture plates into a warm sterile incubator. In addition, no collagen was applied before seeding the hCMEC/D3 cells, so the extracellular matrix in the observed large space between the cell layers was likely produced by the cells themselves. Astrocytes, pericytes and endothelial cells are all capable of forming the extracellular matrix *in vivo*.

The purpose of developing “*triculture II*” was to obtain a more closely spaced stack of cell layers that would reduce the large extracellular space observed in **Figure 3.8**. Thin cross-sections of *triculture II* specimen revealed a minimization of the large extracellular space observed in initially in “*triculture I*” where cells were not allowed time to settle on the surface of a basal support before transferring them into the sterile incubator. In addition, characteristic cell junctions and organelles became clearer when preparing the second set of the BBB *triculture* cross-sections because a small angle of view was used to get a better focus of the tight junctions and other cross-sectional features.

Several ultrastructural characteristics of endothelial cells were observed at the top layer of the *triculture*. The first and more interesting feature was the formation of densely populated vesicles in the upper layer corresponding to the hCMEC/D3 cells. Such features are associated with endothelial cells of tumor microvessels [Skog et al., 2008]. Thus, the *triculture* model developed in this study may be used as a surrogate BBB model in research programs related to

cancer drug delivery. The second important ultrastructural feature in the top layer of the triculture was that it contained the characteristic cell-cell junctions of a continuous endothelial layer (see **Figure 3.9-A**). This is a unique property that makes the in vivo BBB more restrictive towards paracellular permeants.

Some of the thin cross-sections in the triculture specimen showed features of astrocytes in the middle and lower layers. Upon close inspection of **Figure 3.9-A**, it appeared that there were characteristic mitochondrial structures in the stellate projections of astrocytes. The observation of prominent mitochondria in the end-foot processes of astrocytes was expected based on the reference micrograph of the BBB in vivo (see **Figure 3.1**). In addition, the localization of mitochondria in the stellate projections of astrocytes supports previous studies showing that astrocytes exchange mitochondria with other cells in the CNS via end-foot projections [Stephen et al., 2014]. This high density of mitochondrial structures may be used as a distinguishing characteristic between end-foot processes belonging to the astrocytes or pericytes. For example, cells in the bottom layer in **Figure 9-B** were identified as pericytes since they lacked long stellate projections containing any large mitochondria. **Figures 9-A and 9-B** showed that parts of the triculture were layers of either astrocytes located directly underneath the hCMEC/D3 layer or pericytes also located directly underneath the hCMEC/D3 layer.

Further analysis revealed that there were regions in the triculture that contained all the three types of cells (astrocytes, pericytes and the hCMEC/D3 cells) directly stacked to form a trilayer in which the hCMEC/D3 cells formed a continuous layer at the top section of the triculture. **Figure 3.9-C** represents regions in which a pericyte cell is sandwiched between a bottom layer of astrocyte and a top layer of hCMEC/D3 cells. It should be noted that cells at the top layer shown in **Figure 3.9-C** formed a network of tightly knit cells that formed a continuous endothelial barrier. The middle cell, a single pericyte, did not form side connections with other cells. Instead, it formed clear physical contacts with cells underneath it or above it. Features observed in **Figure 3.9** represent the kind of configuration found among the three types of BBB cells in an in vivo setting.

In summary, a triculture model of the human BBB showing a physiologically relevant configuration was developed and characterized microscopically in a cross-sectional TEM analyses. Current TEM micrographs revealed that the hCMEC/D3 cells in the triculture were grown to form a continuous layer on a combined basement of astrocytes and pericytes. This is a physiologically

representative configuration of the BBB *in vivo* as observed in the reference micrograph (see **Figure 3.1**) where parts of the endothelium capillary are mainly covered by the astrocytes or a combination of astrocytes and pericytes. Analyses based on cell-specific ultrastructural features were used as a guide to identify cells in cross-sectional layers of a triculture model of the BBB. In the future, a more accurate identification may be achieved using cell-specific immunostaining techniques to find the relative positions of each BBB cell type in the triculture arrangement.

3.7.3 The expression pattern of F-actin in the BBB cells: astrocytes, pericytes and the hCMEC/D3

i) The expression pattern of F-actin in the monoculture controls

Further cell imaging assessments were conducted by determining the pattern of F-actin microfilaments in the BBB cells through staining of the monocultures of astrocytes, pericytes and the hCMEC/D3 cells with rhodamine phalloidin (**Figure 3.10**). A fluorescent micrograph of the astrocytes monoculture indicated that the expression of F-actin was distributed throughout their cell body in a way that reflected their overall morphology. The expression pattern of F-actin in the astrocytes in this study is like the pattern observed in other literature reports on the expression of the F-actin filaments in astrocytes [[Brozzi et al., 2009](#); [Lau et al., 2011](#)].

The distribution of F-actin in the cytoskeleton of astrocytes was different from that of pericytes and the hCMEC/D3 cells. The F-actin filaments in pericytes were more fibrous and formed parallel thin thread-like bundles. On the contrary, the expression pattern in the hCMEC/D3 cells seemed to be more diffuse and gave rise to a spindle-shaped morphology of the hCMEC/D3 cells. Since the fluorescence pattern obtained in the monoculture controls was different for each cell type, it was hoped that each layer would be detected at distinct optical sections in a confocal microscope. Fluorescent-sections obtained from the triculture are discussed in the next section.

ii) The expression pattern of F-actin in the optical sections of a triculture model of the BBB:

Different optical sections of a triculture were scanned along the Z-axis using a confocal microscope to establish if distinct fluorescent layers (or distinct fluorescent optical sections) formed in the triculture (see **Figure 3.11**). While three distinct layers corresponding to the hCMEC/D3 cells, pericytes, and the astrocytes were expected, there seem to be only two distinct layers detected in the triculture. The first unclear layer had a fluorescent pattern resembling that of

the hCMEC/D3 monoculture (at Z=48um) while the second one had a pattern that seem to be a mix of two patterns corresponding to the pericytes and astrocytes (at Z=96um). Therefore, based on the detection of two fluorescent optical sections, it was concluded that rhodamine phalloidin was well absorbed in the layers of the BBB triculture and could be used in future studies involving optical sectioning of the triculture model. A more definitive immunostaining approach involving cell-specific monoclonal antibodies for the visualization of distinct layers in the triculture, is under development in the **Knipp's lab** (Purdue University_IPPH department)

3.8 Conclusions

Various microscopic images showed that a layer of hCMEC/D3 cells cultured on a combined basement of astrocytes and pericytes would form a physiological representation of a human BBB in vitro. The identity of each cell layer was analyzed based on the characteristic ultrastructural features of each cell type. Current and future studies are ongoing in the Knipp's lab to better delineate the localization of specific cell layers and validate the observed multicellular configuration in the current triculture model of a human BBB.

3.9 Acknowledgements

I thank Dr. Andy Schaber of Purdue Bindley Imaging Facility, Laurie Mueller of Purdue Life Science Microscopy Facility, and Jun Xu, a member of Dr. Yoon Yeo' Lab for providing access and technical assistance in the use of microscopes used in this study.

3.10 References

Aday, S., Cecchelli, R., Hallier-Vanuxeem, D., Dehouck, M., & Ferreira, L. (2016). Stem Cell-Based Human Blood–Brain Barrier Models for Drug Discovery and Delivery. *Trends in Biotechnology*, 34(5), 382-393. doi:10.1016/j.tibtech.2016.01.001

Anders, S., Minge, D., Griemsmann, S., Herde, M. K., Steinhauser, C., & Henneberger, C. (2014). Spatial properties of astrocyte gap junction coupling in the rat hippocampus. *Philosophical Transactions of the Royal Society B: Biological Sciences*, 369(1654), 20130600-20130600. doi:10.1098/rstb.2013.0600

Armulik, A., Genové, G., & Betsholtz, C. (2011). Pericytes: Developmental, Physiological, and Pathological Perspectives, Problems, and Promises. *Developmental Cell*, 21(2), 193-215. doi:10.1016/j.devcel.2011.07.001

Banerjee, S., & Bhat, M. A. (2007). Neuron-Glial Interactions in Blood-Brain Barrier Formation. *Annual Review of Neuroscience*, 30(1), 235-258. doi:10.1146/annurev.neuro.30.051606.094345

Bonni, A., & Ikeuchi, Y. (2008). Faculty of 1000 evaluation for Glioblastoma microvesicles transport RNA and proteins that promote tumour growth and provide diagnostic biomarkers. F1000 - Post-publication peer review of the biomedical literature. doi:10.3410/f.1129814.586895

Brown, J. A., Pensabene, V., Markov, D. A., Allwardt, V., Neely, M. D., Shi, M., ... Wikswow, J. P. (2015). Recreating blood-brain barrier physiology and structure on chip: A novel neurovascular microfluidic bioreactor. *Biomicrofluidics*, 9(5), 054124. doi:10.1063/1.4934713

Brozzi, F., Arcuri, C., Giambanco, I., & Donato, R. (2009). S100B Protein Regulates Astrocyte Shape and Migration via Interaction with Src Kinase. *Journal of Biological Chemistry*, 284(13), 8797-8811. doi:10.1074/jbc.m805897200

Cabezas, R., Ávila, M., Gonzalez, J., El-Bachji, R. S., Bájez, E., García-Segura, L. M., ... Barreto, G. E. (2014). Astrocytic modulation of blood brain barrier: perspectives on Parkinson's disease. *Frontiers in Cellular Neuroscience*, 8. doi:10.3389/fncel.2014.00211

Chen, Q., Boire, A., Jin, X., Valiente, M., Er, E. E., Lopez-Soto, A., ... Massagué, J. (2016). Carcinoma-astrocyte gap junctions promote brain metastasis by cGAMP transfer. *Nature*, 533(7604), 493-498. doi:10.1038/nature18268

Conchello, J., & Lichtman, J. W. (2005). Optical sectioning microscopy. *Nature Methods*, 2(12), 920-931. doi:10.1038/nmeth815

Daneman, R., Zhou, L., Kebede, A. A., & Barres, B. A. (2010). Pericytes are required for blood-brain barrier integrity during embryogenesis. *Nature*, 468(7323), 562-566. doi:10.1038/nature09513

Dvorak, A. M., & Feng, D. (2001). The Vesiculo-Vacuolar Organelle (VVO): A New Endothelial Cell Permeability Organelle. *Journal of Histochemistry & Cytochemistry*, 49(4), 419-431. doi:10.1177/00221552104900401

Farkas, E., & Luiten, P. G. (2001). Cerebral microvascular pathology in aging and Alzheimer's disease. *Progress in Neurobiology*, 64(6), 575-611. doi:10.1016/s0301-0082(00)00068-x

Garbuzova-Davis, S., Hernandez-Ontiveros, D. G., Rodrigues, M. C., Haller, E., Frisina-Deyo, A., Mirytl, S., ... Sanberg, P. R. (2012). Impaired blood-brain/spinal cord barrier in ALS patients. *Brain Research*, 1469, 114-128. doi:10.1016/j.brainres.2012.05.056

García-Cabezas, M. Á., John, Y. J., Barbas, H., & Zikopoulos, B. (2016). Distinction of Neurons, Glia and Endothelial Cells in the Cerebral Cortex: An Algorithm Based on Cytological Features. *Frontiers in Neuroanatomy*, 10. doi:10.3389/fnana.2016.00107

Giaume, C., & McCarthy, K. D. (1996). Control of gap-junctional communication in astrocytic networks. *Trends in Neurosciences*, 19(8), 319-325. doi:10.1016/0166-2236(96)10046-1

- Goldberg, M., De Pittà, M., Volman, V., Berry, H., & Ben-Jacob, E. (2010). Nonlinear Gap Junctions Enable Long-Distance Propagation of Pulsating Calcium Waves in Astrocyte Networks. *PLoS Computational Biology*, 6(8), e1000909. doi:10.1371/journal.pcbi.1000909
- Hatherell, K., Couraud, P., Romero, I. A., Weksler, B., & Pilkington, G. J. (2011). Development of a three-dimensional, all-human in vitro model of the blood–brain barrier using mono-, co-, and tri-cultivation Transwell models. *Journal of Neuroscience Methods*, 199(2), 223-229. doi:10.1016/j.jneumeth.2011.05.012
- Hawkins, B. T. (2005). The Blood-Brain Barrier/Neurovascular Unit in Health and Disease. *Pharmacological Reviews*, 57(2), 173-185. doi:10.1124/pr.57.2.4
- Herland, A., Van der Meer, A. D., FitzGerald, E. A., Park, T., Sleeboom, J. J., & Ingber, D. E. (2016). Distinct Contributions of Astrocytes and Pericytes to Neuroinflammation Identified in a 3D Human Blood-Brain Barrier on a Chip. *PLOS ONE*, 11(3), e0150360. doi:10.1371/journal.pone.0150360
- Hurtado-Alvarado, G., Cabañas-Morales, A. M., & Gómez-González, B. (2014). Pericytes: brain-immune interface modulators. *Frontiers in Integrative Neuroscience*, 7. doi:10.3389/fnint.2013.00080
- Hubbard, J. A., & Binder, D. K. (2016). Gap Junctions. *Astrocytes and Epilepsy*, 265-289. doi:10.1016/b978-0-12-802401-0.00011-9
- Jinga, V., Gafencu, A., Antohe, F., Constantinescu, E., Heltianu, C., Raicu, M., ... Simionescu, M. (2000). Establishment of a Pure Vascular Endothelial Cell Line from Human Placenta. *Placenta*, 21(4), 325-336. doi:10.1053/plac.1999.0492
- Jeffrey, P., & Summerfield, S. (2010). Assessment of the blood–brain barrier in CNS drug discovery. *Neurobiology of Disease*, 37(1), 33-37. doi:10.1016/j.nbd.2009.07.033
- Kassner, A., & Merali, Z. (2015). Assessment of Blood–Brain Barrier Disruption in Stroke. *Stroke*, 46(11), 3310-3315. doi:10.1161/strokeaha.115.008861
- Larson, D. M., Carson, M. P., & Haudenschild, C. C. (1987). Junctional transfer of small molecules in cultured bovine brain microvascular endothelial cells and pericytes. *Microvascular Research*, 34(2), 184-199. doi:10.1016/0026-2862(87)90052-5
- Lau, C., O'Shea, R., Broberg, B., Bischof, L., & Beart, P. (2011). The Rho kinase inhibitor Fasudil up-regulates astrocytic glutamate transport subsequent to actin remodelling in murine cultured astrocytes. *British Journal of Pharmacology*, 163(3), 533-545. doi:10.1111/j.1476-5381.2011.01259.x
- Le, H. T., Sin, W. C., Lozinsky, S., Bechberger, J., Vega, J. L., Guo, X. Q., ... Naus, C. C. (2013). Gap Junction Intercellular Communication Mediated by Connexin43 in Astrocytes Is Essential for Their Resistance to Oxidative Stress. *Journal of Biological Chemistry*, 289(3), 1345-1354. doi:10.1074/jbc.m113.508390

Lucq, J., Tixier, D., Guinault, A. M., Greffard, A., Loisanche, D., & Pilatte, Y. (2000). The target antigens of naturally occurring human anti-beta-galactose IgG are cryptic on porcine aortic endothelial cells. *Xenotransplantation*, 7(1), 3-13. doi:10.1034/j.1399-3089.2000.00041.x

Nagy, J. I., & Rash, J. E. (2000). Connexins and gap junctions of astrocytes and oligodendrocytes in the CNS. *Brain Research Reviews*, 32(1), 29-44. doi:10.1016/s0165-0173(99)00066-1

Naik, P., & Cucullo, L. (2012). In Vitro Blood–Brain Barrier Models: Current and Perspective Technologies. *Journal of Pharmaceutical Sciences*, 101(4), 1337-1354. doi:10.1002/jps.23022

Nakano, M., Atobe, Y., Goris, R. C., Yazama, F., Ono, M., Sawada, H., ... Kishida, R. (2000). Ultrastructure of the capillary pericytes and the expression of smooth muscle α -actin and desmin in the snake infrared sensory organs. *The Anatomical Record*, 260(3), 299-307. doi:10.1002/1097-0185(20001101)260:33.0.co;2-v

Raposo, G., & Stoorvogel, W. (2013). Extracellular vesicles: Exosomes, microvesicles, and friends. *The Journal of Cell Biology*, 200(4), 373-383. doi:10.1083/jcb.201211138

Skog, J., Würdinger, T., Van Rijn, S., Meijer, D. H., Gainche, L., Curry, W. T., ... Breakefield, X. O. (2008). Glioblastoma microvesicles transport RNA and proteins that promote tumour growth and provide diagnostic biomarkers. *Nature Cell Biology*, 10(12), 1470-1476. doi:10.1038/ncb1800

Sondermann, H. (2016). Faculty of 1000 evaluation for Carcinoma-astrocyte gap junctions promote brain metastasis by cGAMP transfer. F1000 - Post-publication peer review of the biomedical literature. doi:10.3410/f.726361991.793519087

Stephen, T., Gupta-Agarwal, S., & Kittler, J. (2014). Mitochondrial dynamics in astrocytes. *Biochemical Society Transactions*, 42(5), 1302-1310. doi:10.1042/bst20140195

TUMA, P. L., & HUBBARD, A. L. (2003). Transcytosis: Crossing Cellular Barriers. *Physiological Reviews*, 83(3), 871-932. doi:10.1152/physrev.00001.2003

Toth, A., Veszelka, S., Nakagawa, S., Niwa, M., & A. Deli, M. (2011). Patented In Vitro Blood-Brain Barrier Models in CNS Drug Discovery. *Recent Patents on CNS Drug Discovery*, 6(2), 107-118. doi:10.2174/157488911795933910

Tytell, M., & Robinson, M. (2016). Faculty of 1000 evaluation for Transfer of mitochondria from astrocytes to neurons after stroke. F1000 - Post-publication peer review of the biomedical literature. doi:10.3410/f.726577022.793523112

Velandia-Romero, M. L., Calderón-Peláez, M., & Castellanos, J. E. (2016). In Vitro Infection with Dengue Virus Induces Changes in the Structure and Function of the Mouse Brain Endothelium. *PLOS ONE*, 11(6), e0157786. doi:10.1371/journal.pone.0157786

Winey, M., Meehl, J. B., O'Toole, E. T., & Giddings, T. H. (2014). Conventional transmission electron microscopy. *Molecular Biology of the Cell*, 25(3), 319-323. doi:10.1091/mbc.e12-12-0863

Winkler, E. A., Bell, R. D., & Zlokovic, B. V. (2011). Central nervous system pericytes in health and disease. *Nature Neuroscience*, 14(11), 1398-1405. doi:10.1038/nn.2946

Yan, Q. (2010). Membrane Transporters and Drug Development: Relevance to Pharmacogenomics, Nutrigenomics, Epigenetics, and Systems Biology. *Methods in Molecular Biology*, 1-21. doi:10.1007/978-1-60761-700-6_1

Zaheer, A., Mathur, S. N., & Lim, R. (2002). Overexpression of glia maturation factor in astrocytes leads to immune activation of microglia through secretion of granulocyte-macrophage-colony stimulating factor. *Biochemical and Biophysical Research Communications*, 294(2), 238-244. doi:10.1016/s0006-291x(02)00467-9

Zernike, F. (1955). How I Discovered Phase Contrast. *Science*, 121(3141), 345-349. doi:10.1126/science.121.3141.345

CHAPTER 4. POTENTIAL APPLICATIONS OF THE BLOOD-BRAIN BARRIER TRICULTURE MODEL AS A DRUG ABSORPTION AND PERMEABILITY SCREENING TOOL

4.1 Summary

Background and objectives: Of critical concern to the screening of BBB permeation is determining the *in vitro* model's potential for multidrug resistant efflux-transporters to either inhibit drug permeation or be subject to drug-drug interactions that alter neuronal exposure. Therefore, it is necessary to determine if the models will predict potential *in vivo* clinical drug-drug interactions prior to advancing novel CNS-drug candidates. The present study is aimed at comparing the effect Pgp/BCRP inhibition on the absorption of digoxin (a neurotoxic drug) using the hCMEC/D3 monoculture or our novel direct contact triculture model. The comparison also included a coculture of astrocytes together with pericytes since Pgp expression in the astrocytes has been reported in numerous publications. In addition, our studies focused on developing a basic permeability scale established using rapid and slow transcellular BBB permeants.

Methods: The mole fraction of digoxin absorbed across the aforementioned BBB cell culture models was determined in the absence or presence of elacridar, a potent Pgp and BCRP inhibitor, by HPLC analysis. Permeability assays were conducted using a set of radiolabeled compounds consisting of fast BBB/brain permeants and slow BBB/brain permeants. Liquid scintillation counting was employed to detect the rate at which molecules were ferried across the triculture model of the BBB. A basic permeability scale was developed by defining high permeability boundary as the position of L-histidine on the scale and low permeability boundary as the position of verapamil.

Results: The mole fraction of digoxin absorbed in a coculture of astrocytes and pericytes was found to be 14% in the absence of elacridar, and 20% in the presence of elacridar. For the monoculture of hCMEC/D3, there was a 13% mole fraction absorbed in the absence of elacridar, and a 17% mole fraction absorbed in the presence of elacridar. There was no detectable effect on the cellular uptake of digoxin in the triculture containing both layers of astrocytes/pericytes and the hCMEC/D3 cells when Pgp/BCRP inhibition was carried the monoculture of revealing 13% digoxin uptake in the absence or presence of elacridar. The position of L-histidine on the

transcellular permeability scale, developed using the direct triculture method, was at 1.2×10^{-5} cm/s, while verapamil's position was at 1.35×10^{-6} cm/s.

Conclusions: Under similar inhibition conditions, it appeared to be more difficult to inhibit Pgp/BCRP (transcellular barriers) in the triculture model of the BBB than in the monoculture model. Therefore, the hCMEC/D3 monoculture model could predict different potential for drug-drug interactions from that of the triculture model. The triculture model is more in agreement with previous studies, which showed that *in vivo* Pgp-inhibition might not be easily achieved by most currently available inhibitors. Based on the preliminary triculture transcellular-permeability scale, CNS-drug candidates would be characterized as negative BBB permeants if they show $P_{app} < 1.35 \times 10^{-6}$ cm/s and as positive BBB-permeants if their $P_{app} \geq 1.2 \times 10^{-5}$ cm/s. However, there is still a significant number of known CNS-positive and negative permeants that still need to be investigated prior to establishing a more robust scale. Furthermore, *in vitro in vivo permeability correlations* would be the subject of future validation studies in the laboratory.

Keywords: Blood-Brain Barrier, Efflux Transporters, Permeability Scale

4.2 Introduction

Transcellular drug transport at the Blood-Brain Barrier is regulated by different kinds of membrane-bound transporters expressed by cells of the neurovascular BBB unit [Miller, 2015]. Membrane transporters at the BBB are classified into two broad categories; the Solute Carrier (SLC) or the efflux (predominantly the ATP-Binding Cassette or ABC) transporters [Urquhart and Kim, 2009]. Numerous transporters falling into each of these categories have been demonstrated to be critical determinants of CNS-drug penetration across the BBB [Chaves et al., 2014]. The expression of key transporters at the BBB-endothelium is highly polarized to enhance active efflux of select molecules back into the blood stream while promoting the uptake of nutrients and other molecules required by the neurons [Cornford and Hyman, 2005]. Therapeutic molecules circulating in the lumen of brain capillaries may be absorbed across the BBB-endothelium by facilitated transport or by active carrier-mediated route [Yudilevich et al., 1972].

The multidrug resistant efflux-transporters (Pgp, BCRP or MRP isoforms) clear drugs circulating in the brain parenchyma by actively pumping them from neuronal environment across the BBB back into the blood stream thus acting as a natural mechanism to protect the neuronal

environment from neurotoxic compounds entering brain parenchyma by circumventing BBB mechanisms [Kurihara et al., 1988; Loscher and Potschka, 2005]. For example, Pgp expressed in the apical membranes of BBB-endothelial capillaries protects neurons from toxic compounds, such as digoxin [Mayer et al., 1996]. However, in the presence of a drug that potently inhibits Pgp, digoxin may cross the BBB in high amounts to elicit neurotoxicity [Eyal et al., 2009]. Thus, drug-efflux activities due to BBB-transporters are investigated routinely in preclinical drug screening to minimize potentially toxic drug-drug interactions and to enhance lead candidate selection and advancement into later clinical drug-development [Hutzler et al., 2011].

Animal BBB-cell models have been routinely utilized in preclinical studies for predicting drug permeation and detecting potentially relevant clinical drug-drug interactions although pharmacogenomic differences between human and animal derived cells may limit translational efficiency [Martinez, 2011]. For a long time, the need for a proliferative, human brain microvessel endothelial cell (BMEC) line has been recognized and then finally realized in 2005 by the establishment of the hCMEC/D3 cells by Couraud and colleagues [Weksler et al., 2013]. The study described in this chapter evaluates the use of a human BBB cell model (the hCMEC/D3 cell line) for a potential application in drug-drug interactions as a triculture model.

Here we examined the effect of elacridar, a potent inhibitor of the ABC efflux transporters Pgp and BCRP, on the cellular absorption of digoxin in the hCMEC/D3 cell monoculture, the co-culture of pericytes on astrocytes and the direct-contact triculture of hCMEC/D3 layered on a co-culture of pericytes and astrocytes on the filter support of *Transwell*TM. We hypothesized that the effect of Pgp-inhibition on the cellular absorption of digoxin would be significantly lower in the triculture, in comparison to the effect of Pgp-inhibition on the absorption of digoxin in the hCMEC/D3 monoculture or the co-culture of astrocytes and pericytes (separate BBB cellular components). Note that efflux activity in the astrocyte-pericyte layers of the triculture model of the BBB may be masked by a higher efflux activity in the hCMEC/D3 cells, thus the need to delineate the effects of each layer would be informative in establishing efflux activity in the non-endothelial cells of the BBB system.

It should be noted that some researchers grow the hCMEC/D3 cells under selective pressure to induce Pgp function [Noack et al., 2014]. This approach may be suitable in studying how drugs that induce Pgp function would affect the absorption and permeability of novel CNS-drug

candidates across the direct-contact triculture model, and if the observations made would predict similar effects *in vivo*. While additional primary human brain microvessel endothelial cell lines (other than the hCMEC/D3) have been developed as novel BBB cell models, the hCMEC/D3 is still one of the most widely utilized cell line in the BBB research and was therefore selected for studies described in this chapter [Weksler et al., 2013].

In order to verify the expression of Pgp function at the astrocyte-pericyte sections of a BBB triculture model, the fraction of digoxin absorbed in the presence or absence of elacridar was conducted using the coculture to begin delineating if non-endothelial components of the BBB-system offer additional efflux pumps that could limit permeation of Pgp substrates such as digoxin. A significant difference in the fraction of digoxin absorbed under Pgp-inhibition would potentially indicate the expression of efflux-system pumps in the astroglial region of the BBB, which may further limit drug penetration even if Pgp function at the BMEC level is inhibited.

In addition, efflux activity in the astrocyte and pericyte lawn of a BBB-triculture model would suggest the formation of a backup efflux system for reinforcing efflux activity of the endothelial cells during normal and potentially disrupted BBB-endothelial protection for the brain. Furthermore, astrocytes have been shown to respond to changes in the biochemical environment of neurons by expressing Pgp [Zhang et al., 1999]. While *in vitro* Pgp function has been shown in the monoculture of astrocytes, Pgp-studies involving a combination of astrocytes and pericytes in a direct coculture setting have not been reported [Ronaldson et al., 2004]. The present study investigates Pgp-function in a direct coculture of astrocytes and pericytes, and comparisons to the hCMEC/D3 monoculture and direct triculture containing astrocytes, pericytes and the hCMEC/D3 cells are made to delineate separate roles of the cellular components of a human BBB.

Lastly, the potential of a direct triculture model of the BBB to rank Pgp-mediated permeability of transcellular permeants is evaluated in this chapter. L-histidine (a non-Pgp substrate rapidly transported into the brain parenchyma) was used as a marker for fast BBB-permeant; thiamine (a Pgp substrate, needed by the brain cells for metabolic requirements) was used as a marker of a rapid BBB-permeant but was expected to be slower than L-histidine. Propranolol (a lipophilic Pgp-substrate) was expected to have slower permeability than L-histidine and thiamine. Taxol (another lipophilic Pgp-substrate) was expected to have slower permeability than L-histidine and thiamine.

Verapamil (a lipophilic Pgp-substrate used as a marker of very slow BBB-permeant) was expected to be slower than all the compounds used in the transcellular permeability assays.

L-histidine is an essential amino acid required for proper functioning of the brain cells, hence it should be readily absorbed across a physiologically relevant cell culture model of the human BBB [Sakurai et al., 2009, Carl et al., 2010]. Thiamine is required for energy production from glucose metabolism in the brain cells, and is transported across the BBB by a carrier-mediated mechanism [Greenwood et al., 1982]. However, thiamine is also a substrate of efflux transporters at the BBB, which may reduce its permeability across the BBB relative to the permeability of L-histidine [Lockman et al., 2003].

Propranolol, paclitaxel and verapamil diffuse passively through the BBB-cell membranes, and they may be cleared from intracellular space by efflux transporters such as Pgp [Yang et al., 2013]. The rates of efflux clearance for propranolol, taxol and verapamil would depend on the extent of Pgp polarization at the BBB-endothelium. If Pgp-efflux transporters were more expressed on the luminal (blood facing apical) side, then the rates of clearance from intracellular space back to the luminal side would be more than the rate of clearance from the intracellular space towards abluminal (astrocyte-pericyte and neuronal basolateral) side of the BBB-endothelium. Efflux ratios are used commonly as indicators of the effective direction for efflux activity [Thiel-Demby VE et al., 2004].

The present study assumes that the distribution of efflux transporters is polarized towards the luminal membranes of the cells used in seeding the BBB-triculture model, thus favoring efflux of Pgp/BCRP substrates on the apical side of the *Transwell*TM filter supports used in the permeability assays. The potential of the triculture model to rank permeability coefficients of Pgp substrates (thiamine, propranolol, taxol, and verapamil) lower than a non-Pgp substrate (L-histidine, a substrate for uptake transporter across the BBB) is therefore evaluated for its physiological relevance as a tool for screening novel CNS-drug candidates in drug discovery and development programs.

4.3 Hypothesis

Under similar inhibitory concentration, it would be more difficult to inhibit Pgp/BCRP function in the direct contact triculture model of the BBB in comparison to the separate endothelial or astrocytes- pericytes constituent cell cultures.

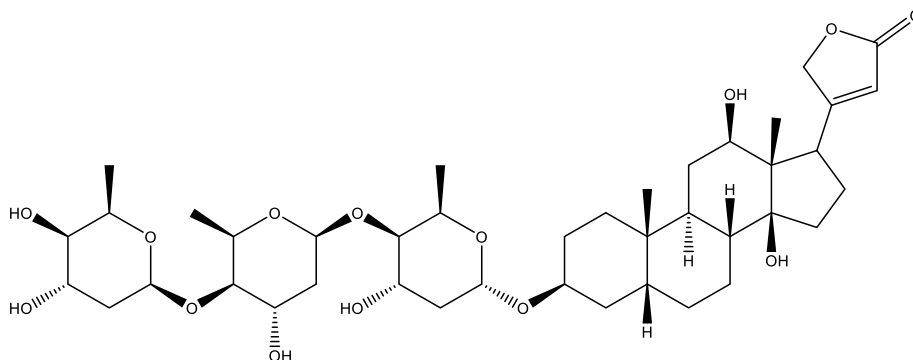
4.4 Test parameters

4.4.1 Mole fraction absorbed

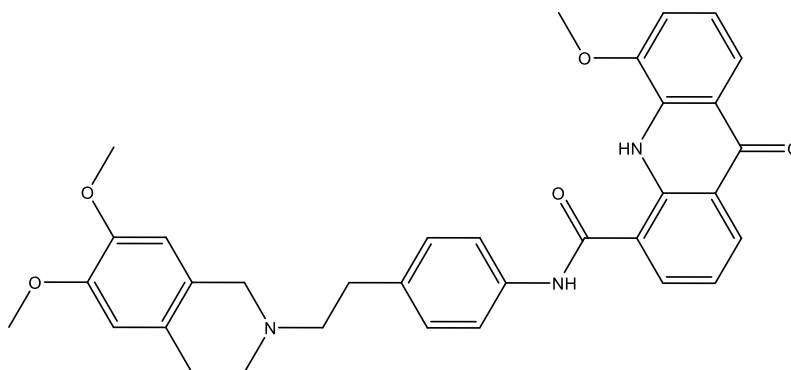
If Pgp/BCRP function is well expressed in the hCMEC/D3 cell line or the astrocytes, then the mole fraction of digoxin (a Pgp probe molecule recommended by the FDA) absorbed when Pgp is inhibited by elacridar (a potent inhibitor of Pgp/BCRP activity) would be greater than the mole fraction absorbed under non-inhibitory conditions. A summary description of physico-chemical properties of digoxin and elacridar is provided in **Table 4.1**. The choice of digoxin concentration to use in the donor chamber of a *Transwell*TM was made in part due to the fact that it is a well-established and accepted molecular probe for Pgp function [Fortuna et al., 2011]. However, it is worth noting that BCRP has overlapping substrates with Pgp that can obfuscate the interpretation of efflux data where elacridar is a substrate for Pgp and BCRP (Bankstahl et al., 2013). Therefore, inhibitory effects caused by elacridar would be likely due to inhibition of both BCRP and Pgp functions in the cell cultures tested as described in the methods section.

Table 4.1. Pgp probe substrate (digoxin) and inhibitor (elacridar)

Pgp probe (Digoxin): Aqu. Solubility = 0.127mg/mL, log P = 2.37, pKa = 7.15, and MW = 780.9 g/mol



Pgp inhibitor (Elacridar): Aqu. solubility = 0.003mg/mL, log P = 6.81, pKa = 8.35, and MW = 600g/mol



4.4.2 Permeability of transcellular permeants

There are several transcellular permeation pathways for small molecules to traverse the BMECs including passive diffusion, facilitated diffusion, active influx and efflux transport as explained in **Figure 4.1**. The purpose of this study is not the contribution of each of these routes in the effective permeability, but instead to evaluate how the direct-contact triculture model ranks the expected apparent permeability values of known BBB-permeants.

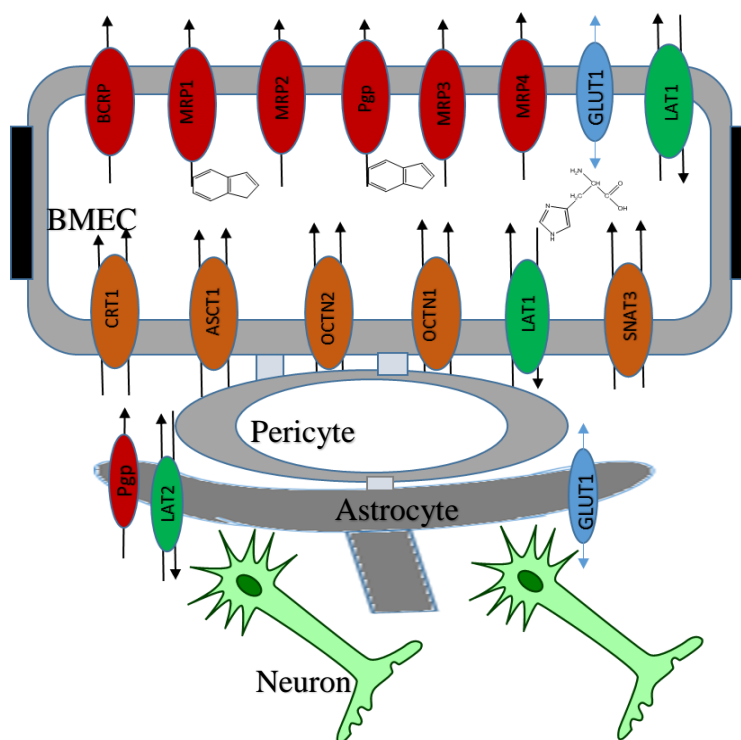
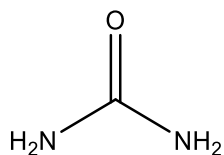
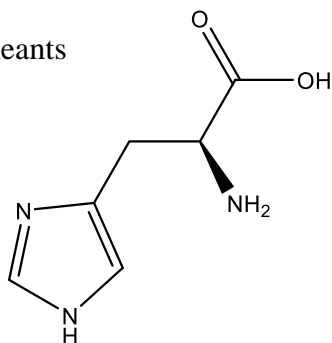


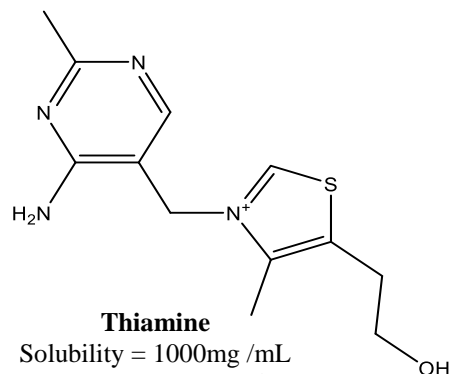
Figure 4.1. Transcellular transport systems at the BBB-glia unit. BCRP stands for Breast Cancer Resistance Protein. MRP1, -2, -3, -4 stands for Multidrug Resistance associated-Protein 1, -2, -3, -4. GLUT1 stands for Glucose Transporter 1. Pgp stand for P-glycoprotein transporter. LAT1 stands for Large neutral-Amino Acid Transporter. CRT1-Creatinine Transporter 1, ASCT1-neutral Amino Transporter 1, OCTN 1, -2 stands for Organic Cation/Carnitine Transporter 1, -2 and SNAT3 stands for Special Amino Acid Transporter 3. Note that transport out of the brain is more favored than transport into the brain parenchyma.

Table 4.2. Transcellular test-permeants**(A) Hydrophilic test-permeants****Urea**

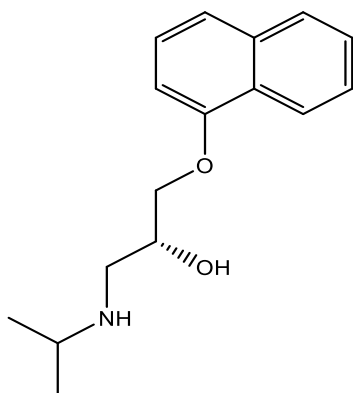
Solubility= 412.0 mg/mL
 MW= 60.6g/mol
 pKa = 0.1
 BBB Transporter: UT-B
 [Li et al., 2012]

**L-histidine**

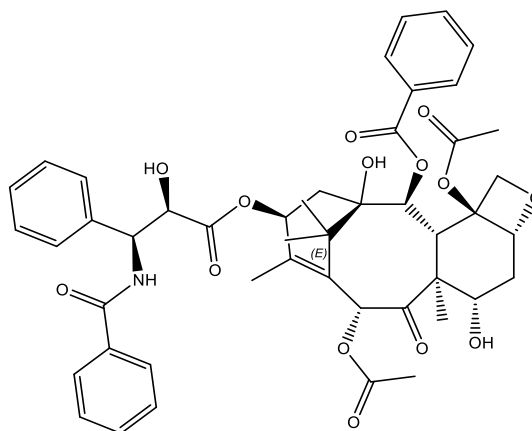
Solubility = 62.0mg/mL
 MW = 155.16g/mol
 pKa = 2.6
 BBB Transporter: LAT 1
 [Peura et al., 2013]

**Thiamine**

Solubility = 1000mg /mL
 MW = 265.35 g/mol
 pKa =5.5
 Transporter: hTHTR2
 [Greenwood et al., 1982; Subramanian et al., 2005]

(B) Lipophilic test-permeants**Propranolol**

Aqu. Solubility 61.7mg/mL
 MW = 259g/mol
 logP = 3.48
 pKa = 9.42

**Taxol**

Aqu. Solubility 0.006mg/mL
 MW = 259g/mol
 logP = 3.0
 pKa = NA

L-histidine is known as positive BBB-permeant [Brenton and Gardiner, 1988; Yoshikawa et al., 2014], thiamine, a hydrophilic vitamin that is transported across the BBB by an uptake transporter even though it has been reported to be susceptible to Pgp efflux [Lockman et al., 2003]. Propranolol and paclitaxel are lipophilic substrates of Pgp used in this study as markers of slow BBB-permeation while verapamil was used as a marker of negative permeability boundary as following the example of Nakagawa et al., in previous studies involving indirect BBB cell culture models [Ballatore et al., 2003; Nakagawa et al., 2009]. A detailed description of the physicochemical properties of the compounds that are considered in this study as BBB-transcellular permeants is done in **Table 4.2**.

The long-term goals of this study is to establish robust permeability scales for screening neuroactive agents or brain drug delivery systems with optimal BBB permeability. Thus, the small set of compounds used in the current study may be further improved by incorporating more compounds that are known to be either positive or negative BBB-permeants (following the example of Nakagawa et al., while using a truly direct-contact triculture methodology)

4.5 Materials and Methods

4.5.1 Materials

Digoxin, elacridar, poly-L-lysine, collagen, trypsin and dimethyl sulfoxide were purchased from Sigma-Aldrich (St. Louis, MO, USA). [3H]- propranolol and [3H]-verapamil were purchased from Perkin Elmer (Boston MA, USA); [14C]-taxol, [14C]-L-histidine, [14C]-thiamine, and [14]-urea were purchased from Moravek Biochemicals company. Hank's Balanced Salt Solution (HBSS), human brain astrocytes, the astrocyte media, human brain vascular pericytes and pericyte media were supplied from ScienCell Research Laboratories (Carlsbad, CA, USA) and Dr. Pierre Couraud of Institut Cochin (Paris, France) kindly donated the hCMEC/D3 cell line used in this study. Endothelial Basal Medium-2 (EBM-2 media) was purchased from Lonza Group (Walkersville, MD, USA). The 12-well format *Transwell*TM plates (polycarbonate inserts, 12 mm in diameter, 0.4 um pore size) were supplied from Corning Lifesciences (Corning, NY, USA). See **Tables 4.1 and 4.2** for a detailed description of the physico-chemical properties for the tested BBB-permeants.

4.5.2 Enhancement of Digoxin Absorption by a Pgp/BCRP inhibitor

The mole fraction absorbed was determined in the **AP** coculture (**A**= astrocytes, **P** = pericytes) the hCMEC/D3 monoculture, and the triculture. Briefly, the coculture of astrocytes and pericytes was seeded at a density of [(4 x 10⁴A): (4 x 10⁴ P)] cells/cm² and used at day 7 post pericytes seeding. The hCMEC/D3 monoculture was seeded on a filter support of a *Transwell*TM as described in section 4.4.3.1, and the triculture as described in section 4.4.3.2. For control the control studies, cell-cultures were first incubated with a solution of digoxin (at 112 uM in 0.5% DMSO) on the apical chamber of a *Transwell*TM for a period of 120 minutes. A change in the concentration of digoxin at the end of 120 minutes was used to calculate the number of moles absorbed in the cell layers.

To evaluate the effect of inhibiting Pgp and/or BCRP on the absorption of digoxin, solutions containing digoxin and elacridar (112 µM and 5µM respectively, all in 0.5% DMSO) were incubated on the apical chamber containing the cell cultures for a period of 120 minutes. The number of digoxin moles absorbed under Pgp/BCRP inhibitory conditions was calculated from the change in the free concentration of digoxin in the apical chamber of the *Transwell*TM at the end of 120 minutes. Mole fractions absorbed under AP coculture, the hCMEC/D3 monoculture, and triculture methods were calculated using the ratio of the number of digoxin moles absorbed, to the initial number digoxin of moles present in the apical chamber. Analytical detection of digoxin was achieved using HPLC methods with where the mobile phase was water and acetonitrile at 70:30, v/v, and volume of injection was 100 µL, column temperature was set at 24°C, the flow rate was 1mL/min, and the UV-detector was set at 218 nm. Addition of 5µM of elacridar in the samples of digoxin did not lead to analytical interference in the analysis of standard solutions of digoxin.

4.5.3 Permeability assays for transcellular permeants

4.5.3.1 Control assay in the monocultures of hCMEC/D3 cells

Immortalized hCMEC/D3 cells (frozen at passage 32) were thawed, reconstituted in the EBM-2 media, and then passaged in vented T-75 flasks in an incubator set at 37°C and 5% CO₂. The hCMEC/D3 cells were used after three or more passages in a T-75 flask pre-coated with 100ug/mL collagen. Confluent hCMEC/D3 cells were detached from T-75 flask using trypsin. Trypsin was removed by centrifugation at 1500 rpm and the re-suspended hCMEC/D3 cells were

plated in a triplicate at 8×10^4 cells/cm² on the collagen-coated apical surface of filter inserts of a *Transwell*[®] (0.4 μ m pore size). The hCMEC/D3 monocultures on *Transwell*TM were placed in a sterile incubator for 7 days, with the media was changed on them every 48hrs. The hCMEC/D3 monocultures were pre-incubated with HBSS (Hank's Balanced Salt Solution containing 25 mM Hepes buffer, pH ~ 7.4) for 15 minutes before carrying out transport studies.

At the start of transport studies, 1.5mL of fresh HBSS buffer was placed in the receiver chamber and 0.5mL of fresh HBSS containing radio labelled marker compound were added at the donor chamber. Concentrations used were 0.25uCi/mL for L-histidine, 0.25 uCi/mL for thiamine, 1uCi/mL for propranolol, 1uCi/mL for taxol and 1uCi/mL for verapamil. Samples from the receiver chamber were collected at 15, 30, 45, 60, 90 minutes intervals during permeability assays for paracellular permeants, and at 15, 30, 45, 60, 90, and 120 minutes during assays for transcellular permeants (propranolol, taxol and verapamil were pre-incubated for 30 minutes before sample collection from the receiver chamber). Transport assays were carried out on a rocking plate at 65 rpm. Radioactivity in the donor samples was detected using a liquid scintillation counter. Rates of mass transfer from the donor chamber to the receiver chamber were used to calculate permeability coefficients using **Equations 4.1** and **4.2** as follows:

$$\frac{1}{P_{apparent}} = \frac{1}{P_{Layers}} + \frac{1}{P_{Filter}} \quad (\text{Equation 4.1}), \quad \& \quad P_{apparent} = \frac{V_R \times dC_R}{dt \times A \times C_{D0}} \quad (\text{Equation 4.2})$$

Where $P_{apparent}$ = Apparent permeability, P_{Layers} = Permeability across cell layers, P_{Filter} = Permeability across a free filter support, V_R = Volume of the receiver chamber, C_R = Concentration of the test permeant in the receiver chamber A = Area of the permeability barrier C_{D0} = Concentration of the test permeant in the donor chamber at $t = 0$.

4.5.3.2 Assay in the triculture model of the human BBB

The direct contact, layered triculture of astrocytes, pericytes and hCMEC/D3 was carried out on the apical surface of a *Transwell* filter support as described in Chapter 2. Briefly, astrocytes were first plated at $\sim 4 \times 10^4$ cells/cm² on filter inserts that were pre-coated with 10ug/mL poly-L-lysine overnight. At the end of 48hrs, astrocytes were incubated with 0.5mL of 10ug/mL poly-

lysine on the apical side for 10 minutes at 37°C and 5% CO₂ atmosphere. Once the poly-L-lysine solution was removed, pericytes were then plated on top of astrocyte layer at a seeding density of $\sim 4 \times 10^4$ cells/cm². At the end of 48hrs, the coculture of astrocytes and pericytes layers was rinsed using HBSS and incubated (on the apical side) with 0.5mL, 100ug/mL of rat-tail collagen type I for 10 minutes at 37°C and 5% CO₂. At the end of 10 minutes, the collagen solution was removed and the hCMEC/D3 cells are plated on top of the coculture layers at a density of $\sim 8 \times 10^4$ cells/cm² to form a full triculture model of the BBB vascular unit. Permeability values were obtained as described in subsection **4.4.3.1**.

4.5.4 Statistical analysis

All experimental data were expressed as means \pm SEM obtained in three or more independent experiments. Studies were compared using unpaired one-tailed student's t-test where two independent means were compared, or one-way ANOVA followed by Tukey's post hoc tests where a control experiment was compared to two or more distinct experimental methods. A non-overlapping 95% confidence interval (CI) was used to establish a significant difference between two closely spaced mean values.

4.6 Results and discussion

4.6.1 Effects of elacridar on the absorption of digoxin

Efflux transporters at the BBB can affect CNS-drug disposition and pharmacodynamics [Golden and Pollack, 2003]. The FDA recommends preclinical evaluation of new drug candidates as potential substrates for several transporters including Pgp, BCRP, OCT2, OATP1B3, OAT1, and OAT3 (see the **FDA-Draft guidance on clinical drug interaction studies, 2017**). Upon establishing if a drug candidate is a substrate, it is recommended that prior to advancement, potential for drug-drug interactions ought to be investigated with assays focused on Pgp, BCRP and other multidrug resistant efflux transporters to assess the potential for clinical toxicity due to inhibition related increases in exposure [Reynolds et al., 2011; Nix et al., 2011].

In the present study, a novel direct contact triculture model of the BBB seeded on a *Transwell*TM filter support was evaluated to verify if it would lead to different Pgp/BCRP mediated drug-drug interactions in comparison to the corresponding monoculture of hCMEC/D3 cells and

the coculture of pericytes that were directly seeded on a lawn of astrocytes. Digoxin, an FDA-recommended preclinical probe for Pgp activity, was used as Pgp/BCRP test substrate and Elacridar, an FDA-recommended preclinical inhibitor for Pgp activity, was utilized as a test inhibitor in the study.

While there was a noticeable efflux inhibition for digoxin in the monoculture of hCMEC/D3 cells and in the coculture of astrocytes with pericytes, similar inhibitions of digoxin efflux were not observed in the BBB triculture when elacridar solution was used to inhibit efflux transporters (112 μ M for Digoxin & 5 μ M for Elacridar, see **Figure 4.2**). Initial results of this study suggest that the hCMEC/D3 monoculture may predict a higher potential for Pgp/BCRP mediated drug-drug interactions at the human BBB while the triculture model containing the hCMEC/D3 layer may predict no Pgp/BCRP mediated drug-drug interactions between digoxin and elacridar at the human BBB. It should be noted that an increase in the absorption/exposure of digoxin by a factor of **1.25** or greater indicates potential Pgp/BCRP mediated clinical drug-drug interactions [De la Pena et al., 2017].

Therefore, the hCMEC/D3 monoculture model would provide different predictions on the effect of a Pgp/BCRP inhibitor on the brain absorption of a neurotoxic compound such as digoxin. The gain in the absorption of digoxin, upon the presence of elacridar was greater by a factor of **1.25** in contrast to the triculture model, which indicated no significant gain in the absorption of digoxin in the presence of elacridar (**Figure 4.2**)

The amount of digoxin absorbed, at the end of 120 minutes, in the coculture of astrocytes and pericytes was increased significantly when elacridar was applied onto the coculture containing digoxin; a 20% mole fraction was absorbed when elacridar (a Pgp/BCRP inhibitor) was applied versus 14% in the absence of elacridar. In the hCMEC/D3 monoculture, 17% of digoxin moles were absorbed under efflux inhibition, while the extent of uptake with no-inhibition was moderately lower at 13%. Though the percentage increase in the uptake of digoxin observed in the hCMEC/D3 monoculture or the coculture of astrocytes with pericytes due to efflux inhibition are minimal, they may be clinically relevant for a toxic drug like digoxin with a minimal therapeutic window [Goldberger et al., 2012].

Contrary to the observations made under cocultured lawn of astrocytes with pericytes or the hCMEC/D3 monoculture, there was no statistically significant increase in the absorption of

digoxin in the direct contact triculture containing the hCMEC/D3 due to efflux inhibition with elacridar. The mole fraction absorbed under inhibitory or non-inhibitory conditions remained the same at 13%. The lack of increased uptake under efflux inhibition indicated that, under similar conditions, it might be more difficult to inhibit the transcellular barrier function of Pgp and BCRP transporters in the triculture model than in the hCMEC/D3 monoculture or in the coculture of astrocytes layered under pericytes. Efflux action on digoxin may not be easily inhibited by using moderate concentrations of elacridar. However, one should be careful not to use higher concentrations of the toxic elacridar since such an approach may not provide reliable predictions for *in vivo* or clinical studies where high concentrations of elacridar would cause toxicity.

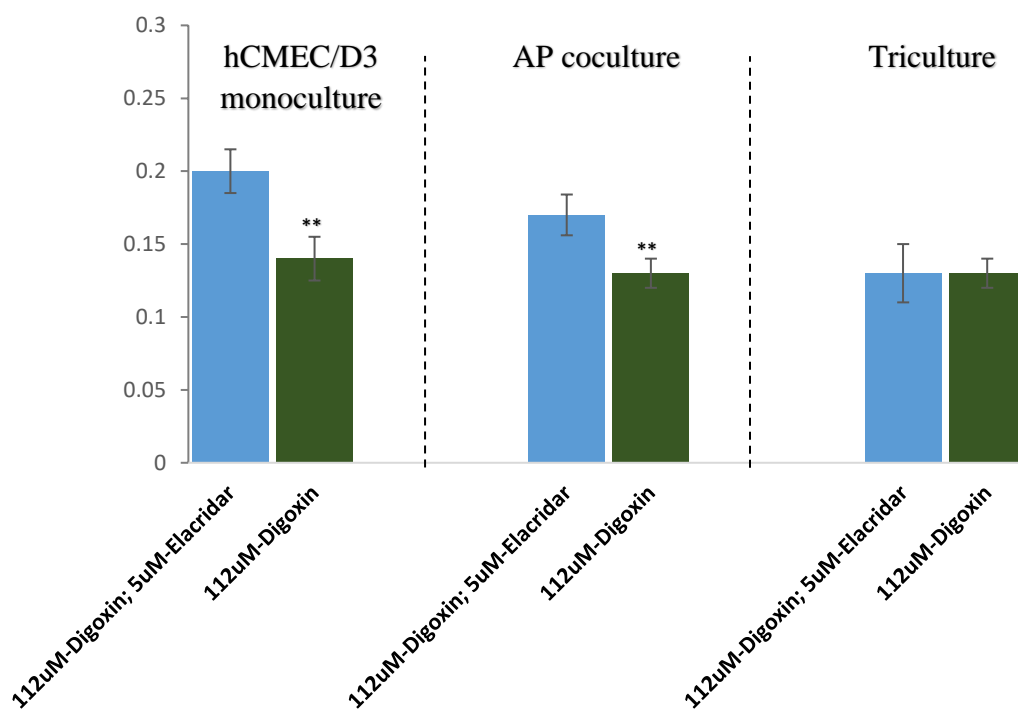


Figure 4.2. A comparison of drug-interactions (elacridar and digoxin) in the AP-coculture versus hCMEC/D3 monocultures, and the triculture containing hCMEC/D3 cells on a basement of pericytes layered directly on the astrocytes. AP stands for Astrocytes Pericytes coculture. The confidence intervals (CI) for the difference in the mean molar fraction absorbed indicated a significant difference for values obtained under the hCMEC/D3 monoculture (n=6, at 95% CI = 0.06 ± 0.009), and for values obtained under the AP-coculture (n=6, at 95% CI = 0.04 ± 0.007). There was no significant increase of digoxin absorption in the triculture when elacridar, a potent Pgp inhibitor, was incubated in the triculture prior to the addition of digoxin (n=6, at 95% CI = 0 ± 0.009).

In preclinical drug-interaction studies, the triculture would predict no potential drug-drug interaction between elacridar and digoxin at the human BBB, while the hCMEC/D3 monoculture would predict increased risk for Pgp/BCRP mediated drug-drug interaction at the human BBB and hence potential neurotoxicity arising from increased levels of digoxin absorption at the BBB. Confirmatory experiments using higher but non-toxic concentrations of elacridar are warranted to validate whether Pgp/BCRP inhibition in the hCMEC/D3 monoculture would consistently lead to higher absorption or permeability of digoxin in comparison to the triculture model, which currently indicates that inhibition of Pgp/BCRP with elacridar does not lead to higher absorption of digoxin across the human BBB. Note that observation made under the triculture model are more in agreement with the published data showing that it is difficult to increase BBB permeation of a Pgp/BCRP substrate in healthy human subjects by simply co-administering a potent Pgp inhibitor such as Tariquidar [Bauer et al., 2012].

4.6.2 Permeability of hydrophilic transcellular permeants

The BBB acts as a nutritional conduit for delivering hydrophilic nutrients such as amino acids and vitamins from blood in circulation, and may be involved in clearing hydrophilic metabolic products such as urea, and carbon dioxide [Friss et al., 1980; Doran et al., 2006; Marchi et al., 2016]. A comparison of permeability coefficients for urea, L-histidine, and thiamine was expected to show a higher permeability for L-histidine and urea when compared to thiamine, which may be susceptible to efflux transport at the BBB [Lockman et al., 2003]. In addition, it was expected that the transcellular permeation rates of hydrophilic urea, histidine, and thiamine in the monoculture of hCMEC/D3 cells would be different in comparison to the triculture. As expected, the permeability of urea was greater than that of thiamine (1.6 x greater than the permeability of thiamine across the hCMEC/D3 monoculture, and 1.7 x greater than permeability of thiamine across the triculture; see **Figure 4.3**).

The permeability of L-histidine, a substrate for uptake transporters at the BBB, was greater than that of thiamine under the mono- and –triculture models. L-histidine permeability was 1.9 x greater than thiamine permeability under the hCMEC/D3 monoculture and 1.6 x greater under the triculture. The lower permeability of thiamine may be attributed to its interaction with efflux transporters as previously reported in animal studies (Lockman et al., 2003) but additional

confirmatory studies are needed to validate this observation at various concentrations and efflux inhibition preferably using a human cell line with higher Pgp expression.

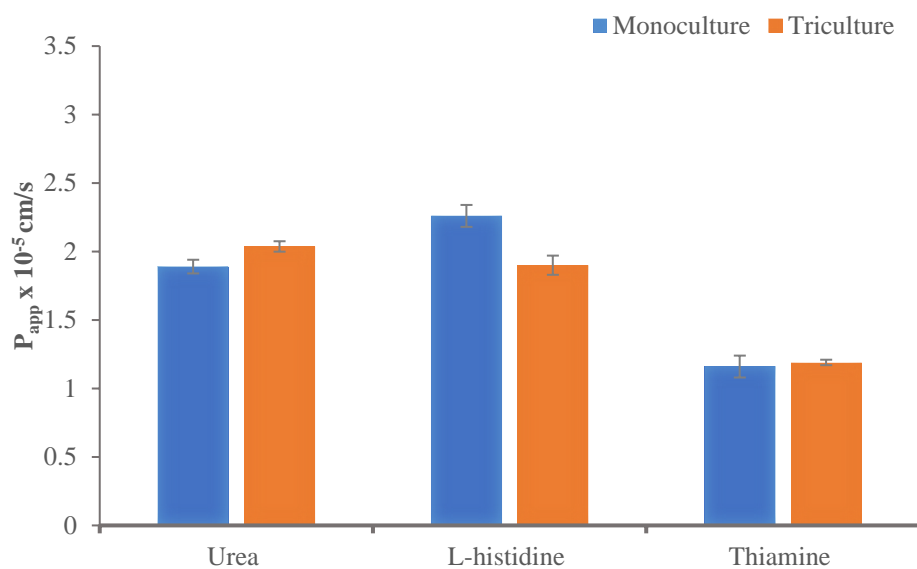


Figure 4.3. A comparison of hydrophilic transcellular permeability coefficients across mono- and tri-culture models. There was no significant difference in the permeability of hydrophilic transcellular permeants across mono- and tri-culture models of the human BBB. Urea seem to have a higher permeability across the triculture than across the monoculture (the 95% CI = 0.15 ± 0.073). On the contrary L-histidine exhibited a lower permeability in the triculture (the 95% CI = 0.36 ± 0.121). Thiamine showed similar permeability across the mono- and triculture models of the BBB in this study with a 95% CI of (0.03 ± 0.094)

A hypothetical permeability data set would include positive hydrophilic BBB-permeants such as guanidine compounds and essential amino acids (leucine, valine tyrosine, tryptophan, phenylalanine, and isoleucine) and a negative data set corresponding to poor BBB-permeants such as glutamate, norepinephrine, and the catecholamines dopamine [Bothe et al., 2014; Kostrzewa, 2007]. A resulting permeability scale might be used in defining boundaries between BBB-positive/negative permeants in the triculture model. Ultimately, a better-defined permeability scale could be useful in deciding whether novel CNS-drugs, prodrugs, or nutrients might have the required permeability at the BBB *in vivo*.

4.6.3 Permeability of lipophilic transcellular permeants

The BBB is implicated in a selective passive transcellular (lipophilic) permeation, allowing certain lipophilic molecules such as propranolol or diazepam to diffuse through its cell membranes more easily than certain others such as verapamil or chloroquine [Eigenmann et al., 2016]. Various physicochemical factors such as molecular size, shape, weight and solvent accessible surface areas influence BBB selectivity for transcellular diffusion of molecules into the brain parenchyma [Ghose et al., 2012; Geldenhuys et al., 2015]. Though consideration of optimal physicochemical properties is crucial in CNS drug design, predictions based on physicochemical properties often have to be verified in cell-based assays or animal models for BBB-permeability [Rankovic, 2015]. The present study aimed at establishing if the proposed triculture model of a human BBB would rank the permeability of an initial small set of transcellular permeants in a reasonable order based on the published literature.

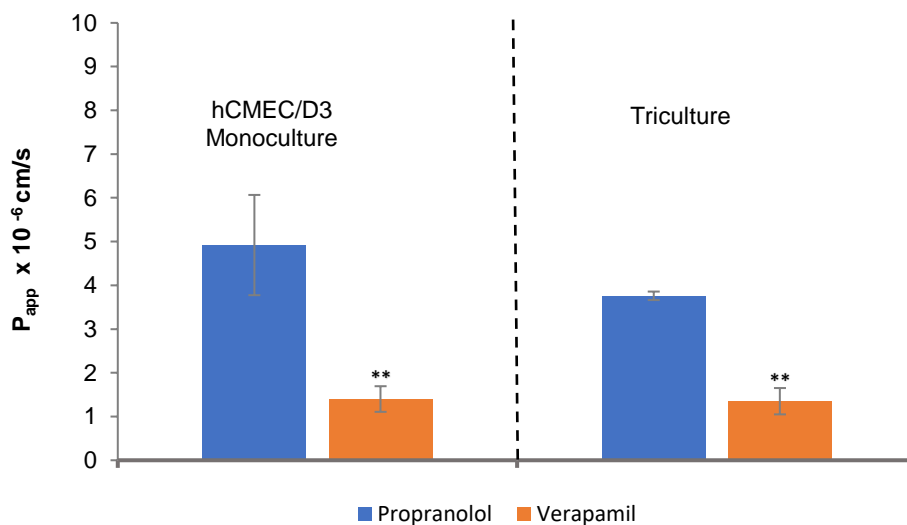


Figure 4.4. A comparison of lipophilic permeability coefficients for propranolol and verapamil. There was no significant difference in the permeability of lipophilic transcellular permeants (propranolol and verapamil) under the mono- and tri-culture models. The 95% CI for the difference in the mean P_{app} values were 1.16 ± 1.734 for propranolol and 0.05 ± 0.802 for verapamil. However, the permeability value of verapamil, a Pgp-marker compound, was significantly lower than that of propranolol, a marker of fast transcellular permeation, both in the mono- and triculture settings (the 95% CI intervals for the differences in the mean P_{app} values were 3.52 ± 1.792 under the monoculture settings, and 2.41 ± 0.634 under the triculture settings).

For example, propranolol a lipophilic positive BBB-permeant was expected to exhibit higher permeability than verapamil, another lipophilic agent that is a potent substrate of efflux transporters including Pgp and BCRP which restrict its permeability across the BBB much more than propranolol (see **Table 4.2 for details on physicochemical properties**). Under the hCMEC/D3 monoculture model, the permeability of verapamil was 3.6 x lower than permeability of propranolol. However, in the triculture model, the permeability of verapamil was 2.8 x lower. This indicates that the monoculture shows a better permeability resolution between fast and slow transcellular permeants; however, more permeability assays are required to verify this observation (see **Figure 4.4** for details).

A transcellular permeability scale based on the proposed triculture model should be developed for a wider industrial application in studies related to brain drug delivery across a human BBB. For example, the permeability of propranolol may be used to set a permeability boundary that defines moderate BBB-permeants, while verapamil may be used to set a boundary for negative BBB-permeants as exemplified by a commercial permeability scale used at Alpha Bioregen [[Alpha Bioregen webpage, accessed on June 2017](#)]. Similarly, the permeability of verapamil could be used to define a lower permeability boundary for impermeable compounds.

4.6.4 A basic permeability ranking scale for transcellular permeants

A transcellular permeability scale containing both hydrophilic and lipophilic compounds with reference positions defining high and low permeability points may better reflect a selective transport property in the direct contact triculture model of the BBB proposed in this thesis. The high transcellular permeability positions on the scale could be defined by essential nutrients known to cross the BBB rapidly to meet nutritional demands for neurons in the brain parenchyma. Certain neutral amino acids such as L-tyrosine, L-phenylalanine, L-leucine, and L-histidine get absorbed into the brain parenchyma via carrier-mediated transporters across the BBB into neuronal environment in order to fulfill nutritional and metabolic requirements [[Yudilevic et al., 1972](#)]. Therefore, L-histidine was selected to be used in defining a high permeability threshold based on the triculture model. Similarly, Thiamine was selected as an essential vitamin needed for proper functioning of the brain cells and hence was expected to show either moderate or high permeability values relative to the permeability of propranolol, paclitaxel or verapamil, lipophilic molecules

that may cause brain neurotoxicity [Harata et al., 1995; Olesen et al., 1978; Fellner et al., 2002; Fang et al., 2013].

Therefore, propranolol, paclitaxel and verapamil were selected to define moderate to low permeability positions on the permeability scale for transcellular permeants across the proposed triculture model. These three compounds are known to be substrates of Pgp and hence were expected to show lower permeability values in comparison to L-histidine and thiamine that should enter the brain via BBB to fulfill certain nutritional demands by the brain neurons [Pires et al., 2008; CEREP application notes, 2013]. Note that, a more robust scale would require additional compounds to define extremely low permeability positions. Compounds such as digoxin, tariquidar and elacridar may be employed to establish low permeability positions on the permeability scales [Alphabioregen application notes, 2017].

Therefore, the small data set illustrated in **Figure 4.5** was used to provide a “Proof of Concept” for advancing the triculture methodology as a physiologically relevant approach for ranking permeability coefficients of novel CNS-drugs/drug delivery systems. Note that, the hCMEC/D3 cell line is not stably transfected with a Pgp plasmid; thus a human BBB cell line showing higher expression of Pgp will be required for use in the development of a more robust permeability scale for commercial applications.

Based on initial data, permeability of L-histidine was 14x higher than that of verapamil, but only 5x higher than that of paclitaxel or propranolol, which are moderate Pgp substrates. Similarly, the permeability of thiamine was 9x higher than that of verapamil, and only 3x higher than that of paclitaxel and propranolol. It is speculated that the higher permeability of L-histidine may be due to lack of interaction with efflux pumps such as Pgp and BCRP and a rapid transport by the uptake transporters such as LAT1 and other amino acid transporters expressed in the hCMEC/D3 cells.

The permeability boundaries defined by the current compounds indicate that low-permeability compounds would have an apparent permeability coefficient in the neighborhood of 1.35×10^{-6} cm/s (i.e., verapamil’s placement on the scale). Intermediate-permeability compounds would show values around 3.8×10^{-6} cm/s (i.e., propranolol’s position), and high-permeability compounds would show 1.2×10^{-5} cm/s or higher (thiamine and L-histidine’s position).

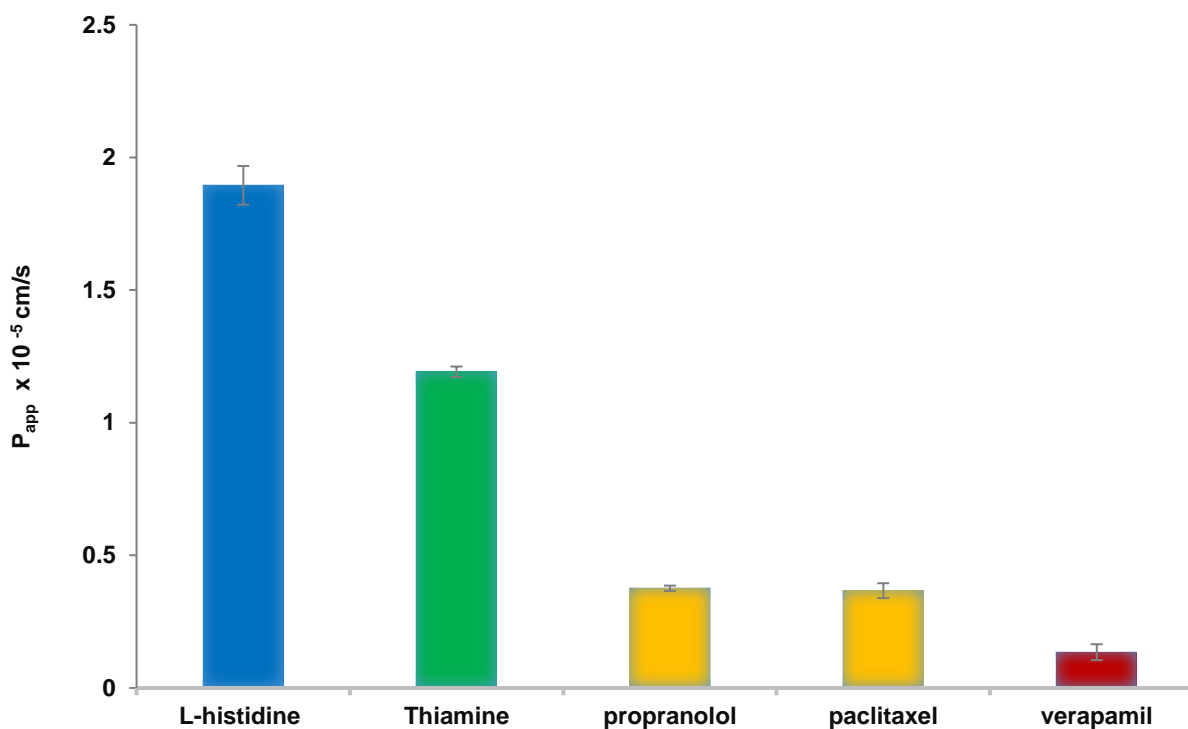


Figure 4.5. A basic permeability scale for a small set of transcellular BBB-permeants. **Blue** and **Green** compounds represent high BBB permeant-markers, **yellow** compounds are indicative intermediate permeability markers, and the **red** compound indicates lower permeability. The triculture model is capable of ranking different permeants in different permeability categories (a one-way ANOVA test indicated the difference where $n = 3$ in each category, with a p -value < 0.001). A post hoc Tukey's Honestly Significant Difference value of 0.036 indicated that propranolol and paclitaxel had similar apparent permeability values with a non-significant difference ($HSD > 0.009$) in the mean values.

Note that this is a dynamic scale and the boundary positions may be defined differently as new compounds are screened and new permeability rankings become well established on the scale.

4.7 Conclusions

One of the main objectives in this study was to compare the effect of inhibiting Pgp in a direct coculture of astrocytes and pericytes that mimics a component of the BBB system, then the hCMEC/D3 monoculture that partially mimics the BBB system and finally a triculture model. The

direct contact triculture model mimicked a full BBB system, containing three principal cellular components (the hCMEC/D3 seeded directly onto a lawn co-culture of pericytes on astrocytes). Under similar inhibitory concentrations, there was more absorption of digoxin molecules in the coculture of astrocytes and pericytes as well as in the monoculture of hCMEC/D3 cells than in the triculture model. These initial results therefore indicate that the proposed direct-contact triculture model may predict different potential for Pgp/BCRP mediated drug-drug interactions at the human BBB. It is worth noting that the proposed direct-contact triculture model showed that Pgp/BCRP did not lead to a highly significant increase in the absorption of digoxin (a Pgp substrate). This observation is in agreement with other reports in the literature showing that only minimal increases in brain exposure of a Pgp drug substrate is achieved in healthy human subjects upon co-administration with a potent Pgp inhibitor.

Another aim of the study was to develop an initial transcellular permeability scale in order to define high and low permeability thresholds. Under current scale, a permeability position between positions of propranolol and L-histidine permeability coefficients would be defined as high. However, a permeability position between propranolol and verapamil positions would be defined as intermediate, while below verapamil position would be defined as a negative permeability value. The author's opinion in this thesis is that a novel CNS compound showing a permeability value similar or less to that of verapamil would be less likely to permeate through the human BBB *in vivo*. Certainly, further validation work is still needed before adopting the triculture model as a screening tool in research programs related to CNS-drug discovery and development.

4.8 Acknowledgement

I acknowledge Kelsey E Lubin for providing technical support in the development of HPLC methods used in the present study.

4.9 References

Ballatore, C., Zhang, B., Trojanowski, J. Q., Lee, V. M., & Smith, A. B. (2008). In situ blood-brain barrier permeability of a C-10 paclitaxel carbamate. *Bioorganic & Medicinal Chemistry Letters*, 18(23), 6119-6121. doi:10.1016/j.bmcl.2008.10.024

Bankstahl, J. P., Bankstahl, M., Romermann, K., Wanek, T., Stanek, J., Windhorst, A. D., ... Kuntner, C. (2013). Tariquidar and Elacridar Are Dose-Dependently Transported by P-

Glycoprotein and Bcrp at the Blood-Brain Barrier: A Small-Animal Positron Emission Tomography and In Vitro Study. *Drug Metabolism and Disposition*, 41(4), 754-762. doi:10.1124/dmd.112.049148

Bothe, M. K., & Stover, J. F. (2014). The Branched Chain Amino Acids in the Context of Other Amino Acids in Traumatic Brain Injury. *Branched Chain Amino Acids in Clinical Nutrition*, 111-125. doi:10.1007/978-1-4939-1914-7_9

Brenton, D. P., & Gardiner, R. M. (1988). Transport of L-phenylalanine and related amino acids at the ovine blood-brain barrier. *The Journal of Physiology*, 402(1), 497-514. doi:10.1113/jphysiol.1988.sp017217

Carl, S. M., Lindley, D. J., Couraud, P. O., Weksler, B. B., Romero, I., Mowery, S. A., & Knipp, G. T. (2010). ABC and SLC Transporter Expression and Pot Substrate Characterization across the Human CMEC/D3 Blood-Brain Barrier Cell Line. *Molecular Pharmaceutics*, 7(4), 1057-1068. doi:10.1021/mp900178j

Chaves, C., Shawahna, R., Jacob, A., Scherrmann, J., & Declèves, X. (2014). Human ABC Transporters at blood-CNS Interfaces as Determinants of CNS Drug Penetration. *Current Pharmaceutical Design*, 20(10), 1450-1462. doi:10.2174/13816128113199990466

Cornford, E. M., & Hyman, S. (2005). Localization of brain endothelial luminal and abluminal transporters with immunogold electron microscopy. *NeuroRX*, 2(1), 27-43. doi:10.1602/neurorx.2.1.27

De la Peña, A., Cui, X., Geiser, J., & Loghin, C. (2017). No Dose Adjustment is Recommended for Digoxin, Warfarin, Atorvastatin or a Combination Oral Contraceptive When Coadministered with Dulaglutide. *Clinical Pharmacokinetics*, 56(11), 1415-1427. doi:10.1007/s40262-017-0531-7

Doran, J. J. (2005). Tissue distribution of UT-A and UT-B mRNA and protein in rat. *AJP: Regulatory, Integrative and Comparative Physiology*, 290(5), R1446-R1459. doi:10.1152/ajpregu.00352.2004

Eigenmann, D. E., Jähne, E. A., Smieško, M., Hamburger, M., & Oufir, M. (2016). Validation of an immortalized human (hBMEC) in vitro blood-brain barrier model. *Analytical and Bioanalytical Chemistry*, 408(8), 2095-2107. doi:10.1007/s00216-016-9313-6

Eyal, S., Hsiao, P., & Unadkat, J. D. (2009). Drug interactions at the blood-brain barrier: Fact or fantasy?. *Pharmacology & Therapeutics*, 123(1), 80-104. doi:10.1016/j.pharmthera.2009.03.017

Fang, W., Lv, P., Geng, X., Shang, E., Yang, Q., Sha, L., & Li, Y. (2013). Penetration of verapamil across blood brain barrier following cerebral ischemia depending on both paracellular pathway and P-glycoprotein transportation. *Neurochemistry International*, 62(1), 23-30. doi:10.1016/j.neuint.2012.10.012

- Fellner, S., Bauer, B., Miller, D. S., Schaffrik, M., Fankhänel, M., Spruß, T., ... Fricker, G. (2002). Transport of paclitaxel (Taxol) across the blood-brain barrier in vitro and in vivo. *Journal of Clinical Investigation*, 110(9), 1309-1318. doi:10.1172/jci0215451
- Fortuna, A., Alves, G., & Falcão, A. (2011). In vitro and In vivo Relevance of the P-glycoprotein Probe Substrates in Drug Discovery and Development: Focus on Rhodamine 123, Digoxin and Talinolol. *Journal of Bioequivalence & Bioavailability*, 01(02). doi:10.4172/jbb.s2-001
- Friis, M., Paulson, O., & Hertz, M. (1980). Carbon dioxide permeability of the blood-brain barrier in man. *Microvascular Research*, 20(1), 71-80. doi:10.1016/0026-2862(80)90020-5
- Geldenhuis, W. J., Mohammad, A. S., Adkins, C. E., & Lockman, P. R. (2015). Molecular determinants of blood-brain barrier permeation. *Therapeutic Delivery*, 6(8), 961-971. doi:10.4155/tde.15.32
- Ghose, A. K., Herbertz, T., Hudkins, R. L., Dorsey, B. D., & Mallamo, J. P. (2012). Knowledge-Based, Central Nervous System (CNS) Lead Selection and Lead Optimization for CNS Drug Discovery. *ACS Chemical Neuroscience*, 3(1), 50-68. doi:10.1021/cn200100h
- Goldberger, Z. D., & Goldberger, A. L. (2012). Therapeutic Ranges of Serum Digoxin Concentrations in Patients With Heart Failure. *The American Journal of Cardiology*, 109(12), 1818-1821. doi:10.1016/j.amjcard.2012.02.028
- Golden, P. L., & Pollack, G. M. (2003). Blood-Brain Barrier Efflux Transport. *Journal of Pharmaceutical Sciences*, 92(9), 1739-1753. doi:10.1002/jps.10424
- Greenwood, J., Love, E. R., & Pratt, O. E. (1982). Kinetics of thiamine transport across the blood-brain barrier in the rat. *The Journal of Physiology*, 327(1), 95-103. doi:10.1113/jphysiol.1982.sp014222
- Harata, N., & Iwasaki, Y. (1995). Evidence for early blood-brain barrier breakdown in experimental thiamine deficiency in the mouse. *Metabolic Brain Disease*, 10(2), 159-174. doi:10.1007/bf01991863
- Hutzler, J. M., Cook, J., & Fleishaker, J. C. (2011). Drug-Drug Interactions: Designing Development Programs and Appropriate Product Labeling. *Pharmacokinetics in Drug Development*, 21-56. doi:10.1007/978-1-4419-7937-7_2
- Kemper, E. M., Cleypool, C., Boogerd, W., Beijnen, J. H., & Van Tellingen, O. (2003). The influence of the P-glycoprotein inhibitor zosuquidar trihydrochloride (LY335979) on the brain penetration of paclitaxel in mice. *Cancer Chemotherapy and Pharmacology*, 53(2), 173-178. doi:10.1007/s00280-003-0720-y
- Kostrzewa, R. M. (2007). The blood-brain barrier for catecholamines-Revisited. *Neurotoxicity Research*, 11(3-4), 261-271. doi:10.1007/bf03033571

- Kurihara, A., Suzuki, H., Sawada, Y., Sugiyama, Y., Iga, T., & Hanano, M. (1988). Transport of Digoxin into Brain Microvessels and Choroid Plexuses Isolated from Guinea Pig. *Journal of Pharmaceutical Sciences*, 77(4), 347-352. doi:10.1002/jps.2600770414
- Li, X., Chen, G., & Yang, B. (2012). Urea Transporter Physiology Studied in Knockout Mice. *Frontiers in Physiology*, 3. doi:10.3389/fphys.2012.00217
- Lockman, P. R., Mumper, R. J., & Allen, D. D. (2003). Evaluation of blood-brain barrier thiamine efflux using the in situ rat brain perfusion method. *Journal of Neurochemistry*, 86(3), 627-634. doi:10.1046/j.1471-4159.2003.01888.x
- Löscher, W., & Potschka, H. (2005). Blood-brain barrier active efflux transporters: ATP-binding cassette gene family. *NeuroRX*, 2(1), 86-98. doi:10.1602/neurorx.2.1.86
- Martinez, M. N. (2011). Factors Influencing the Use and Interpretation of Animal Models in the Development of Parenteral Drug Delivery Systems. *The AAPS Journal*, 13(4), 632-649. doi:10.1208/s12248-011-9303-8
- Marchi, N., Banjara, M., & Janigro, D. (2016). Blood–brain barrier, bulk flow, and interstitial clearance in epilepsy. *Journal of Neuroscience Methods*, 260, 118-124. doi:10.1016/j.jneumeth.2015.06.011
- Mayer, U., Wagenaar, E., Beijnen, J. H., Smit, J. W., Meijer, D. K., Asperen, J., ... Schinkel, A. H. (1996). Substantial excretion of digoxin via the intestinal mucosa and prevention of long-term digoxin accumulation in the brain by the mdrla P-glycoprotein. *British Journal of Pharmacology*, 119(5), 1038-1044. doi:10.1111/j.1476-5381.1996.tb15775.x
- Miller, D. (2015). Regulation of ABC transporters at the blood-brain barrier. *Clinical Pharmacology & Therapeutics*, 97(4), 395-403. doi:10.1002/cpt.64
- Nakagawa, S., Deli, M. A., Kawaguchi, H., Shimizudani, T., Shimono, T., Kittel, Á., ... Niwa, M. (2009). A new blood–brain barrier model using primary rat brain endothelial cells, pericytes and astrocytes. *Neurochemistry International*, 54(3-4), 253-263. doi:10.1016/j.neuint.2008.12.002
- Nix, D. E., & Gallicano, K. (2011). Design and Data Analysis in Drug Interaction Studies. *Drug Interactions in Infectious Diseases*, 655-682. doi:10.1007/978-1-61779-213-7_20
- Noack, A., Noack, S., Hoffmann, A., Maalouf, K., Buettner, M., Couraud, P., ... Löscher, W. (2014). Drug-Induced Trafficking of P-Glycoprotein in Human Brain Capillary Endothelial Cells as Demonstrated by Exposure to Mitomycin C. *PLoS ONE*, 9(2), e88154. doi:10.1371/journal.pone.0088154
- Olesen, J., Hougaard, K., & Hertz, M. (1978). Isoproterenol and propranolol: ability to cross the blood-brain barrier and effects on cerebral circulation in man. *Stroke*, 9(4), 344-349. doi:10.1161/01.str.9.4.344

- Peura, L., Malmioja, K., Huttunen, K., Leppänen, J., Hämäläinen, M., Forsberg, M. M., ... Laine, K. (2013). Design, Synthesis and Brain Uptake of LAT1-Targeted Amino Acid Prodrugs of Dopamine. *Pharmaceutical Research*, 30(10), 2523-2537. doi:10.1007/s11095-012-0966-3
- Pires, M. M., Emmert, D., Hrycyna, C. A., & Chmielewski, J. (2008). Inhibition of P-Glycoprotein-Mediated Paclitaxel Resistance by Reversibly Linked Quinine Homodimers. *Molecular Pharmacology*, 75(1), 92-100. doi:10.1124/mol.108.050492
- Rankovic, Z. (2015). Designing CNS Drugs for Optimal Brain Exposure. *Blood-Brain Barrier in Drug Discovery*, 385-424. doi:10.1002/9781118788523.ch18
- Reynolds, K. S. (2011). Drug Interaction Considerations Throughout Drug Development. *Drug Interactions in Infectious Diseases*, 613-630. doi:10.1007/978-1-61779-213-7_18
- Ronaldson, P. T., Bendayan, M., Gingras, D., Piquette-Miller, M., & Bendayan, R. (2004). Cellular localization and functional expression of P-glycoprotein in rat astrocyte cultures. *Journal of Neurochemistry*, 89(3), 788-800. doi:10.1111/j.1471-4159.2004.02417.x
- Sakurai, E., Sakurai, E., Watanabe, T., & Yanai, K. (2009). Uptake of L-histidine and histamine biosynthesis at the blood-brain barrier. *Inflammation Research*, 58(S1), 34-35. doi:10.1007/s00011-009-0656-8
- Stieger, B. (2013). Faculty of 1000 evaluation for Variability in P-Glycoprotein Inhibitory Potency (IC50) Using Various in Vitro Experimental Systems: Implications for Universal Digoxin Drug-Drug Interaction Risk Assessment Decision Criteria. F1000 - Post-publication peer review of the biomedical literature. doi:10.3410/f.718043074.793480891
- Subramanian, V. S., Marchant, J. S., & Said, H. M. (2005). Targeting and Trafficking of the Human Thiamine Transporter-2 in Epithelial Cells. *Journal of Biological Chemistry*, 281(8), 5233-5245. doi:10.1074/jbc.m512765200
- Tachikawa, M., & Hosoya, K. (2011). Transport characteristics of guanidino compounds at the blood-brain barrier and blood-cerebrospinal fluid barrier: relevance to neural disorders. *Fluids and Barriers of the CNS*, 8(1), 13. doi:10.1186/2045-8118-8-13
- Thiel-Demby, V. E., Tippin, T. K., Humphreys, J. E., Serabjit-Singh, C. J., & Polli, J. W. (2004). In Vitro absorption and secretory quotients: Practical criteria derived from a study of 331 compounds to assess for the impact of P-glycoprotein-mediated efflux on drug candidates. *Journal of Pharmaceutical Sciences*, 93(10), 2567-2572. doi:10.1002/jps.20166
- Trinh-Trang-Tan, M., Lasbennes, F., Gane, P. ..., Roudier, N., Ripoche, P., Cartron, J., & Bailly, P. (2002). UT-B1 proteins in rat: tissue distribution and regulation by antidiuretic hormone in kidney. *American Journal of Physiology - Renal Physiology*, 283(5), F912-F922. doi:10.1152/ajprenal.00359.2001
- Urquhart, B. L., & Kim, R. B. (2009). Blood-brain barrier transporters and response to CNS-active drugs. *European Journal of Clinical Pharmacology*, 65(11), 1063-1070. doi:10.1007/s00228-009-0714-8

- Weksler, B., Romero, I. A., & Couraud, P. (2013). The hCMEC/D3 cell line as a model of the human blood brain barrier. *Fluids and Barriers of the CNS*, 10(1), 16. doi:10.1186/2045-8118-10-16
- Yang, C., Zhang, T., Li, Z., Xu, L., Liu, F., Ruan, J., ... Zhang, Z. (2013). P-glycoprotein is responsible for the poor intestinal absorption and low toxicity of oral aconitine: In vitro, in situ, in vivo and in silico studies. *Toxicology and Applied Pharmacology*, 273(3), 561-568. doi:10.1016/j.taap.2013.09.030
- Yoshikawa, T., Nakamura, T., Shibakusa, T., Sugita, M., Naganuma, F., Iida, T., ... Yanai, K. (2014). Insufficient Intake of L-Histidine Reduces Brain Histamine and Causes Anxiety-Like Behaviors in Male Mice. *Journal of Nutrition*, 144(10), 1637-1641. doi:10.3945/jn.114.196105
- Yudilevich, D. L., De Rose, N., & Sepúlveda, F. V. (1972). Facilitated transport of amino acids through the blood-brain barrier of the dog studied in a single capillary circulation. *Brain Research*, 44(2), 569-578. doi:10.1016/0006-8993(72)90319-8
- Zhang, L., Ong, W. Y., & Lee, T. (1999). Induction of P-glycoprotein expression in astrocytes following intracerebroventricular kainate injections. *Experimental Brain Research*, 126(4), 509-516. doi:10.1007/s002210050759

CHAPTER 5. DISSERTATION HIGHLIGHTS AND LONG-TERM PERSPECTIVES ON THE DEVELOPMENT OF LAYERED CELL CULTURE MODELS OF THE HUMAN BLOOD-BRAIN BARRIER

5.1 Dissertation highlights

A major goal of this thesis was to develop a direct-contact triculture model for mimicking the BBB-physiology *in vitro*. A mini-review on the BBB-physiology and transport functions was written in chapter one to justify why a direct layer-by-layer methodology for the preparation of a BBB-model on a *Transwell*TM would lead to a more physiologically representative configuration of the BBB *in vitro*. The relevance of optimal direct-contacts (e.g., gap and peg-socket junctions) in molecular exchange/signaling between the BBB cells was highlighted. The direct-contact triculture methodology and its variant approaches in a *Transwell*TM chamber were proposed to allow for the development of a more physiologically relevant cell culture model of the BBB with a cellular arrangement and interactions resembling those of the BBB in an *in vivo* setting.

Initial development and characterization of a direct-contact triculture method for mimicking the BBB *in vitro* was described in Chapter II. Initial studies described in Chapter II indicated that a layer-by-layer coculture of astrocytes and pericytes form a resistant paracellular barrier to the flux of mannitol with a similar magnitude to that measured in the monoculture of hCMEC/D3 cells. Thus, the popular view that astrocytes and pericytes influence the BBB-functions only through inductive effects may not be completely accurate. Based on our initial data, astrocytes together with pericytes may be important direct contributors in restricting permeation in an additive or potentially synergistic fashion across the BBB system contrary to the contemporary notion that non-endothelial BBB cells do not form a distinct physiological barrier to the absorption of small or large molecules across the BBB.

Although both astrocytes and pericytes showed similar effect on reducing the paracellular permeation when directly co-cultured in layers with the hCMEC/D3 cells, the observed reduction in the effective permeability of a small paracellular permeant such as sucrose was not additive in the triculture where both astrocytes and pericytes were present. It seemed as if there was a limited extent by which the permeability of small paracellular markers due to the inclusion of the astrocytes or pericytes in the triculture model. Further mechanistic studies on the role of interactions between cells found in the neurovascular unit on the effective permeation of small or

large hydrophilic molecules across the BBB *in vitro*, may assist in delineating the extent by which astrocytes and pericytes influence paracellular permeation routes across the BBB system.

Nevertheless, it was noted that a direct-contact triculture model of the BBB, containing a combined basement of astrocytes and pericytes, and a continuous top layer of hCMEC/D3 cells was consistently more restrictive than the corresponding monoculture of hCMEC/D3 cells based on the results from permeability assays using the established small and large hydrophilic paracellular permeants. Therefore, the proposed triculture model better mimicked the paracellular tightness associated with the BBB physiology *in vivo*.

While Chapter II dealt with establishing a stable triculture model of the human BBB on a *Transwell*TM, Chapter III described imaging of ultrastructural features in the cultures of BBB cells used in the preparation of the triculture model. Monocultures of separate BBB cells (astrocytes, pericytes and hCMEC/D3 cells) were used as controls to identify distinct ultrastructural characteristics in the layers corresponding to the astrocytes, pericytes or the hCMEC/D3 cells in the triculture model of the BBB containing all these cells on a *Transwell*TM support. The observed ultrastructural features in the cross-sectional specimens of a BBB-triculture were finally compared to the ultrastructural features published in a reference micrograph of a human BBB by Farkas et al., 2001.

A major objective in Chapter III was to establish the unique physical and morphological features corresponding to the layers of hCMEC/D3 cells (a transformed primary human brain microvessel endothelial cell model), human brain vascular pericytes, and human brain astrocytes. The hCMEC/D3 layer was continuous due to the formation of tight cell-cell junctions between adjacent hCMEC/D3 cells. The hCMEC/D3 layer contained several vesicles spanning across cell membranes indicating that transcytosis may be a contributing transport process occurring within the hCMEC/D3 cell layer. There is a wide scientific interest in using vesicular transcytosis for CNS-drug delivery across the BBB [Lajoie et al., 2015; Mäger et al., 2016]; the proposed triculture model may find useful applications in preclinical evaluation of receptor mediated drug delivery strategies for treating neurological diseases.

To the contrary, monolayers of pericytes or astrocytes lacked a consistent formation of tight cell-cell junctions, based on the analysis of TEM micrographs, and hence could not form continuous cell layers. More specifically, numerous gaps were observed at the cell-cell junctions in the monocultures of astrocytes and pericytes, suggesting that astrocytes or pericytes, on their

own, may not form an effective paracellular barrier to the flux of hydrophilic molecules. Since both astrocyte and pericyte densities may vary regionally along the brain endothelial capillaries/the neurovascular system, it is not clear if the seeding densities examined in the current studies would be representative of the coverage densities along the cerebral endothelial capillary system. The extent by which astrocytes and pericytes cover brain capillaries may determine the BBB physiology and functions [Watkins et al., 2014]. Therefore, more astroglial and pericytes seeding density ratios may have to be explored in the future, to understand how seeding density ratios would affect the formation of cell-cell junctions of among astrocytes or pericytes and to delineate how changes in the astrocytes or pericytes coverage of the BBB capillary would influence its functions.

The layered, direct-triculture model in which astrocytes and pericytes provided a physiologically relevant basement on which the hCMEC/D3 cells grew to form a continuous layer showing tight cell-cell junctions in TEM analyses. The cross-sectional TEM analyses of the triculture specimen showed that a consistent layer of hCMEC/D3 cells was formed at the top section, while the bottom layer contained areas of astrocytes or astrocytes mixed with pericytes. Thus, the cross-sectional configuration of the triculture model resembled the cross-sectional configuration of the BBB-glia vascular unit *in vivo*, where either the astrocytes or pericytes or both cell types cover brain capillaries.

After establishing the similarity in physiological configuration between the BBB-triculture model and the BBB *in vivo* by TEM analyses, the next objective was to evaluate the potential application of the triculture model in drug transport assays. A select set of model compounds was used to test the permeability rank order expected in a functional triculture model of the BBB; this set of compounds contained molecules expected to use different pathways of permeation including nutrient-carriers (facilitated diffusion), passive transcellular permeation, and efflux mediated transport. The main goal was to evaluate the potential of a direct-contact triculture model of the BBB to classify the permeability of established BBB permeants into fast or slow categories, and to validate the observed rank order using published literature on the permeability of the test-permeants across the BBB.

L-histidine and thiamine, essential brain nutrients, were expected to traverse the BBB-triculture model more quickly than propranolol, paclitaxel (a Pgp substrate), and verapamil (a substrate of efflux transporters such as Pgp and BCRP) that represent typical neurotoxic drugs that

would be found in blood circulation of cardiac or cancer patients. Recognizing that propranolol (a substrate of Pgp), paclitaxel (a Pgp substrate) and verapamil (a Pgp substrate) are known substrates of efflux transporters, they were expected to be much slower in traversing the BBB-triculture in comparison to L-histidine or thiamine. There, the permeability ranking function for these test-permeants was examined in the triculture model to establish its potential application as a permeability screening tool of novel CNS-drugs or CNS-drug delivery technologies.

The direct-contact triculture model revealed its potential for ranking the expected permeability order from high permeability of L-histidine and thiamine, to moderate permeability values for propranolol and paclitaxel, and to low permeability of verapamil which is an established marker for low permeability across the BBB models. Thus, the triculture exhibited a good potential for application in ranking molecular permeability coefficients based on a small set of test permeants in the present study. Additionally, the effects of Pgp inhibition on the absorption of a typical Pgp substrate (digoxin) were analyzed and compared between the hCMEC/D3 monoculture, the coculture of astrocytes and pericytes, and the triculture which is a full representation of the BBB cellular composition. Elacridar, a non-competitive Pgp inhibitor, was used to make comparisons of the Pgp function in the fore mention cell cultures that offer partial or full representation of the BBB configuration *in vitro*.

Initial results indicated that it is relatively more difficult to inhibit Pgp/efflux function in the triculture model of the BBB than the hCMEC/D3 monoculture model, which is a partial representation of the BBB *in vitro*. This observation further supports the relevance of a triculture methodology in mimicking the BBB *in vitro* as it is more in agreement with previous *in vivo* studies showing that inhibition of Pgp at a healthy BBB did not lead to higher absorption of drugs in the brain. However, additional studies using alternative BBB cell lines should be investigated to determine if high Pgp expressing cells would provide a better comparison to the *in vivo* BBB function.

5.2 Long-term strategies for advancing the triculture-methodology

Numerous approaches have been proposed, in various literature on the BBB, on how to improve tightness in the BBB cell-culture models. In one of the most recent publication, Katt et al. reported using retinoic acid to modulate the expression of important tight junctions and efflux transporters [Katt et al., 2016]. The use of retinoic acid led to high TEER values in the hCMEC/D3 cell line (a

BBB-cell model) from low values of around $50 \Omega\text{-cm}^2$ to high values of around $2000 \Omega\text{-cm}^2$. In a different approach, the hCMEC/D3 cell-layer grown under flow-dynamic conditions demonstrated a 20-fold increase in TEER values relative to the hCMEC/D3 cells grown on a *Transwell*TM chamber under minimal shaking conditions [Cucullo et al., 2007].

Therefore, the issue in the BBB cell culture models may no longer be how to tighten the paracellular pathway, but rather how to mimic the BBB *in vitro* in a configuration that resembles that of the BBB as observed in an *in vivo* setting. A physiologically relevant model ought to mimic the diffusional paths that a novel CNS-drug or drug delivery system would traverse across the BBB to get to the brain parenchyma. The direct contact triculture model invented in this research represents the initial step towards providing true physiological relevancy for enhanced prediction of novel molecules with optimal BBB permeation properties or drug delivery technologies with enhanced capability for permeating through a neuro-defensive BBB system. Suggestions on how to implement the triculture methodology in an industrial setting where high throughput screening technologies may be available are discussed next.

5.2.1 High throughput implementation of the triculture methodology

The Blood-CNS interfaces, including the BBB, act as neuroprotective barrier that control molecular trafficking between the CNS and peripheral systems [Bauer et al., 2014]. The BBB achieves its selective restrictive properties through a complicated network of protein-protein interactions in the cell-cell junctions of the BBB endothelial capillaries and biochemical signals transmitted through non-endothelial cellular components of the neurovascular unit [Alvarez et al 2011; Tietz and Engelhardt 2015]. Thus, the effect of exogenous chemical agents on the normal/abnormal functions of the neurovascular unit would be a subject of interest in CNS-drug discovery and delivery programs where effects of novel CNS-drug candidates and CNS-drug delivery technologies on the BBB physiology or functions may have to be established before realizing a successful clinical outcome. Failure to follow this approach may result in deleterious neurotoxicity or a lack of clinical efficacy in the later stages of drug development.

The chemical space of interest in general drug discovery programs is of astronomical order ($10^{20} - 10^{24}$ molecules of interest to medicinal chemists) [Reymond et al 2012; Reymond et al 2015]. Therefore, a high throughput screening approach is traditionally employed to discover molecules with therapeutic actions on biological targets of interest by screening several thousands

of molecules. For example, 10,000 molecules per day in high throughput screening or 100,000 molecules may be evaluated per day in ultra-high throughput screening with the goal of increasing the probability of getting a hit molecule from such a large chemical space [Szymański et al 2012].

Efforts to discover molecular chemotypes that have interesting chemical action on the neuroprotective functions of the BBB may involve large sets of compounds (0.5 to 2.8 million, a typical library of compounds for a big pharmaceutical company like Pfizer) [Hansen et al., 2016]. Implementation of the direct triculture methodology within HTS technologies in drug discovery and early development programs may provide better prediction of *in vivo* performance than the conventional indirect triculture techniques.

Probing drug actions on a triculture model of the BBB in a high throughput-screening manner would require fast and well-designed assays. A direct layering of BBB cells on the apical surface of a *Transwell*TM chamber to create a direct-contact triculture model for mimicking the BBB may be more amenable in high throughput screening technologies. It would be faster and easier to automate direct seeding of BBB cells on the apical surface of a *Transwell*TM in comparison to indirect methodologies, where manual seeding may be required to plate cells on different sides of a *Transwell*TM filter support.

Application of the triculture methodology in probing chemical effects on the normal (or abnormal) BBB-signaling functions may require a unique triculture configuration depending on the analytical method used. For example, if a high content imaging detection is required on the neurons cultured in a BBB-environment, it may be suitable to design automated experiments in which BMECs would be plated on the apical surface of a *Transwell*TM first, pericytes second, astrocytes third, and neurons of interest (diseased or normal) fourth to form a multilayered configuration *in vitro*.

Once the resulting neuronal-BBB culture is stable, it may be transferred to a well containing a compound of interest in the basolateral chamber to evaluate its BBB-permeability and neuronal effects, all in a single assay. Thus, a library of compounds may be screened in phenotypic assays and correlation models relating physical-chemical properties and neuronal effects might be obtained using a triculture model of the BBB in a neurological environment.

Implementation of the triculture methodology in a high throughput screening assays would need to fulfill many more requirements. These may include a well-designed automation scheme, well-validated assays to reduce the number of false negatives or positives, digital capability to

collect, store, and analyze large data sets, and finally a lot of time since high throughput screening projects may take months or years before obtaining useful data sets for applications in modeling [Macarron and Hertzberg, 2009]. The time and resources in high throughput screening projects may also vary depending on the purpose; CNS-drug formulation studies or drug delivery projects may require less time in comparison to the BBB-target identification and validation projects.

5.2.2 Inclusion of brain neurons in the direct-contact triculture model of the blood-brain barrier

The current opinion from BBB-experts is that the main problem with neuronal drug delivery is how to deliver a neurotherapeutic drug candidate across the BBB-unit in a sufficient amount to elicit a desired pharmacological effect [Banks, 2016; Pardridge 2016]. Thus, a BBB cell culture model in a *Transwell*TM that truly mimics all the cellular barriers that a drug molecule destined to a diseased neuron in the brain parenchyma would encounter, may be more useful than a model that partially represent its diffusional path towards neurons in the brain parenchyma.

Prediction of a free fraction of a drug that escapes BBB protective mechanisms to gain access to the brain parenchyma and its neurological effects are the most important goals in the successful application of the *in vitro* triculture model of a human BBB described in the preceding chapters. Inclusion of an additional direct layer of neurons in the model may render it to be more robust in the prediction of the free fraction of a drug that would be bioavailable to neurons in the brain parenchyma. In addition, other pharmacological parameters of interest may be better predicted when the BBB is mimicked in neurological environment as depicted in **Figure 5.1**.

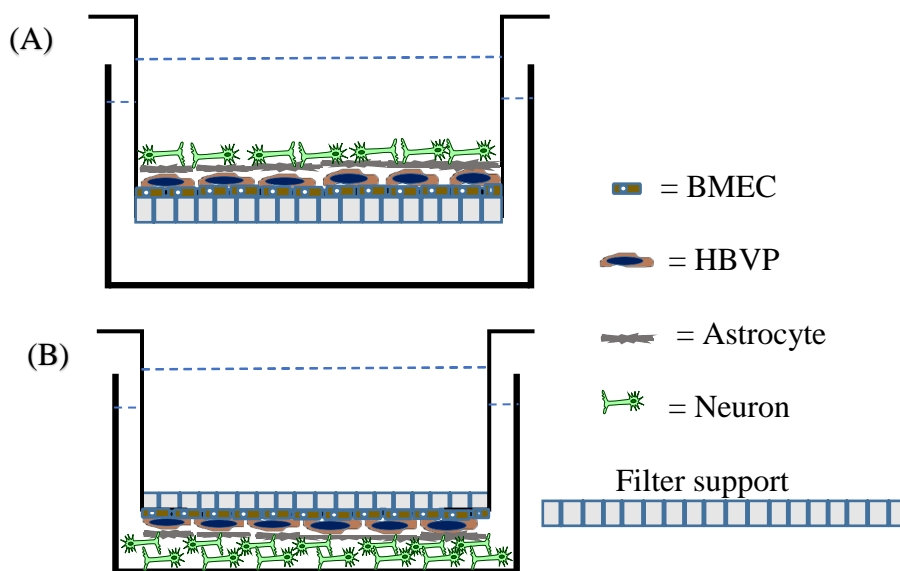


Figure 5.1. Conceptual designs on how to mimic a preclinical BBB-glia unit system in a neuronal environment. Panel (A) shows a direct-contact model of the BBB in a neuronal environment on the apical chamber of a *Transwell*TM. Panel (B) illustrates a direct-contact model maintained in a neuronal environment on the basolateral chamber of a *Transwell*TM.

5.2.3 Development of *In Vitro In Vivo* correlation models, refinements and commercialization

The ability to predict neuronal drug exposure using *in vitro* techniques is highly complex and may not be achievable in a short period. However, if *in vitro* data on the permeability of drugs across a triculture model of the human BBB including the free fraction of drugs that escape BBB protective mechanisms, and data on the required concentration of drugs for causing desirable neurological effects are available, then robust predictions regarding *in vivo* brain pharmacokinetics and pharmacodynamics may be attained from *in vitro* studies that mimic well the BBB physiology and function.

In this endeavor, the Positron Emission Technology (PET available at Purdue University) may be useful in providing *in vivo* data sets regarding brain pharmacokinetic parameters that would be used in the development of IVIVC models for routine applications in CNS drug research and development programs. While IVIVC studies in brain drug disposition may require a large collaboration between various groups, the BBB cell culture models may be used to collect *in vitro* transport parameters. Examples of relevant pharmacokinetic parameters would include the free

fraction of drug available to the neurons- F_a , the apparent permeability- P_{app} , transporter kinetic parameters- K_m , and V_{max} , or the link between *in vitro* transport parameters and *in vitro* neuronal phenotypes of interest to medicinal chemists. Such *in vitro* pharmacokinetic and pharmacodynamic data sets could then be correlated with *in vivo* data sets collected or published from other BBB researchers from around the world.

Ultimately, the 3D-cell culture models conceived in this study may be commercialized to companies in the business of neurological drug discovery and development. Companies like Neuromics (Edina, Maine, USA) or Alphabio Regen (Boston, Massachusetts, USA) may be interested in a 3D-model of the BBB cultured in a neuronal environment to allow for coupling of drug permeability and phenotypic assays in one BBB-kit.

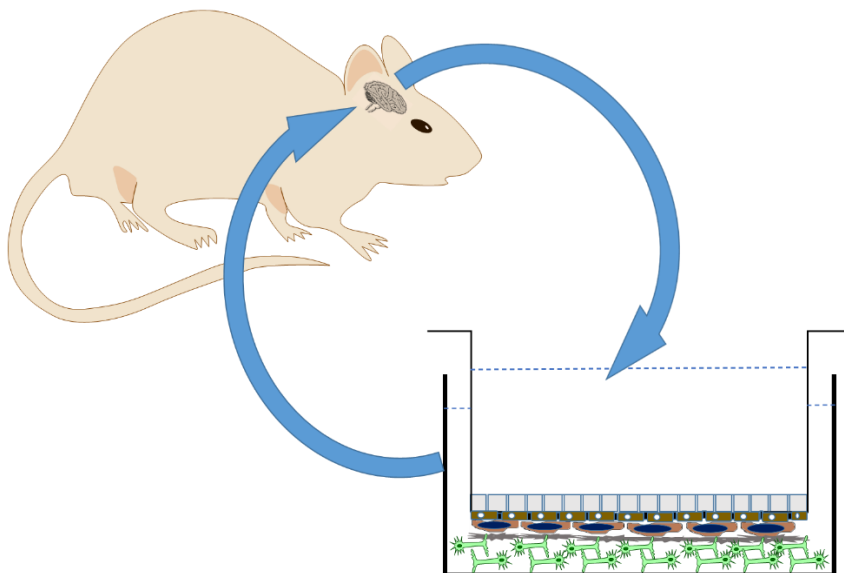


Figure 5.2. A framework for the application of BBB cell culture methods in the development of IVIVC models. The ultimate goal is to generate robust IVIVC models capable of predicting pre-clinical or clinical pharmacokinetic and pharmacodynamic parameters of interest in CNS-drug development. For example, data sets from pre-clinical models such as a mouse could be used to assist in the development of IVIVC models for predicting drugs/drug delivery systems that would lead to optimal drug exposure to the brain parenchyma. IVIVC models may be continually refined as more data from *in vivo* and *in vitro* studies become available from various researchers.

Therefore, one of the most important steps in the final development of the layered 3D-BBB cell culture models would be to establish a reliable preservation technique that would allow one to

sell precultured BBB models to companies involved in the development of neurological drug delivery technologies. Initially it would be beneficial to develop the direct contact 3D-BBB kits and test if they can be preserved at -80°C and if they can be thawed to recover the original BBB-drug transport properties in a few days (~7 days), as done in the current 3D-BBB kits at Neuromics. To summarize, a 3D-human BBB cell culture model showing robust disease specific IVIVC models and potential for development into a commercial kit would bring good financial returns from the time and money invested in its conception and development.

5.3 A declaration of conflict of interests

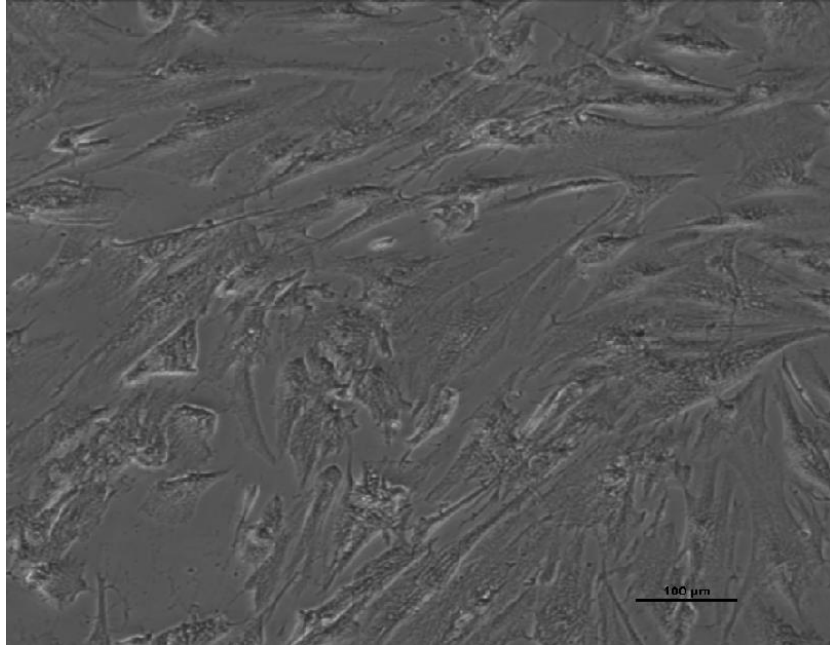
All novel concepts, designs, and prototypes developed in this dissertation are related to claims of the **US Provisional Patent Application Serial No. 62/384,380**, filed September 7, 2016 and **US Patent Application Serial No. 15697699**, filed September 7, 2017. Invention of the Blood Brain Barrier models and methods described in this dissertation were supported by the grant number RO1-65448 awarded by the National Institute of General Medical Sciences. The US government has certain rights on the intellectual properties described in the present dissertation.

5.4 References

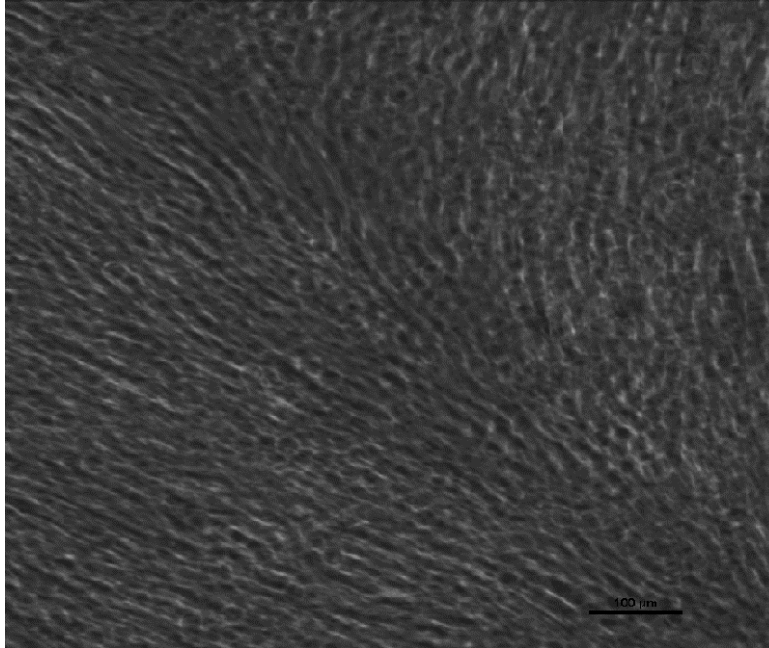
- Alvarez, J. I., Dodelet-Devillers, A., Kebir, H., Ifergan, I., Fabre, P. J., Terouz, S., ... Prat, A. (2011). The Hedgehog Pathway Promotes Blood-Brain Barrier Integrity and CNS Immune Quiescence. *Science*, 334(6063), 1727-1731. doi:10.1126/science.1206936
- Banks, W. A. (2016). From blood–brain barrier to blood–brain interface: new opportunities for CNS drug delivery. *Nature Reviews Drug Discovery*, 15(4), 275-292. doi:10.1038/nrd.2015.21
- Bauer, H., Krizbai, I. A., Bauer, H., & Traweger, A. (2014). “You Shall Not Pass”-tight junctions of the blood brain barrier. *Frontiers in Neuroscience*, 8. doi:10.3389/fnins.2014.00392
- Cucullo, L., Couraud, P., Weksler, B., Romero, I., Hossain, M., Rapp, E., & Janigro, D. (2007). Immortalized Human Brain Endothelial Cells and Flow-Based Vascular Modeling: A Marriage of Convenience for Rational Neurovascular Studies. *Journal of Cerebral Blood Flow & Metabolism*, 28(2), 312-328. doi:10.1038/sj.jcbfm.9600525
- Hansen, E. C., Pedro, D. J., Wotal, A. C., Gower, N. J., Nelson, J. D., Caron, S., & Weix, D. J. (2016). New ligands for nickel catalysis from diverse pharmaceutical heterocycle libraries. *Nature Chemistry*, 8(12), 1126-1130. doi:10.1038/nchem.2587

- Katt, M. E., Xu, Z. S., Gerecht, S., & Searson, P. C. (2016). Human Brain Microvascular Endothelial Cells Derived from the BC1 iPS Cell Line Exhibit a Blood-Brain Barrier Phenotype. *PLOS ONE*, 11(4), e0152105. doi:10.1371/journal.pone.0152105
- Lajoie, J. M., & Shusta, E. V. (2015). Targeting Receptor-Mediated Transport for Delivery of Biologics Across the Blood-Brain Barrier. *Annual Review of Pharmacology and Toxicology*, 55(1), 613-631. doi:10.1146/annurev-pharmtox-010814-124852
- Macarrón, R., & Hertzberg, R. P. (2009). Design and Implementation of High-Throughput Screening Assays. *Methods in Molecular Biology*, 1-32. doi:10.1007/978-1-60327-258-2_1
- Mäger, I., Meyer, A. H., Li, J., Lenter, M., Hildebrandt, T., Leparc, G., & Wood, M. J. (2017). Targeting blood-brain-barrier transcytosis – perspectives for drug delivery. *Neuropharmacology*, 120, 4-7. doi:10.1016/j.neuropharm.2016.08.025
- Pardridge, W. M. (2016). CSF, blood-brain barrier, and brain drug delivery. *Expert Opinion on Drug Delivery*, 13(7), 963-975. doi:10.1517/17425247.2016.1171315
- Reymond, J. (2015). The Chemical Space Project. *Accounts of Chemical Research*, 48(3), 722-730. doi:10.1021/ar500432k
- Reymond, J., & Awale, M. (2012). Exploring Chemical Space for Drug Discovery Using the Chemical Universe Database. *ACS Chemical Neuroscience*, 3(9), 649-657. doi:10.1021/cn3000422
- Szymański, P., Markowicz, M., & Mikiciuk-Olasik, E. (2011). Adaptation of High-Throughput Screening in Drug Discovery—Toxicological Screening Tests. *International Journal of Molecular Sciences*, 13(12), 427-452. doi:10.3390/ijms13010427
- Tietz, S., & Engelhardt, B. (2015). Brain barriers: Crosstalk between complex tight junctions and adherens junctions. *The Journal of Cell Biology*, 209(4), 493-506. doi:10.1083/jcb.201412147
- Watkins, S., Robel, S., Kimbrough, I. F., Robert, S. M., Ellis-Davies, G., & Sontheimer, H. (2014). Disruption of astrocyte–vascular coupling and the blood–brain barrier by invading glioma cells. *Nature Communications*, 5. doi:10.1038/ncomms5196

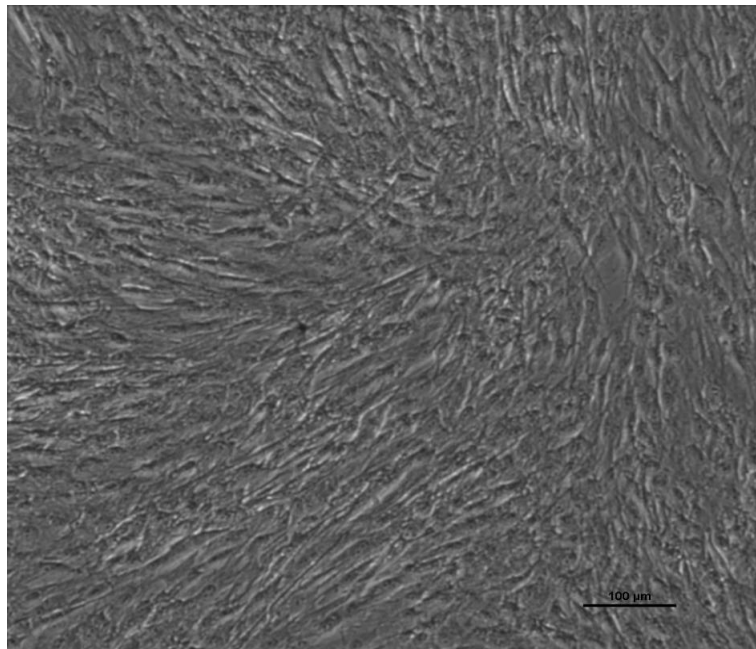
APPENDIX A. SUPPLEMENTAL DATA ON THE BASAL CULTURE OF ASTROCYTES AND PERICYTES



Supplemental Figure 1. Pericytes cultured alone on the surface of a *Transwell*TM filter support. Pericytes did not grow to cover the surface completely even at the end of day 7. The bar represents 100 μm

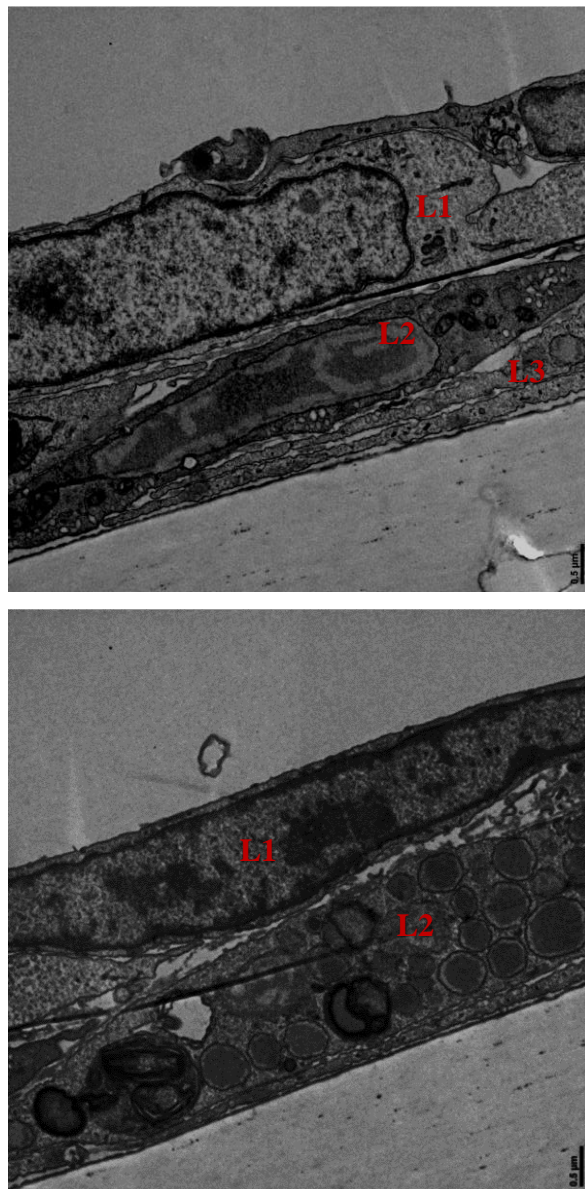


Supplemental Figure 2. Pericytes grown on a basal culture of astrocytes multiplied to cover the underneath astrocytes completely at the end of day 7. The bar represents 100μm



Supplemental Figure 3. Astrocytes cultured on a basal layer of pericytes for 7 days. Astrocytes on the top layer multiplied to cover most of the underneath pericytes. The characteristic needle-like projections, which are unique features to the astrocytes, were clearly visible on the astrocytes. The bar scale represents 100 μm

APPENDIX B. SUPPLEMENTAL TEM MICROGRAPHS OF THE BBB TRICULTURE



Supplemental Figure 4. Thin cross-sectional TEM micrographs of a BBB triculture. Panel **A** shows a section where three layers (**L1**, **L2**, and **L3**) formed. Panel **B** shows a section where two cell layers are formed (**L1**, and **L2**). It is hoped that a non-ambiguous identification of the cell layers of the BBB triculture will be made using cell-specific staining antibodies as a continuation of the research presented in the current dissertation. The bar scale represents 0.5 μm